Coordinatore
Fernando Fraternali

Tutor
Rosario Montuori
Industrial tutor
Maria Gabriella Castellano
Academic Co-tutor
Ιωάννης Βάγιας

Bonaventura TAGLIAFIERRO

Seismic Protection of Adjustable Pallet Racking Structures with Isolation Systems

Novel devices for practical uses

UNIVERSITÀ
DEGLI STUDI
DI SALERNO

dciv Dipartimento di
Ingegneria Civile

PhD Rischio e Sostenibilità
*nei Sistemi dell'Ingegneria Civile,
Edile ed Ambientale*

Copyright for this work belongs to the author.

UNIVERSITÀ DEGLI STUDI DI SALERNO

Dipartimento di Ingegneria Civile

Dottorato di Ricerca
in
Rischio e sostenibilità
nei sistemi dell'ingegneria civile, edile ed ambientale

XXXIV (2018-2021)

Seismic Protection of Adjustable Pallet Racking Structures with Isolation Systems

Bonaventura Tagliafierro

Academic Tutor	**PhD Coordiantor**
Prof. Rosario Montuori	*Prof. Fernando Fraternali*
Industrial Tutor	**Academic Co-tutor**
Dr. Maria Gabriella Castellano	*Prof. Ιωάννης Βάγιας*

Foreword

The investigation of warehouse pallet-rack structures presented in this thesis follows from a specific research project funded and envisioned by the HORIZON 2020 European call. Due to its multidisciplinary and multi-tier views, whose elaboration and articulation were strengthened by such high-level financial support, the scope of the project has been fully explored in conjunction with two key partners, one industrial and the other academic, both of whom have greatly contributed to enhancing the quality of the main outcomes of this project.

The reader will find that the document is arranged in a textbook format that provides a didactic overview of the comprehensive framework within which the investigation is presented. The fragility of warehouse pallet-rack structures has been evidenced by the enormous losses experienced in warehouses when induced lateral motion has resulted in partial or total structural collapse, with consequences of disproportionate magnitude.

Warehouse structures that constitute key links in industrial supply chains have been subject to disasters that cast serious doubts on current seismic classification as well as the reliability of design approaches and procedures. Although the ability of code specifications to accurately contemplate the uncommon features of pallet racks has always been a priority of the scientific community, and those specifications have therefore been subjected to thorough evaluation, there is clearly a need for new and better feedback that could provide the basis for the introduction of novel methodologies able to more adequately cope with such specificities.

The introduction to this work is arranged to picture the state-of-the-art technology for the design of pallet-racking systems using standard procedures, widely recognized for the design of building structures. As a matter of course, most of the consolidated body of knowledge for the design of seismically resistant frames is based on certain hypotheses that are, at best, not always fulfilled by the geometrical and mechanical layouts that are often put forward for warehouses. This is addressed in the second part of the introduction to this work and represents necessary background knowledge for correct understanding of the need for the special care that must be used when tackling the design of racks in seismic areas.

The Emilia 2012 earthquake brought to light the delicate problem of supply-chain disruption, underlining the susceptibility of old industrial structures to potential lateral loads that at the time of their construction were either not taken into account or were poorly handled for various reasons. The support of FIP Industriale, an Italian company that leads the R&D sector in developing and manufacturing cutting-edge anti-seismic devices, has been of vital importance for providing a clear understanding on the best routines to follow to guarantee a successful deployment of the available hardware. The company patented a novel device that was purposely developed to fit the specific behavior of racks, triggered by recognized needs, which was henceforth physically tested; the ensuing post-processing analytical/numerical investigation has unveiled a number of features of IsolGOODS®, providing invaluable information for its deployment in seismic areas.

The present document, however, explores a more classic yet alternative technological solution in an attempt to augment the spectrum of available devices that can be of interest to the engineer who is approaching the design of pallet-racking frames to be installed in seismic-prone areas; moreover, the outcomes of this research program are not limited to new structures but could as well be applicable to the refurbishment of existing racks. The concept was engineered and tested using established procedures that have delivered a general design model that is usable with most of the software currently used for structure modeling. The numerical model, which originates from a carefully designed analytical model, is validated and then implemented in the well-known open-source OpenSEES numerical model to investigate the possibilities provided by the proposed device to improve the seismic resilience of upright frames for racks.

Rosario Montuori, Ph.D.
Editor of Ingegneria Sismica International Journal

Summary

The importance of storage facilities along the supply chain is something that is becoming vital to a sector that has seen a skyrocketing increase in demand during the past decade. Yet, designing reliable and functional racking systems does still pose a great challenge to the engineers due to the lack of specifications that clearly address their extremely fragile mechanisms for resisting seismic-induced lateral forces. The great level of structure optimization that characterizes pallet racking systems as a whole represents their conspicuous weak spot, for they possess little to no overstrength to be deployed when unforeseen events strike.

The main strategy that has been pursued, in accordance with the initial impetus given to this research, is the seismic isolation technique, widely exploited for the design of civil structures such as bridge decks, nuclear plants, and building lateral resistance frames, with successful results in Western countries (Chapter 2). Although perfectly legitimate in principle, most of the hardware developed in response to the increased demand for those specific types of construction cannot be used to provide similar performance with pallet-racking structures – at least not as they now exist; new devices need to be developed, from initial concept to system patent and eventually reaching the marketplace. Chapter 3 reviews the anti-seismic devices readily available on the market for creating a horizontal layer with reduced lateral stiffness, capable of decoupling the ground motion from the structure foundations. Beyond isolation systems, classic solutions may be used for improving the seismic performance of racks; the most significant ones are based on the mainstream approaches for the seismic design of structures; Chapter 4 reviews some of the major applications to racking systems.

Aiming at accomplishing the main goal of this research, the results of experimental shaking table tests performed using real-time earthquake records are used to investigate the suitability of tailor-made devices to create isolation systems for standard pallet racks; Chapter 5 describes the physical tests and the data interpretation. Particularly, a curved-surface sliding (CSS) bearing is considered for the physical tests, which had been engineered and preliminarily tested by FIP Industriale (Padova, Italy) under the patented name IsolGOODS®. The tests were carried out in the FIP Laboratory, and the processed results are twofold. In a first investigative study, the system response under six ground motions has allowed drawing first and useful conclusions on the practical effectiveness of the novel device. Secondly, numerical modeling techniques have provided a productive tool that is then employed to unveil the range of applicability of IsolGOODS®to a different spectrum of seismic demands, giving clear indications on when and where CSSs can provide the best economic-to-performance ratio (Chapter 6).

A novel concept, based on well-recognized seismic principles, was therefore conceived with the aim of providing a middle-range solution for improving the performance of pallet-racking systems along the cross-aisle direction (Chapter 7). The proposed base-plate connection, designed for promoting upright uplift when the lateral forces exceed a certain threshold, was tested in the NTUA Laboratory of Steel Structures using monotonic and cyclic protocols. A more comprehensive picture of the behavior of upright frames when equipped with the proposed device is formed as the result of numerical investigation (Chapter 8). Firstly, a scheme to reproduce base-plate connections, encompassing a general analytical representation, is validated using output data retrieved from the prior experimental campaign. Hence, numerical-simulation result interpretation has led to drafting the framework in which the proposed device can represent an opportunity to enhance structure performance, and at a relatively low cost.

Acknowledgment

PhD Title: Seismic Protection of Adjustable Pallet Racking Structures with Isolation Systems

PhD Student: Bonaventura TAGLIAFIERRO

Supervisor: Rosario MONTUORI[1]

Industrial Tutor: Maria Gabriella CASTELLANO[2]

Academic Co-supervisor Ioannis VAYAS[3]

List of published paper

1. B. Tagliafierro, R. Montuori, and I. Vayas. "A hybrid modeling procedure for base-plate connections for pallet racking systems in seismic areas based on experimental tests and nonlinear numerical analyses." In: *Under review In: Thin-Walled Structures* (2022)
2. B. Tagliafierro, R. Montuori, and M. G. Castellano. "Shake table testing and numerical modelling of a steel pallet racking structure with a seismic isolation system." In: *Thin-Walled Structures* 164 (2021), p. 107924. ISSN: 0263-8231. DOI: https://doi.org/10.1016/j.tws.2021.107924
3. M. Simoncelli, B. Tagliafierro, and R. Montuori. "Seismic devices for steel storage structures." In: vol. 2021-June. National Technical University of Athens, 2021
4. B. Taglafierro et al. "Experimental testing campaign and numerical modelling of an innovative base-plate connection for pallet racking systems." In: vol. 2021-June. National Technical University of Athens, 2021
5. M. Simoncelli, B. Tagliafierro, and R. Montuori. "Recent development on the seismic devices for steel storage structures." In: *Thin-Walled Structures* 155 (2020), p. 106827. ISSN: 0263-8231. DOI: https://doi.org/10.1016/j.tws.2020.106827

Other publications

1. R. Montuori, E. Nastri, and B. Tagliafierro. "Residual displacements for non-degrading bilinear oscillators under seismic actions." In: *Mechanics Research Communications* 111 (2021), p. 103651. ISSN: 0093-6413. DOI: https://doi.org/10.1016/j.mechrescom.2020.103651
2. B. Tagliafierro et al. "A new open source solver for modelling fluid-structure interaction: Case study of a point-absorber wave energy converter with power take-off unit." In: ed. by P. C. Papadrakakis M. Fragiadakis M. Vol. 1. European Association for Structural Dynamics, 2020, pp. 657–668. ISBN: 9786188507203
3. R. Montuori, E. Nastri, and B. Tagliafierro. "An Optimal Seismic Force Pattern for Uniform Drift Distribution." In: *Buildings* 9(11) (2019), p. 231. DOI: https://doi.org/10.3390/buildings9110231
4. B. Tagliafierro and E. Nastri. "Seismic design lateral force distributions based on elastic analysis of structures." In: ed. by T. C. Simos T.E. Vol. 2116. American Institute of Physics Inc., 2019. ISBN: 9780735418547. DOI: 10.1063/1.5114273

[1]Department of Pharmacy, University of Salerno, Italy

[2]Senior Research Engineer, Research and Development Department, FIP MEC srl, Italy

[3]National Technical University of Athens, Institute of Steel Structures, Greece

Contents

IV	Conclusions

List of Figures

List of Tables

Problem Definition

1. Introduction

1.1 Structures for racking systems

While materials are cross-docked, there must be some place where goods are stored, for short- and long-term storage. Commonly, these places – warehouses – are organized as massive containers for all the facilities that allow goods to be stored and retrieved.

■ **Vocabulary 1.1 — Racks.** Adjustable pallet racking systems are often identified using the term *racks*.

The warehouse management system (WMS) is used throughout the supply chain to efficiently increase storage density and minimize the fetching time [6]. Another vital aspect of warehouses is the versatility of the storage systems that physically store the items, and indeed one of their main features is the capability of easily yielding to change in geometric layout over time. *Steel storage racking systems* satisfy all these requirements. More often than not, racking and shelving structures are made of thin-walled cold-formed steel elements [7], with connection details [8] that make it possible to make any changes to the rack layout.

There are a great variety of three-dimensional steel structure racking systems available, each of which fits the unit-load to be stored [9, 10]. One of the most common unit-loads is the pallet because palletising is an effective way to manage, store, and transport goods. Once goods are stacked on a pallet, it is easy to ship and store loose goods as a unit. *Adjustable pallet racking systems* are of interest when the wares are accessible at any time (Figure 1.1). In contrast to the usage density of ARWS, racks are characterized by a low rating of space exploitation. Lately, their use has also been growing in popularity for use in big-box stores, where goods are stored for bulk and retail sale. If the particular location in which adjustable pallet racking systems are in use lies in a seismic-prone area, the proximity of people to the racking systems poses an important customer safety issue, which must be taken into account when designing either the containers or the storage racks.

1.2 Lessons from the past

Each time a large earthquake strikes a certain area, the effects on the building stock make apparent the need to adjust seismic codes for earthquake-resistant structures to the state-of-the-art of the knowledge and technologies. For instance, the *1994 Northridge, CA*, which underlined the poor

---

The picture reported above shows a typical warehouse with racks (credits: NEDCON B.V.).
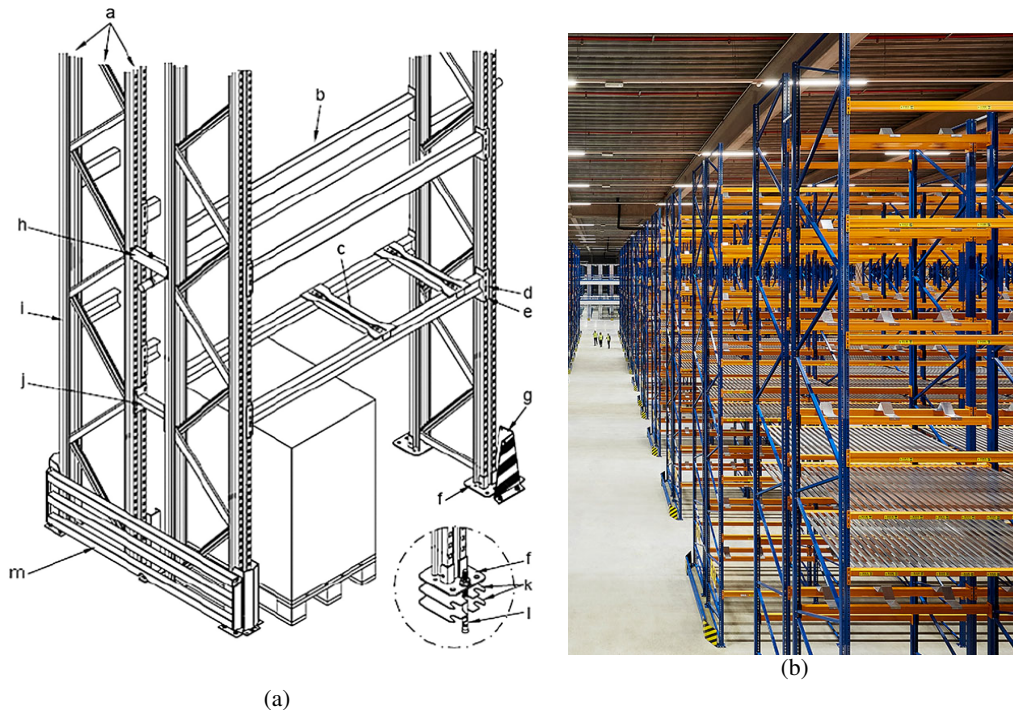
Figure 1.1: Pallet racking structure in its main components (a) : a) upright frame, b) beam, c) pallet support, d) beam-upright connection, e) safety clip, f) base plate, g) post protector, h) sprinkler bearing, i) upright, j) run spacers, k) base plate, i) leveling shims, l) anchor bolt, m) row-end protector. Warehouse store with pallet racks (b) (courtesy of NEDCOV B.V.).

performance of welded connections, influenced a new practice in detailing the steel joints [11]; the *2011 Great East Japan Earthquake and Tsunami, Japan* has led to many improvements on coastal defense structures, building damage assessment and warning systems [12]. Over the years, this process of enhancing and reappraisal has result in a reduction of the death toll after seismic events, as far as advanced countries are considered[1]. The current seismic design methods ground on the *performance based design*, which stood in for the strength approach. The goal is reached by successfully spreading plastic deformations all over the structures, attaining energy dissipation through structural damage. Presently, however, the evidence of great economical losses for the stake-holders raises a new challenge, questioning the cost effectiveness of repairing buildings. A new philosophy for earthquake-resistant design seems to catch on [13].

In the wake of many past failures, most of which showed disproportionate losses [14–16], many countries worldwide have issued codes and recommendations specifically addressing steel storage rack structures with the specific aim to provide higher levels of safety in locations open to the general public [for example, 127]. No less important is the safety of personnel who operate the warehouses. According to the base principles of the Performance Based Design [17], depending on incremental degrees of reliability, the framework that allows to stock/store/retrieve goods must be designed to met the *damage limitation* and the *no-collapse* requirements.

Most modern pallet racking systems have been designed without complying with any seismic provisions [18]. The long-established design and optimisation methods for such structures have mostly delivered small degrees of overstrength and only occasionally have such design procedures accounted for lateral actions coming from impacts during working conditions [see 19] and from imperfections . As such, it is no surprise that the performance of such structures during earthquakes is relatively poor. A brief review of damages suffered by pallet racks can highlight what was previously said. In the aftermath of the *2010 Darfield earthquake* event, Crosier et al. (2010) [20]

---

[1]Wikipedia::List of natural disasters by death toll

(a)   (b)   (c)
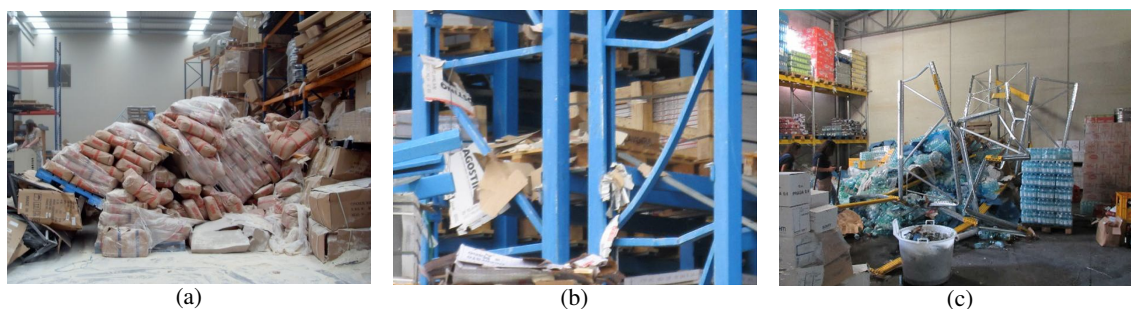
Figure 1.2: Damage inside miscellaneous storage provider site (a) (reproduced from [20]); pottery warehouse close to Roversetto (Ferrara, Italy) (b); a collapsed storage rack in an industrial building (reproduced from [15]).

surveyed industrial steel structures in Christchurch (New Zealand). Though the event resulted in little damage to buildings, steel racks exhibited more sensitivity with several collapses taking place (refer to Figure 1.2(a)). Liberatore et al. (2013) [21] extensively surveyed industrial structures within the *Emilia region* of Italy after the seismic sequence of 2012. The research confirmed that the high vulnerability of steel stands seems to be related to inadequate longitudinal bracing Figure 1.2(b). Perrone et al. (2016) [15] focused on damage reported by *non-structural elements* during the *2016 Central Italy earthquake*, which have indeed underlined the need to design racks racks that are safer under seismic effects.

Overall, it is recognised that the poor performance that rack structures have shown during past seismic events stems from inadequate design procedure [22]. Moreover, the high degree of fragility of cross-aisle frames, which stand out for column buckling failures [23] and ground anchoring failures [14], seems to be the most likely failure mode.

1.2.1 Standards evolution for racks

Following, after having collected the main characteristics that can influence the seismic performance of adjustable pallet racks, the standards in force in the three countries are reviewed through a detailed description that aims to highlight the most important differences between their approaches.

For good reasons, steel storage racks are not treated as building structures by the major codes worldwide, and different, purposely developed standards have been issued on this regard: the [128] used in the USA (Specification for the Design, Testing and Utilization of Industrial Storage Racks); the [129] used in Europe (Steel Static Storage Systems – Adjustable Pallet Racking Systems – Principles for Seismic Design); and the NZS 1170.5:2004 [130] and BRANZ Design Guide Version 12 [131] used in New Zealand. Hence, the codes (for example, EN 1993 [132] in Europe and ANSI/AISC 303-16 [133] in the US) for the design of steel structures are not sufficient to guarantee an adequate level of performance. There are several good reasons for steel storage racks to be treated differently. The main concerns are related to the self-weight of steel storage racks, which account for about 5% of their pay-load, and also relate to the structure elements forming procedure and their relative connections, making it quite complex to predict structural behavior [24].

Although codes should provide general principles and rules that have undergone a supervised process [25], racking structures clearly call for more appropriate prescriptions due to their different scope. For instance, along with provisions related to structures subject to static loads (e.g. EN 15512 [134] in Europe; ANSI MH 16.1 [128] in the US), specific structure design requirements have been compiled through research projects focused on the seismic behavior of storage racking systems (e.g. SEISRACK: Storage racks in seismic areas [135]; Seisracks2 – Storage Racks in Seismic Areas [26]) that have led to issue new code provisions for the seismic design of storage racking structures, porting the Code of Practice FEM 10.2.08 [136] to the state of in-force documentation.

The focus of the newly-established frameworks is on the seismic safety of rack structures,

accounting for the stored goods as well, which becomes much more sensible when these structures, along with the stored goods, are located in publicly accessible areas. It is widely recognised that safeguard measures must be purposely put in place if it is possible for the housed items to fall. For instance, EN 16681 and FEMA 460 [127] consider the *movement of the unit loads* as damage; FEMA 460 suggests several restraint practices to be adopted (see [27, 28]). Goods motion may be caused by sliding of pallets, which can be induced by excessive floor accelerations that, clearly, can not be reduced either via stiffening or strengthening the structures. It becomes necessary to deploy innovative design procedures and solutions.

Within the European Framework, steel structures are designed according to the principles issued by the Eurocode3 (EC3) [132]. Pallet racks are designed for static loads according to the EN 15512 specifications, "Steel static storage systems-Adjustable pallet racking systems - Principles for structural design" [134], an updated version of which was issued in 2021. It is the evolution of the recommendations FEM1 0.2.08 [136], published by the technical committee Working Group 2 of the "Federation Europeenne de la Manutention" (FEM). The EN 15512 specifies the structural design requirements for adjustable pallet racking systems in which the static actions are predominant. In fact, the EN 16681:2016 [129] specifications, "Steel static storage systems - Adjustable pallet racking systems - Principles for seismic design", which adapt the principle given in the EN 1998-1:2004 (Eurocode 8) [137] to pallet racking systems. In the following, several aspects of the EN 16681 are discussed, with particular reference to the general framework established by Eurocode 8.

It is worth reviewing and discussing the key aspects that are significantly different for rack design with a seismic resistance perspective:

Dead-to-live load ratio In buildings, live loads are always comparable with dead loads while, in racks, the structure weight is very limited – generally not greater than 5% of the overall weight of the pallet units. For the static design, reference must be made to [134]: along with the fully loaded rack condition (100% occupancy), the design can be also governed by the fully loaded rack with the exception of single unloaded bay close to the middle of the structure, at the lowest or at the second storage level. Furthermore, in the seismic design [129], together with the 100% occupancy, it must be considered also: i) the configuration with only the top storage level, used to maximize the design of anchor bolts and base-plates and ii) different occupancy levels (70% and 50% of the total) that can generate mass eccentricities. The most relevant feature related to the load distributions is the inherent seismic masses which may affect the dynamic characteristics of the structure. Contrary to what happens for buildings, the periods of vibration are greatly dependent on the considered level of occupancy, affecting hence both the seismic effects and the structural responses;

Members cross-section Owing to the presence of open thin-walled cross-sections, and to their extreme level of optimization, members are often prone to local and/or distortional buckling phenomena [29–31], which largely precede the attainment of the yielding capacity; holes and slits that are used to accommodate connections can further reduce the cross-sectional resistance [32]. Therefore, for the plastic design of such structures, it is important to rely exclusively on the post-yielding capacity of connections. On the other hand, [132] and [133] do not allow the exploitation of connection post-yielding capacity. Generally, monosymmetric profiles are employed as structural members, which lead to significant and non-negligible torsional effects. For this reason, engineers must be able to account for the calculation of *bimoment distribution* along the members and the associated tangential and normal warping stresses during the design of rack frames. As discussed in [33], neglecting these effects can lead to an unsafe estimation of the load carrying capacity;

Beam-column joint Connections between horizontal elements (pallets beams) and uprights are characterized by a very limited degree of flexural stiffness and bending resistance [30]. Pallet beam-ends are shop-welded brackets with hooks to be located on the slots of the uprights

in view of quick construction of rack skeleton frames [34]. Bolts, in addition to the hooked connection devices, could improve joint performance as proved by [35] and more recently by [36], but frequently skipped because deemed to be too expensive [see 37, 38]. Therefore, the cyclic response of standard beam-column rack joints is characterized by a very unstable behavior due to a remarkable pinching of the cycles [39], which increases as does the level of the imposed rotation.

Reference can be made to Figure 1.3, which proposes an experimentally-retrieved dimensionless bending moment ($\bar{m}$) *versus* the relative upright-beam rotation (ϕ). Note that $\bar{m}$ is obtained by dividing measured joint bending moment over the beam bending resistance, which is in turn determined from tests. The curve [40] the shape of the hysteresis loops changes significantly in subsequent cycles, showing an important loss of stiffness after the first cycle [24]. However, a great issue associated with these connections is the low value of the yielding moments if compared with the ones of the connected beams. It is worth noticing that for structures as intended in [132], the beam-column joints have to be designed to exhibit no plastic deformation. Great values of rotations are however achieved and, as a consequence, a satisfactory level of ductility characterizes joints without brittle fracture [37];
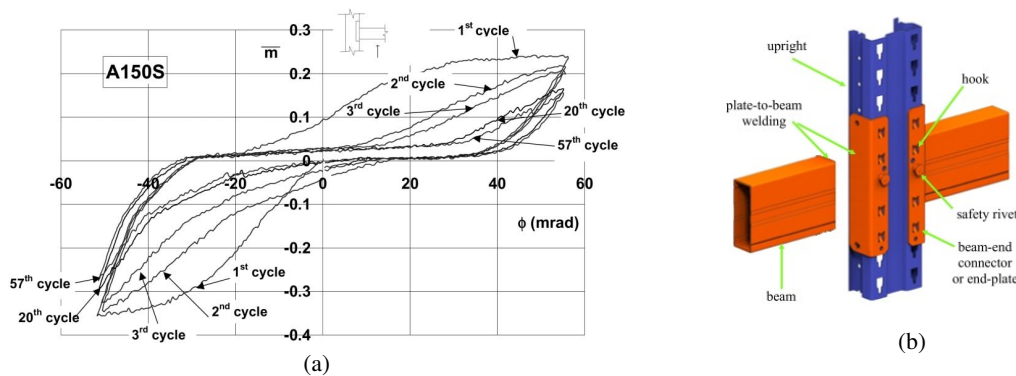
Figure 1.3: Examples of cyclic $\bar{m}$-ϕ relationship for beam-column rack joints (a) (reproduced from [40]); beam to upright connection (b) (reproduced from [41]).

Base-plate connection The connections between uprights and building slabs are characterized by a very limited degree of flexural stiffness and bending resistance. When it comes to the investigation of their performance in the down-aisle direction, a great deal of research has provided a complete understanding on the base connection performance [see,e.g., 38, 42]. In most of the cases, when the cross-aisle direction is considered, the seismic action can pose a risk for the overturning, which becomes the most dangerous limit state. Nevertheless, as happened for the beam-column connections, the nonlinear cyclic behavior can provide a non-negligible ductility to the structure. For this reason, as suggested by [129], attention must be paid on the design of base-connections to be allowed to use a behavior factor q greater than 1.00 (but however lower than 2.00) in the seismic structural analysis;

Dynamic response The seismic response of the two principal directions is rather different. In the down-aisle direction, the great flexibility provided by connections and the absence of spine bracings reflect in significantly high value of the fundamental period of vibrations (T) [44], sometimes up to 3.50 s, which are the typical values observed for high-rise and tall steel buildings [153, 3]. Conversely, in the cross-aisle direction, the presence of bracing systems ensures a fundamental period lower than 1.50 s. Despite their conventional lateral resisting schemes, seismic performance along the transverse direction is utterly dictated by base connections and brace-upright connections [45], where the inelastic deformations take place [46].

As it may seem clear from the previous points discussed, it is a rather complex task to anticipate

Figure 1.4: Schematic representation of a base-plate connection (a) (reproduced from [43]); and a detailed view of the footplate bolted to the upright.(b) (reproduced from systemsdesignuk.com).

the behavior of racks using established approaches, which have been built and found valid in contexts for which some features have been neglected. High engineering skills are required to faithfully reproduce the key characteristics of each item and thus obtain the overall response of the frame, guaranteeing competitive performance with extremely low weight structural systems. The two papers Bernuzzi et al. [24, 47] propose a mixed procedure combining nonlinear time history analyses (i.e., transient analyses) with the low-cyclic fatigue theory approach, which has been developed and applied to rack moment resisting frames. Rack frames are composed of members hardly able to dissipate energy internally, but however able to sustain significant lateral displacements owing to the high level of rotation that can be achieved in post-elastic range by joints. This behavior has been confirmed also recently by pushover analyses on shelving racks [42, 48] and pallet racks [49]. On top of this, the presence of perforations joined with the presence of either compression force and bending moment make the prediction of strength and resistance of these elements quite challenging, and many authors have tried to address these combination of issues mainly by proposing new numerical procedures [24, 31, 32, 50, 51].

1.3 A modern way of thinking: resilient society

The current seismic design methods ground on the *performance based design*, which stood in for the strength approach. The goal is reached by successfully spreading plastic deformations all over the structures, attaining energy dissipation through structural damage. Presently, however, the evidence of great economical losses for the stake-holders raises a new challenge, questioning the cost effectiveness of repairing buildings. A new philosophy for earthquake-resistant design seems to catch on [13]. The problem of the high fragility of upright frames of pallet racking systems against lateral forces raises an important question for researchers. This lack of seismic performance can be attributed to a small degree of internal overdetermination of the system, as is also acknowledged by the European Standard for adjustable pallet racking structures (EN16681), which only takes into account the low-dissipative behavior for these structures.

Seismic isolation (SI) may be the answer to the new demand for a more *resilient society*, though the inception of this technology dates back to almost two centuries ago [52]. Basically, SI can be framed under the theory of vibration-control – seismic vibrations – which is widespread for mechanical applications. Under the same framework, the actual method involved in the dissipation of the seismic-induced energy represents a way of reducing the resonance peaks, that is, *damping* [138]. *Isolation*, on the other hand, can optimize the seismic response of a structure by mitigating the effects of earthquakes on it, for it consists of preventing the propagation of disturbances to sensitive parts of the systems. For what concerns most civil structures applications, the isolation

system is located at ground level, though the discontinuity plane can be introduced at any level of the structure [53]. The system that reduces the transmission of ground vibration is built by placing low-horizontal stiffness elements between foundation – base – and superstructure.

Many examples of base isolation system (BIS) applied to buildings all over the world [54] and also in Italy [55] have proved that the seismic isolation has become effective for either the design of new structures or improving the safety of existing ones [56]. The good performance of the isolation systems applied to buildings and infrastructure is chiefly due to lengthening the natural period of lateral resisting systems, and it is often far from the fundamental period of the most common ground motions ($0.2 - 1.0$ s). In general, the fundamental period of base-isolated structures shifts to more than 2.0 seconds, which assures that most of the high-energetic components of the ground motion are filtered out. As a counter effect, due to the higher flexibility of the lateral resistant system, the structure experiences higher displacements and these must be taken into account when designing the clearance at ground level. However, there is another benefit that helps increase the performance of the BIS, that is, the inherent damping of the isolator devices (i.e. friction pendula, high-damping rubber bearings, lead-rubber bearings).

1.4 Suitability of traditional design methods

For earthquake-resistant steel storage structures, the common practice for their design strictly follows the recognized approaches for civil structures, trending towards safeguarding human lives by ensuring adequate levels of reliability after seismic events and guaranteeing the capability of structures to be rehabilitated in the immediate aftermath [139, 140]. The objective of seismic design is to prevent the collapse of buildings – accepting the occurrence of extensive damage – relying on ductile resources. Of course, in order to maximize the exploitation of local ductility, structures have to be globally guided to exhibit a global collapse mechanism [see 57, 58]. To accomplish this, however, elements must be thoroughly sized to guarantee the failure-control approaches, which act through the *capacity design* principles [59]. The regions where structures have to exhibit plastic deformations are identified and therefore designed with reliable strengths, whereas the brittle-prone regions are designed with hierarchically imposed strengths.

The damage is a consequence of plastic deformations that are inevitable – or desired – to dissipate the input earthquake energy, as long as current seismic code design procedures must be met. As for steel structures, members made up of compact hot rolled rolled profiles inherently possess high ductility, thus allowing for the plastic design of structures. On the other hand, transferring knowledge to rack structures is by no means straightforward. First, low-plastic resources do not allow reliance on such elements to provide structures with sufficient post-elastic deformations. Connections are then identified as the place where plastic deformations can occur - this indeed goes towards capacity design principles, although tabs and slots do not guarantee *ample* and *stable* hysteretic cycles. In fact, the beam-column and base connections inherit their geometries from the static load design procedures and have not yet been updated to the demand for greater ductility. Secondly, the common practice of having the same vertical sections along the elevation constrains the choices of the designers, making the hierarchical criteria not so clearly applicable due to obvious economic feasibility.

Therefore, an unconventional way to design these structures is needed, and isolation techniques are promising solutions for providing the right balance of performance.

1.5 Objectives of this work

The aim of this work is to portray a clear picture of the performance of selective pallet racking systems in the presence of lateral actions, often induced by ground shaking. This PhD thesis proposes two new strategies for the retrofit of non-compliant pallet racking, moving in the panorama of the current hardware know-how, but at the same time pushing the limits of sensible solutions

based on consolidated principles. Racks have been shown, in many cases, to be fragile in response to lateral induced stress and barely possess any degree of overstrength that could help them overcome unexpected scenarios. For this reason, racks appear to be unforgiving of design errors or subtle actions on their columns; both can lead to catastrophic warehouse collapses, causing disproportionate economic losses.

1.6 Document structure

The following list provides a brief description of the content of each chapter:

Chapter 1 provides an introduction to the objectives of this work, providing a critical review of the main issues faced while moving from traditional seismic design procedures to targeting racks.

Chapter 2 is primer to the understanding of seismic isolation working principles and initiates the readers to the issues that are faced by

Chapter 3 reviews the various isolation strategies that have already been put forward during previous investigations.

Chapter 4 introduces the working principles for the design of structures with dissipative behavior and reviews the devices that can be readily used for upright frames.

Chapter 5 reports on the experimental investigation on the IsolGOODS® bearing device performed at full scale on a shake table.

Chapter 6 investigates the performance of IsolGOODS® beyond the seismic intensities considered in the experimental phase.

Chapter 7 presents the proposed design procedure for an innovative base connection to be used for uprights; experimental investigation is performed.

Chapter 8 implements and validates the numerical modeling for dissipative base plates and therefore provides an estimation of cross-aisle frame performance gain when the proposed device is used.

Chapter 9 Conclusive remarks and future work.

2. Seismic Isolation for Racks

2.1 Introduction to seismic isolation

Since the first insights on the feasibility of seismic isolation for civil structures, the available hardware know-how has faced a trial-and-error update procedure, which nowadays has resulted in a great variety of devices and related techniques to be used for the isolation of infrastructure and buildings [54]. Over more than a century of developments, seismic isolation seems presently to be a mature solution for a new approach to earthquake-resistant design of structure [60], which can ensure full post-earthquake functionalities [13]. When the problem is of some concern for medium-rise buildings, base isolation system (BIS) techniques are the most convenient, and effectively capable of mitigating earthquake effects [61]. Some examples of successful applications of mentioned methodologies to improving the seismic performance of RC buildings are reported in [55]. In general, BIS techniques aim at introducing a layer between structures (then referred as *superstructure*) and foundations (or basements, or *substructure*) composed of suitable devices (*isolators*) with low lateral stiffness, which however practically restore the former vertical stiffness. The insertion of an isolation system allows the fundamental vibration period of the structure to be set at will, therefore it can be chosen to be decoupled from the spectral energy contents of most of the seismic events expected in a given area.

2.2 Main principles of base isolation system design

As it is well established, the kinematics of a seismically isolated building can be studied assuming a model with 2 degrees of freedom (2-DOF), after the linear theory presented in [151, 141]. Figure 2.1 depicts the linear elastic 2-DOF model with lumped masses, which may be considered a synthesis of base isolated structures. In terms of *relative* displacements, which are convenient to compare both super-structure displacement u_s and base displacement u_b, the equations of motion are given by:

$$m_s(\ddot{u}_b + \ddot{u}_s) + c_s\dot{u}_s + k_s u_s = -m\ddot{u}_g; \tag{2.1}$$

$$(m_s + m_b)\ddot{u}_b + m\ddot{u}_s + c_b\dot{u}_b + k_b u_b = -(m_s + m_b)\ddot{u}_g, \tag{2.2}$$

The picture reported above shows a typical cheese rack collapsed after the Emilia Romagna Earthquake (2012). Reproduced from [16] (credits: Marco Simoncelli)
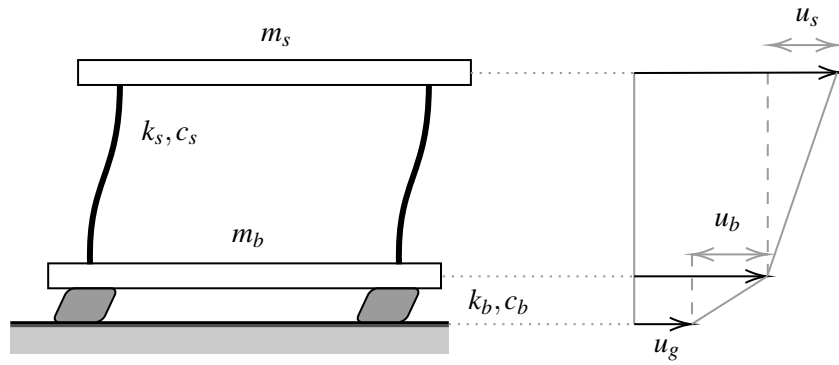
Figure 2.1: 2-DOF base isolation system mechanical model, after De Luca et al. [54].

where m is the mass, c is the damping coefficient, k is the stiffness, subscripts b and s refer to the isolation system and superstructure, respectively. $\ddot{u}_g$ is the ground acceleration. Equation (2.1) is characterized by a circular frequency $\omega_s^2 = k_s/m_s$ that is related to the superstructure (fixed structure), whereas Equation (2.2) by $\omega_b^2 = k_b/(m_s + m_b)$, which is related to the isolation system. It is useful to define the ratio between the periods of the systems $\varepsilon = (T_s/T_b)^2$. The solution of the eigen-problem associated to the system on equation (2.1) and (2.2) yields to identify the two modal periods, approximated to the first order of ε:

$$T_1 = T_b\sqrt{1 - \gamma\varepsilon}, \qquad T_2 = T_s\sqrt{\frac{1 + \gamma\varepsilon}{1 - \gamma}},, \tag{2.3}$$

where $\gamma = m_s/(m_s + m_b)$.

As long as the first order approximation of ε holds, the first period of vibration T_1 is almost the same of the *isolation system T_b*, while the structural period is increased and this effect is as strong as the value of γ increases. This also reflects on the structural damping of the system. The damping ratio of the first mode yields to:

$$\xi_1 = \xi_b(1 - \frac{3\gamma\varepsilon}{2}). \tag{2.4}$$

Equation 2.4 leads to a damping ratio quite similar to the damping ratio that characterizes the dynamic of the isolation system. Additionally, another benefit comes from the participation factor associated to the first mode, which happens to be

$$\Gamma_1 = 1 - \gamma\varepsilon,$$

ensuring that most of the seismic effects set into action the structure with a favorable deformed shape [142]. It can be instructive to consider the first mode shape $\boldsymbol{\phi}_1 = [1, \varepsilon]$, which clearly states, though the structure undergoes deformation, the most of the displacement is gathered at the isolation level.

This heads to the following beneficial effects if compared to buildings without seismic isolation:
1. the significant reduction of the accelerations transmitted to the super-structure, even at the higher levels;
2. the reduction of the inter-storey drifts: in simple terms, under the action of the earthquake the building moves as a rigid block above the isolators.

2.3 Seismic behavior of racks

Even though the pallet racking system response is mostly 3D, the seismic features of racks can be analyzed if two bi-dimensional lateral load resisting systems are taken separately.

The down-aisle lateral resisting system often exhibits a moment resisting frame-like behavior. For sake of common practice, the bracing system is indeed often deprecated. Stiffness and resistance are therefore provided by either beam-to-column and base-plate connections, both of which assure the global stability of the structure. As a matter of fact, the principal issue posed by the down-aisle frame is the side-sway collapse. Numerical models can give an adequate degree of accuracy when analyses are performed to assess the behavior of such frames. Nevertheless, the model must include several characteristic features of pallet racks [47]. More than often there is no horizontal diaphragm and the beam-to-column connections are flexible with different rotational stiffness for hogging and sagging moment [37, 38, 157, 62]. According to the results of the SEISRACKS2 project, unbraced racks can have good performance in terms of strength and ductility if the soft-storey collapse mechanisms are prevented [26, 49, 63]. In [26] the behavior factor was found to be greater than 2, although its value cannot be decoupled from either the geometry layout and the hysteretic properties of the connections [47, 64]. It is important to point out the positive effect of the high lateral flexibility of the down-aisle frame, whose fundamental period of vibration is generally longer than 2 seconds, up to 4 seconds. Additionally, the unit load sliding due to excessive floor accelerations may not represent an issue at all [38, 65]. In fact, the pallet sliding damps some of the seismic-input energy, which is accounted for in EN 16681 [129] by means of the E_{D2} factor.

Cross-aisle frames employ different braced schemes as bearing systems for horizontal forces. Commonly used are X-shaped diagonal pattern -with or without horizontal elements- and D-shaped diagonal patterns. These frames are characterized by high structural slenderness, being the frame often not larger than 1 meters and more than 10 meters tall. The seismic performance of the cross-aisle frames are dictated by the vertical bracing system [66, 67] and the base-plate connections [45, 66]. Hence, structural configurations for the uprights provide a degree of stiffness to the frames themselves, which makes overturning likely to occur if compared to the down-aisle frames. Another important issue is related to the high values of acceleration that can be experienced at the topmost levels. With respect to the typology of goods being stoked, shedding of items may pose a large safety threat. In contrast with what happens for the frame-like down-aisle system, goods may be displaced and fall down within the area that is accessible to people. In fact, this is the main concern that led to promoting awareness about the *movement of contents* [127, 129].

2.4 Seismic isolation for steel storage systems

The general advantages that are brought about by BISs can be beneficial for the rack performance because the reduced likelihood of the overturning of the stored goods, which is a typical problem caused by earthquake-induced lateral forces, as shown in Figure 2.2, and the downtime of seismically protected structures is extraordinarily cut down in case for medium-intensity events for the eventuality of provoking self-induced collapses is greatly diminished. In fact, most of the time, there is a chain collapse originating from just one bay, usually the extremities.

Although a large number of seismic devices are nowadays available on the market [61, 143, 69], it may be complicated to apply them directly to rack systems because of economic and technical reasons; in the following, a detailed review of the key reasons is given:

Rigid diaphragm For a proper installation of base isolation systems, a *rigid diaphragm* must be created immediately above the isolator level to avoid differential displacements between uprights. This can raise a logistic issue because also the pallet slots at ground level must be completely free for the storage of heavier pallets. Moreover, owners avoid using bracing in the down-aisle direction as well;

Load configurations The *loads applied* to the racks can change day by day and very different values of the axial load can be found in the uprights. Only logistic reasons govern the load-unload phases and no attention is given to the structural condition. In many cases, large mass eccentricities are created and consequently torsion effects may become predominant. Mass variability may represent an issue for some kinds of isolation system, which provides

Figure 2.2: Shake table tests on non-isolated steel storage pallet racks [68]

different periods depending on the vertical loads, e.g. the ones composed of rubber devices;

Tensile stress in uprights The lateral resisting system is characterized by high slenderness. The limited plan dimension and the great height of the racks can bring to the *base-uplift* problem along the cross-aisle direction, which could be a problem for the isolator hardware. Most of the seismic devices are not able to bear tension (sliding devices) or cannot work properly (rubber bearing systems). A purposely developed hardware may be considered [70], which is capable of bearing compression as well as tension;

Upright bulk The dimensions of rack uprights are very small if compared to the columns of the traditional building or with bridge piles, where usually the isolators are located. Directly stemming from the latter is that vertical loads are one or even two orders of magnitude less than the usual ones, which are necessary for a certain class of isolators to work efficiently. It is worth referring to the period of vibration of a rubber isolator device, which can be roughly estimated as:

$$T_{dev} \approx 2\pi \sqrt{\frac{\sigma}{G} \frac{n t_r}{g}}, \tag{2.5}$$

where σ is the vertical stress, G is the rubber shear modulus, t_r is the thickness of the rubber layers, n is the number of rubber layers, g is the magnitude of the acceleration of gravity. Equation (2.5) underlines the reason rubber devices cannot apply for the isolation of a system with low mass. The quantities G and $n t_r$, though may be changed, are constrained by technological issues and displacement demand, respectively. Hence, the vertical stress upon the device imposes the period of vibration, which increases with $\sigma^{1/2}$. For instance, considering soft rubber and a shear strain $\gamma = 150\,\%$, reasonable figures are $G = 0.70$ MPa, $n t_r = 0.15$ m and $\sigma = 7.00$ MPa lead to $T_{dev} = 2.46$ s. However, for pallet racks, it is hard to exceed $\sigma = 1.00$ MPa, so that the corresponding period through Equation (2.5) yields to around 0.92 s.

Economics The direct *cost* of common base isolation systems could have a major impact on the total cost of the storage rack frames. Moreover, throughout the rack life, the owner of the warehouse can change as well as the ownership of the stored goods [18]. Often, owners prefer to charge on themselves the risk of a possible collapse rather than investing more in

engineering costs, especially when the costs of the merchandise are not so relevant.

Further readings

A most compelling and complete dissertation on the basic principles that govern the dynamics, and as such the design of isolated buildings, the reader is invited to inspect more specific literature, e.g., Naeim and Kelly [151], Braun [144], Christopoulos and Filiatrault[141], Chopra [142], and Kelly [145], on the matter.

3. Seismic isolators

3.1 Warehouse and high-rack structures

Important studies on high-rack structures with isolation systems have been carried out by Kilar et al. [71, 72], investigating the nonlinear response of *Fixed Base* (FB) and *Base Isolated* (BI) high racks, with various mass eccentricities through nonlinear dynamic time history analyses (NLTH) and pushover analyses (POA) [73]. The presented case study is relative to a real application and its structural model is depicted in Figure 3.1.

The uprights of the rack structure are made of Ω 100×120mm (outer dimensions) cold-formed sections (*H* in Figure 3.1), forming the upright frames by means the use of diagonals realized with C 50x30x3mm profiles (K in Figure 3.1). Uprights have been perforated only where beams have been located. Lateral stability has been increased by means of the use of supporting bracing towers located at both ends of the structure. The columns of the supporting structures are made of hot-rolled HEA200 (A in Figure 3.1) sections. All the beams are made of welded boxed SHS type profiles (B,C,I in Figure 3.1), and the diagonals are double L sections (D,G,J in Figure 3.1). The internal sides of the supporting structures are additionally braced by double L sections (E in Figure 3.1). The top beams are made of HEA100 (F in Figure 3.1) profiles while top bracing are UPN120/55 (L in Figure 3.1). The supporting systems provide an increased rigidity to the racks structure compared to the classical unbraced rack frame.

The base isolation system was designed to ensure that no damage occurs in the fully loaded rack structure under earthquake excitation. The isolation system was composed of 20 rubber bearings with a diameter of 45 cm and a total height of 24 cm (including outer steel plates) [146]. They were made of soft rubber (40 durometer) and had horizontal stiffness of 650 kN/m, with a damping ratio equal to $\xi = 0.10$. Their maximum allowed horizontal displacement is equal to 200 mm and the maximum admitted vertical load was 900 kN under horizontal actions and 3570 kN for static load cases. The rubber bearings were distributed around the perimeter of the structure layout, whereas the middle uprights of the plan layout were vertically supported by flat slider devices. To ensure a uniform distribution of stresses and to create a rigid diaphragm right above the isolation system, a reinforced concrete slab with 30 cm of thickness and a series of concrete tie-beams (b/h=$40/60$ cm), forming a 6×6 m grid, was added beneath the structure. This stiff diaphragm resulted in 633 tons of additional mass at the base-storey. The center of stiffness of the isolation system corresponded to the center of stiffness of the superstructure [71], as well as to the geometrical center of the floor

---

The picture reported above shows a progressively collapsed warehouse during the 2010 Canterbury earthquake (New Zealand). Reproduced from Firouzianhaji et al. [36].
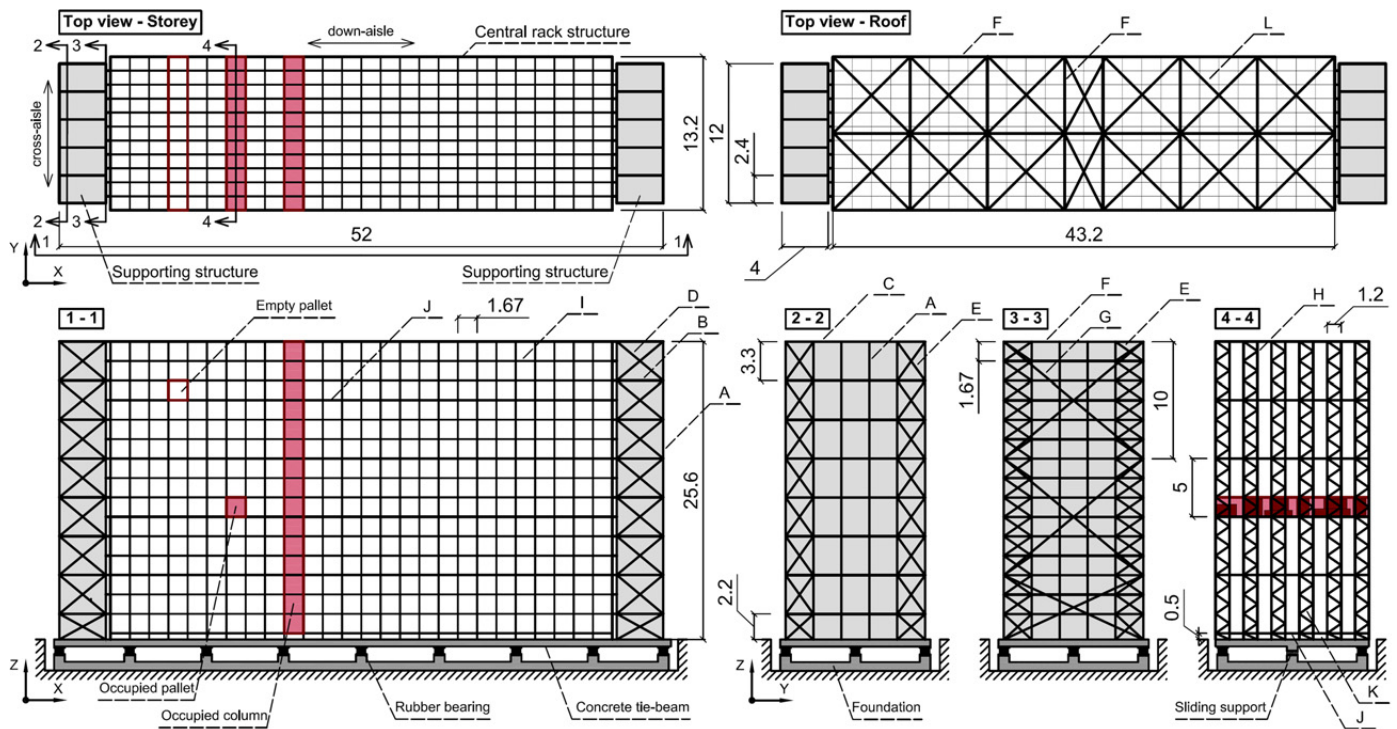
Figure 3.1: Geometry of the base-isolated rack structure with its two outer supporting structures (dimensions in meters) (reproduced from [71]).

plan.

The structure was modeled and analyzed by using the commercial finite element (FE) computer software SAP2000 v12.0.1 [74]. Firstly, a second-order modal analysis was performed to obtain the fundamental period T_1 of both models. FB rack has shown a fundamental period of 1.35 s in the down-aisle and 1.25 s in the cross-aisle direction. As expected, the base isolation system increased those values: 3.47 s and 3.42 s in the down- and cross-aisle directions, respectively. It must be underlined that these preliminary analyses were performed considering the *fully loaded* loading condition. After, a parametric study was carried out by varying the mass eccentricity in both FB and BI models and two different peak ground accelerations (a_g) were selected, namely 0.175g and 0.250g.

The structure sensitivity to asymmetric live load distributions was analyzed with respect to the inherent eccentricity e_{max}, which represents the distance between the center of mass and the geometrical center of the structure. A final summary of the most important outcomes of the analyses carried out in [71] are reported in Figure 3.2. Figure 3.2(a) reports, for each relative eccentricity e_{max}/B (B is the total length of the structure), the relative displacements of the frames on either the stiff and the flexible side, and the center of mass (CM). Similarly, Figure 3.2(a) reports the story drifts for the rack structure (left panel) and the supporting structure (right panel).

From the 4 panels in Figure 3.2, it can be noted that for the FB rack structure the most critical occupancy is not the fully one (100%$\rightarrow e_{max} = 0\%$), but rather occupancy levels ranging between 85% and 55%, which can produce maximum eccentricities ranging from 5% to 15% of the larger floor plan dimension. Incidentally, it must be noticed that also a different structural period can vary the effects of the ground motion on to the super-structure. For the FB structure, the plastic hinges develop either at column-ends and diagonals of the supporting structures and at the base of columns on the flexible side of the central rack structure, which may lead to a dangerous local collapse mechanism. The accidental eccentricity, which is prescribed by Eurocode8 (5% of the floor plan dimension), might be too small to correctly account for an unfavorable asymmetric payload

distribution. On the other hand, the introduction of the base isolation system does flatten the effects of having different occupancy levels, as it can be observed from the 4 panels in Figure 3.2. In fact, the relative displacements as well as the storey drift are hardly affected by eccentricity. Additionally, the system can significantly reduce the unfavorable effects of torsion.

(a)

(b)
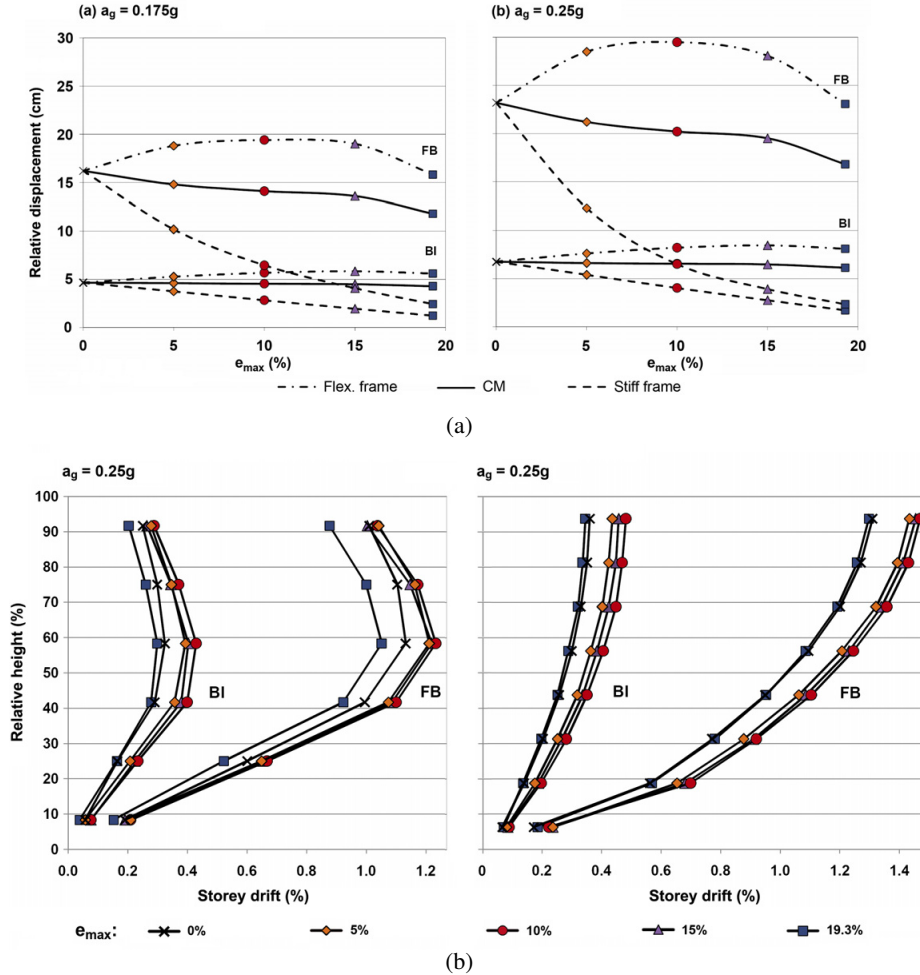
Figure 3.2: Deck rotation of the models for different mass eccentricities (a) and storey drifts of the models for different mass eccentricities (b) (reproduced from [71]).

As a whole, the effects of torsion in the BI structure are smaller than the ones in the FB structure: the reduction in torsional deck rotations was by a factor of 5 (Figure 3.2(a)). Furthermore, the reduction in terms of inter-storey drifts was by a factor of 3 as can be observed from Figure 3.2(b). Overall, the implementation of a BIS can therefore be a very effective solution, since it can get rid of all damages from the rack structures as well as from the supporting structures.

Finally, Kilar et al. [72] presents an interesting cost analysis on the same high rack structure of Figure 3.1. Figure 3.3 reports the data of a cost analysis performed on 2 configurations (i.e. SYM and ASYM, short for *symmetric* and *asymmetric*, respectively) of the same structure and with 2 seismic intensities. The difference between the two cases stands in the way the pay-load is distributed i.e. SYM $e_{max} = 0\%$; ASYM $e_{max} = 10\%$, for they share the same occupancy level. It was shown that a base isolation system is probably not economically feasible for smaller to moderate ground motion intensities, if only the pure repair costs are accounted for. However, if the *downtime* (C_d loss of function) costs and damaged content costs are taken into consideration, along with the structural costs C_s and the damaged content costs C_c, the isolation system could be economically viable for all the analyzed seismic intensity (Figure 3.3). The costs of base isolation are represented by the red straight line, and can be approximated to 10% of initial building costs. If

the total costs are considered, it can be noted that the costs increase as the seismic magnitude does and if full occupancy is considered, the total induced costs could exceed the costs of the original structure. The base isolation solution results are always more convenient. Obviously, the results of this cost analysis are strictly dependent on the Authors' assumptions on the costs and on the duration of different structural recovery operations. The Authors of this work have found that those assumptions are fairly representative of a real-like scenario.
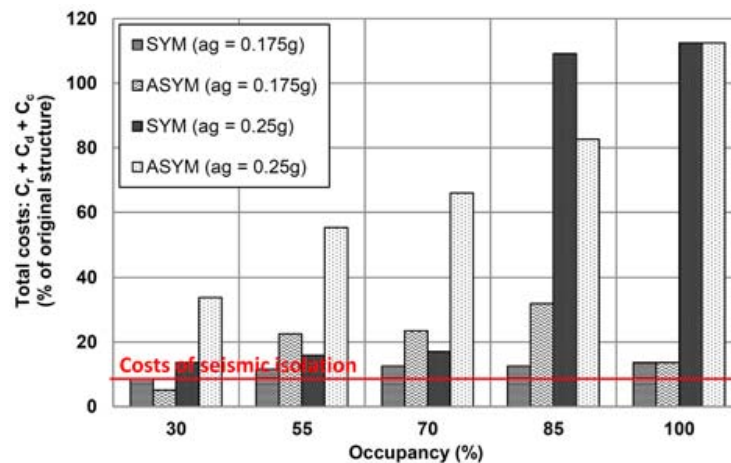
Figure 3.3: Seismic isolation costs *versus* total costs (structural repair, downtime and damaged content) for different occupancy levels and ground motion intensities (reproduced from [72]).

It can be concluded that the discussed isolation strategy can be classified as a *classical* base isolation procedure, commonly used for buildings, and grounds on a well-known theoretical background. Both articles [71, 72] present an interesting application of a base isolation system to non-conventional structures, which requested to develop a more extensive analysis campaign for the high uncertainties related to the mass distribution. Since the isolation system is made up of elastomeric seismic isolators, the great variability of the mass distribution does affect the fundamental structural period which, in turn, implies different seismic effects on the super-structure. In contrast, the seismic isolation of buildings has much fewer degrees of freedom. Nevertheless, a great advantage arises, that is, the main peculiarities of racks systems can be partially faced and the suppliers of such structures could use their long-established know-how also for seismic-prone areas.

3.2   Seismic isolators

3.2.1   Pellegrino® isolation system

The isolation system developed by RIGID-U-RAK (ridgurak.com accessed: 2020) has been named with the trademark Pellegrino®; its layout is such that it can provide seismic isolation exclusively in the cross-aisle direction of pallet type steel storage racks; by incorporating high damped elastomeric bearings and friction plates (Figure 3.4(a)) the device is capable of limiting the lateral displacement. Filiatrault et al. [68] presents a summary of experimental results from tests of isolated pallet racks performed on the triaxial shake table at the University of Buffalo (US). The base isolation system considered in this study is designed to provide base isolation in the cross-aisle direction of a pallet rack system, whereas providing similar restraints as conventional bolted base plates in the down-aisle direction.

The objective of the isolation in the cross-aisle direction is to reduce the horizontal accelerations of the rack in order to avoid content spillage and structural damage during a major seismic event, without interfering with normal material handling operations. The base isolation is not designed to provide isolation in the down-aisle direction, though. The system (Figure 3.4(b)) consists of a

U-shape plate (*Horizontal Support*), inserted inside a steel box (*Box Fabrication*) which is welded on the base plate (*Base Plate*). Actually, the base plate and the steel box make up a one-piece component, which represents the fixed part of the device (refer to Figure 3.4(a)). As it may sound clear, the base plate is anchored to the building slab by means of anchor bolts. In this framework, the two uprights are bolted onto the flange of the U-shape profile. Two seismic mounts make up the connection between the movable part, i.e. the horizontal support plate, and the fixed one, i.e. box fabrication + base plate.

(a)

(b)
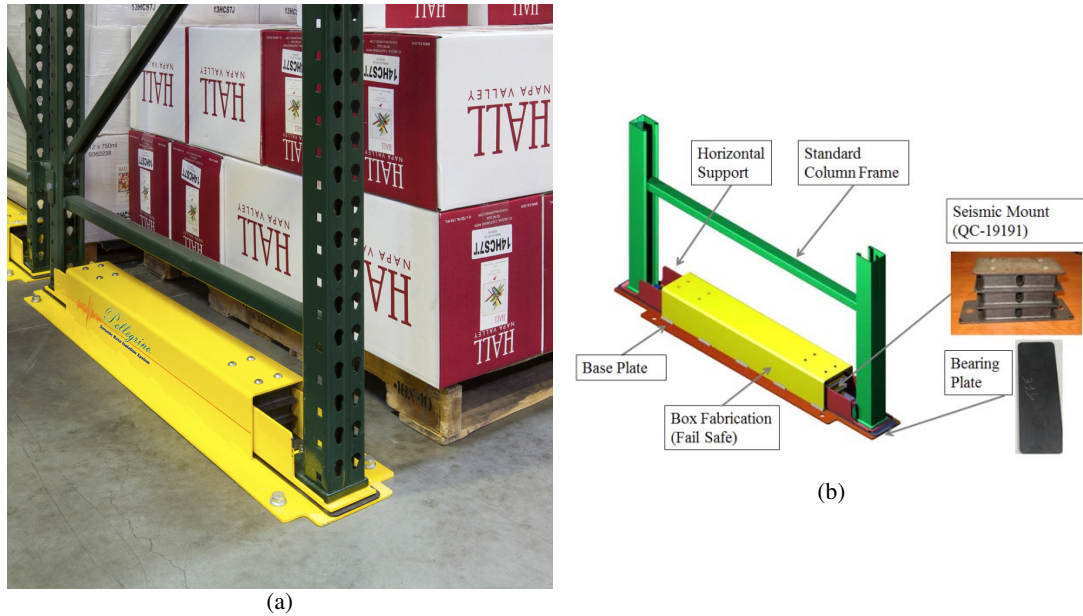
Figure 3.4: Pellegrino® device (a) (font ridgurak.com). Rendered view of the base isolation system Pellegrino® for steel storage racks. The principal components are given (b) after the schematic proposed in [165].

The lateral seismic shear forces are carried by the mounts and by friction between the horizontal support and bearing plates. The horizontal support plate can slide on the base plate of the box, which is coated with low-friction bearing material, when seismic loading is acting along the cross-aisle direction. If the uprights are engaged in compression, the two mounts are mainly engaged in shear stress and little tension. However, if there is an upright in tension, one of the two mounts must be engaged in compression as well as shear. Therefore, the lateral stiffness of the isolation system is provided only by the two parallel mounts. In the down-aisle direction, the rubber mounts are restrained by the side walls of the horizontal support plate, effectively restraining displacements in that direction and enclosing two multi-layered high damping laminated elastomers. It is important to stress that the most of the force along the down-aisle direction is transmitted by contact U-shape plate-steel box, whereas a small amount, by friction mechanism. The Ph.D. thesis developed by [165] describes all the preliminary tests made on this isolation system, whose principal results are summarized in Table 3.1. It can be noted that the lateral and the compression stiffness of the devices are changing with the variation of the hardness of the rubber. On the contrary, the equivalent damping ratios remain about the same. The maximum lateral displacements are for both cases equal to 100 mm.

Full-scale tests were performed on the triaxial shake table in the *Structural Engineering and Earthquake Simulation Laboratory* (SEESL) at the University at Buffalo (US). Several loading distributions were considered and the tests were repeated with increasing intensity of earthquakes. First of all, natural periods of all the tested racks have been determined via pulse tests. Full-cycle acceleration time-history at a frequency of 10 Hz and amplitude of 0.05 *g* was generated by the shake table in the three orthogonal directions of the rack to assess the fundamental periods of

Table 3.1: Principal characteristics for two different configurations of the Pellegrino® base isolation system (reproduced from [68]).

Rubber durometer	Shear stiffness [kN/m]	Equivalent damping ratio	Compression stiffness [kN/m]	Max lateral displacement [mm]
40	47	0.20	373	100
60	93	0.22	634	100

vibration, which are collected in Table 3.2. Tests have been conducted by using different types of weights to simulate the stored products: concrete blocks of 21.8 kN of weight each, light merchandise (23.1 kN total), intermediate merchandise (94.1 kN total) and heavy merchandise (176.5 kN total). In the down-aisle direction fundamental periods of FB racks are significantly longer than those of the cross-aisle (in case of concrete block as pallets e.g. 1.30 s *vs* 0.57 s). In case of light merchandise, the cross-aisle period for FB rack is very small, highlighting the really low value of the weight used for this case. For the base isolated rack configurations, the cross-aisle fundamental periods are much longer than the cross-aisle periods of the conventional rack configurations. Conversely, the periods along the down-aisle direction are slightly longer than those of the FB configurations, meeting the objective of providing base isolation in one direction only.

Table 3.2: Measured initial fundamental periods of rack specimens (reproduced from [68]).

Test Series	Rack configuration	Base Isolator Rubber Durometer	Loading	Fundamental period (s)	
				Down-aisle	Cross-aisle
1A	Base isolated	60	Concrete blocks	1.37	1.71
1B	Fixed based	N/A		1.30	0.57
2, 10	Base isolated	40	Light Merchandise	0.59	1.45
6	Fixed based	N/A		0.47	0.19
3	Base isolated	40	Intermediate Merchandise	0.89	1.75
7	Fixed based	N/A		0.79	0.46
4	Base isolated	40	Heavy Merchandise	1.14	1.71
5, 9	Base isolated	60		1.12	1.75
8, 11	Fixed based	N/A		1.00	0.55

The synthetic seismic input has been generated starting from the maximum considered earthquake (MCE) demand for a site Class D in a high seismic zone (e.g. California), given in the FEMA 460 document [127] where is defined also the Design Earthquake (DE) for the life safety performance. In particular, the 150% seismic input level meets the MCE (0.7g) and the 100% meets the DE (0.47g). Observing the results of the seismic tests, they have clearly demonstrated the improved structural performance of a rack structure incorporating a cross-aisle base isolation system. The base isolation system considered in this study significantly reduced the cross-aisle absolute accelerations and inter-storey drifts (Figure 3.5) of the rack structure compared with the values measured in the same rack conventionally anchored at its base. For the rigid base rack, an inter-storey drift of 4% occurred at the first level of the rack. As it may be clear, the structure exhibits a soft-storey failure mechanism which is the worst scenario ever. On the other hand, the base isolated configuration shows that the inter-storey drift remains under 0.7% at all levels

(Figure 3.5).

<center>(a)   (b)</center>
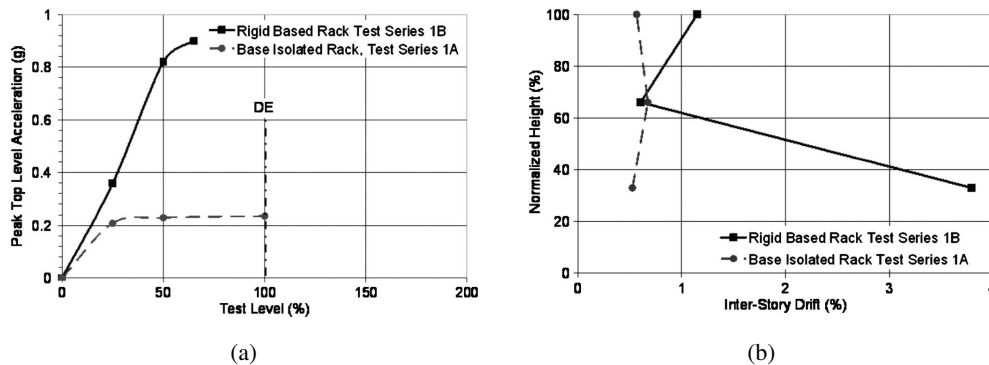
Figure 3.5: Variations of peak top level cross-aisle accelerations with excitation amplitudes (a), and envelopes of peak cross-aisle interstory drifts, cross-aisle seismic excitations (b), 50% test level, Test Series 1A and 1B (reproduced from [68]).

Although the base isolation system is designed to isolate the rack in the cross-aisle direction, it also has some beneficial effects in reducing the accelerations of the racks in the down-aisle direction, up to 1.5 and 2.1 times lower for light and heavy merchandise, respectively. This beneficial effect is due to the slight increase in the down-aisle natural period of the racks (Table Table 3.2). The efficiency of the base isolation system in reducing the cross- and down-aisle accelerations increases with the weight of the merchandise.

For the base isolated rack configurations, no overturning of the merchandise during triaxial excitation, corresponding to 100% test level (life safety performance), has been observed. Under a triaxial seismic excitation at 200% test level, the base isolated rack loaded with light merchandise recorded an item falling from the topmost level. On the other hand, the base isolated rack loaded with heavy merchandise did not sustain any loss. Under the same 200% triaxial excitation, the rigid based rack did lose almost all of the stored items (last panel in Figure 2.2). Moreover, the conventional (rigid based) racks suffered significant structural damage as a result of the triaxial seismic tests. Following a triaxial seismic excitation at 65% test level, yielding, local buckling and cracking at the base of the central uprights were observed (Figure 3.6(a)). On the other hand, damage on the base isolated structure, for the case with heavy merchandise, cracking and tearing across down-aisle connector perforations in uprights was observed (Figure 3.6(b)).

During the seismic test at 150% test level, both central uprights sheared off completely from their base plates just above the welds. Finally, it was judged that the rigid based racks did not meet the expected performance objectives recommended in the FEMA 460 document since serious structural damage occurred at intensity less than the DE.

3.2.2 IsolGOODS® curved surface slider system for storage pallet racking systems

The device which is used to provide base-isolation to the steel storage pallet racking system considered in this work is the IsolGOODS® curved surface slider (CSS) system, which is patented under the framework of FIP MEC. IsolGOODS® is a unidirectional – cross-aisle direction – seismic isolation device designed for adjustable pallet racking systems, which leaves unaltered the behavior of the down-aisle lateral resisting system. The device has been designed in order to minimize its overall dimensions without wasting space for pallets at ground level, which is often used for store unit-loads as well. The IsolGOODS® bearing is arranged in two configurations for single- and double-entry racks, respectively Figure 3.7(b) and Figure 3.7(a). The device is hence installed beneath each upright frame of the rack, and it is anchored to industrial flooring by means of mechanical anchor fasteners according to current seismic standards. The device is also capable of bearing tension forces. However, this property is not investigated in this work.
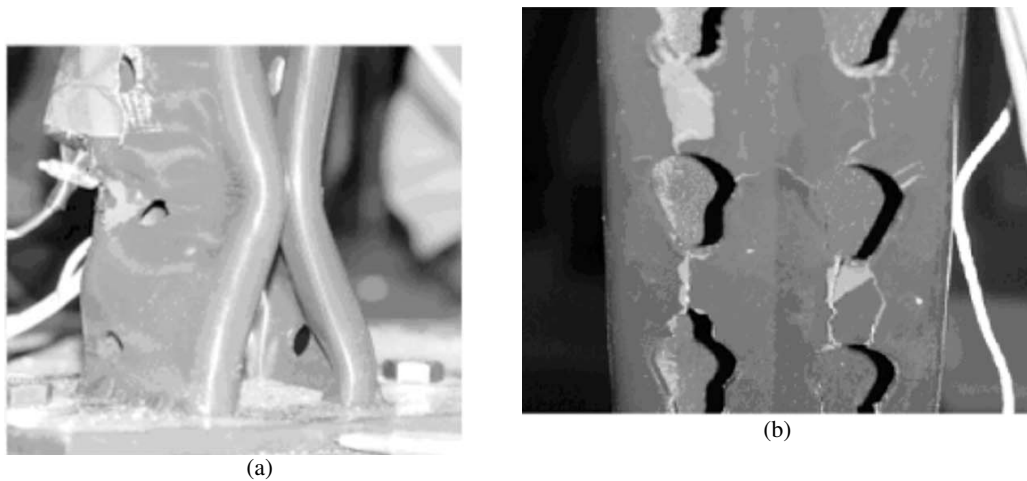
Figure 3.6: Buckling of central upright of rigid based rack, Test Series 1B, 65% test level (a). Cracking and tearing across down- aisle connector perforations in uprights of base isolated racks following Test Series 5 and 9, 200% test level (b) (reproduced from [68]).
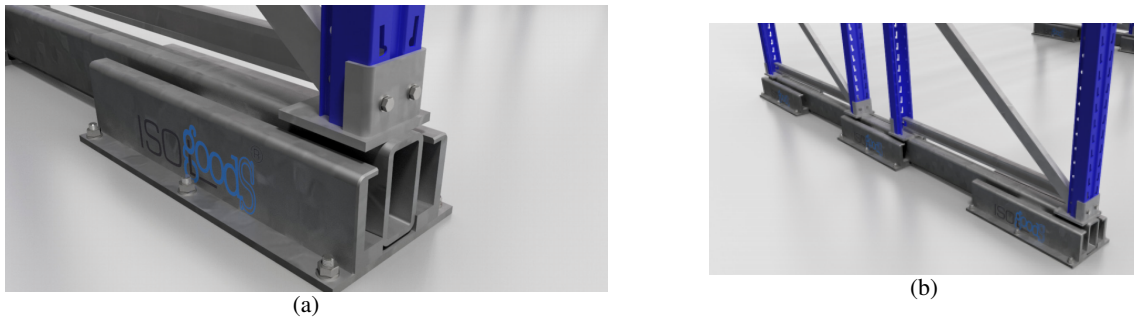
Figure 3.7: Render views of the IsolGOODS® device when installed under a single-entry (b) and a double-entry (a).

The main body of the IsolGOODS® is made up of two twin CSS bearings (single-entry version) that are installed at 0.500 m one each other and are linked together with a rigid beam, which is parallel to the cross-aisle direction. The beam is provided with two welded plates which can accommodate the upright base connections. Each bearing consists of two articulated sliders on a polished stainless steel overlaid, concave surface whose radius of curvature is $R = 2.000$ m and can experience a maximum design displacement of ± 160 mm. The sliders are bound to the rigid beam by means of a hinge connection, which is provided with a low-friction lubricant. A special thermoplastic material is used on the bottom-surface of the slider to govern the system friction. The material utilized is the FIP friction material (FFM), which is an ultra-high molecular weight poly-ethylene (UHMW-PE), which guarantees high load-bearing capacity and wear resistance. Additionally, FFM minimizes the stick-slip and ratio between the break-away and the dynamic friction coefficients as well. The undamped period of the device is $T_{iso} = 2.84$ s with an effective damping ratio of $\xi_{iso} = 0.42$ at the design displacement.

3.2.3 Rubber bearings vs. Curved surface slider bearings

The most important feature of CSS system is represented by its fundamental period of vibration, which, under certain hypotheses, could be computed in the following way:

$$T_b = 2\pi \sqrt{\frac{R}{g}}. \tag{3.1}$$

where R is the equivalent radius of curvature of the device. As it may be apparent, the value of the period of the isolated structure in Equation (3.1) is independent from the mass of the superstructure. Equation (2.5) can also be found in the Design Recommendations for Seismically Isolated Buildings by Architectural Institute of Japan. This feature, as approximate as it can be, is of particular interest for racks, for which the mass distribution is mostly unknown and its high variability may pose an issue to identify the worst load-scenario(s). The effective damping of CSS system can be evaluated as a function of the maximum displacement d and can be expressed as:

$$\xi_b = \frac{2}{\pi} \frac{\mu R}{d}, \tag{3.2}$$

where μ is the friction coefficient.

In the following, to highlight the main issues of designing isolation systems for racks, a simplied, although realistic, procedure that aims at preliminarily sizing devices for a single-depth racking system is presented. Let us get started with the definition of the type of isolators and the structure. The latter is a 5-bay 8-storey pallet rack with a total mass of $M = 85$ Mg, considering that each pair of beams is loaded with three 700-kg-pallets. With this in mind, the axial force for each inner column is around $P = 84$ kN. For the first iteration, rubber bearings with high damping (high damping rubber bearings, HDRB), which can assure an adequate degree of damping inherently ($\xi \approx 15$ %), are taken into account. The material can be characterized by a shear modulus of $G = 0.40$ MPa at $\gamma = 100$ % (shear strain) [75]; thus the minimum diameter for the device that ensures a pressure less than 7.00 MPa is:

$$\phi = 2\sqrt{\frac{P}{\pi\sigma_{lim}}} \approx 0.15m. \tag{3.3}$$

Let us now impose a period T_b to the isolation system; as a value of first attempt, it is used 3.50 s, which yields:

$$k_{iso} = \frac{M(2\pi T_b)^2}{n_{iso}} \approx 34kNm^{-1}, \tag{3.4}$$

where k_{iso} is the stiffness for each bearing, and $n_{iso} = 12$ is the total number of isolators. It is possible to evaluate the rubber thickness necessary to satisfy the required stiffness, that is:

$$nt_r = \frac{GA}{k_{iso}} = 0.28m, \tag{3.5}$$

where A is the rubber area. If a plausible value for the rubber thickness is defined as $t_r = 5$ mm, the primary and the secondary shape factors are $S_1 = 7.5$ and $S_2 = 0.6$, respectively [54]. The figures given so far make clear the ample discrepancies with codified values: the number of rubber layers to build the device, namely $n = 55$, which would need $n - 1$ steel shims thus making the device around 40 cm high: a device as such will never satisfy the stability checks due to excessive slenderness.

The main problem here is that an hypothetical displacement demand of $d_E = 0.20$ m would lead to a shear strain $\gamma = 70\%$. The shear modulus for rubber, in general, increases when the shear strain is decreasing. So, this procedure requires an iterative routine that will finally deliver the geometrical layout for the rubber bearing. As a consequence of higher values of G involved in, though, the height of the device increases as well, leading to non-realistic sizes. The value proposed above and obtained at this first iteration ,k_{iso}, is close to what can be observed in Table 3.1 of the manuscript. The following Figure 3.8 shows the configuration of the device the value refers to.

Figure 3.8 makes clear the ratio between a device able to offer the right amount of lateral stiffness for a pallet rack system. For the sake of clarity, the mount as employed for the work of Filiatrault et al. does not bear any – or almost any – axial force because another strategy has been used to put into practice a system able to deal with the vertical load. The reader, who is interested in more detail about the procedure and the values employed herein, can find examples in [54, 151].
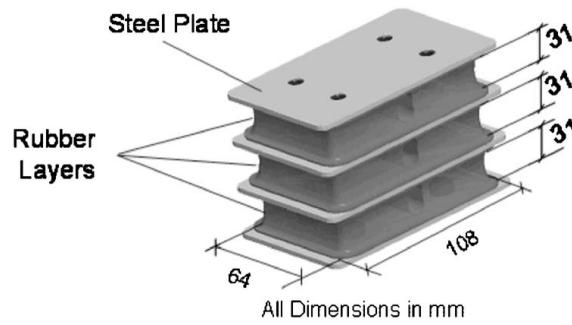
Figure 3.8: Elastomeric rubber mount of base isolation system [68]

Further reading

Candia et al. [76] analytically investigated the behavior of wine barrel configurations, identifying a remarkable increase of forces in the stack's components under earthquakes. Some published research has been focused on the nonlinear rocking behavior of wine barrel stacks during seismic excitation. Chadwell, Stanley, and J.M. [158, 159] conducted research to provide wine barrel stacks with collapse mitigation by using seismic isolation ball bearings. Despite the developed device being clearly efficient, in the process of its development no attention was paid neither to limiting lateral displacements nor to the re-centring capacity after.

The Gilardini System, the LOKIBASE system, is a bi-directional device that hence affects both directions. Though a complete description of the devices is given in [77, 78], no testing campaign for this device and its applicability to racks are available. The first [77] focuses on the analysis of a beam damper, whose experimental tests were run at University of Trento Laboratory (Italy), and then provides a theoretical model for the fully operating device. The latter [78] mostly deals with the optimisation of the beam damper, considering two different cross sections.

4. Dissipative connections for racks

For structural engineers, the selection of the lateral load-resisting system for buildings is a critical decision. While it is easy to understand the requirements to select beams and columns to support the gravitational loads (i.e., self-weight of the building itself and the live loads related to building occupancy), a lateral system is required for any building to resist horizontal loadings. Lateral loads are routinely considered for structure design, mainly either wind- or earthquake-induced ones, although blasts, floods, and tsunamis are also possible [80]. For low-rise buildings, most standards around the world give little to no relevance to the possibility of having wind and earthquake loads at the same time for several reasons; however, it may become relevant [160] especially for high-rise buildings and towers.

Lateral resisting systems can be especially critical when buildings are to be constructed in regions where significant seismic activity is expected. In the case of a steel buildings, a wide variety of lateral resisting arrangements are available [see 147, 148], which can exploit a number of innovative systems based on energy dissipation and damping that have been recently conceived [81, 161, 82–86]. These tested and approved systems have the capability of maintaining structure integrity in the face of significant lateral loads and inelastic behavior. One of the key elements to steel structures resisting seismic loads is properly designed energy-dissipating fuse elements according to the consolidated *capacity design* principles [59], conceptually providing guidance for the definition of the structure strength, stiffness, and absorption capability relationship.

One of the first investigations aiming at improving the understanding of the performance of down-aisle rack frames was performed in Bernuzzi and Castiglioni [40]. In moment-resisting frames (MRFs), beams and columns resist both gravity and lateral loads although typically only the perimeter frames are designed to provide significant lateral stiffness. The first topic debated in [40] concerned the definition of maximum allowable so-called *q-factor* to enforcing design procedures that comprise its use, which has since led to developing specific provisions for racks. Traditionally, for civil and industrial steel structures, beams can accommodate plastic deformation within their cross sections fulfilling the mentioned capacity design principles, mostly by specific cross-section aspect ratios (e.g., Classification of cross sections in [132]). Nevertheless, storage racks can still provide some degree of energy dissipation if other non-conventional mechanisms are considered [see, e.g., 153, 3, 83, 87, 88]. That being said, this is not the case for cold-formed beams employed to build rack frames. As such, beam-column joints (*fuses* using the definition given before) with post-yielding capability have been being developed and implemented to improve the ductility of

Left: bolted t-stub specimen after a cyclic loading protocol test (reproduced from [79]). Right: failure mode of typical beam-upright tab connection under cyclic loading protocol (reproduced from [37]).

these frames. This topic is extended in Subsection 1.2.1.

> **R** Note that the word *dissipative*, along with the related term *dissipation*, is used in this work according to its primary definition given in the code specifications (EC8 and EN16681 [129, 137]) pertinent to the objectives of this work. As it is well-known, devices able to collect irreversible deformation do contribute to the global response of lateral resisting structures through dinamically reducing their stiffness.

Other common lateral resisting systems for steel buildings comprise braced schemes, which, unlike MRFs, provide much more stiffness and then can henceforth be used for slender structural systems. Most of the standards that regulate the use of racks prescribe the use of tests for the estimation of quantities that can be representative of the element' performance [89]. The European Standard [134] requires specific shear stiffness tests (A.2.4 in [134]) for braced upright frames that indicate the diagonal cross-section area, A_g, usually given as a percentage of the actual brace area. The first systematic study on the performance of cross-aisle upright frames, focused on post-yielding resistance of the specimens, was performed during the Seisrack project [135]; uprights were tested considering a slightly different loading procedure that led to more conservative values for A_g. Nevertheless, it is not straightforward to determine the effects of underestimating (or over-) the lateral stiffness. The research report indicates that, albeit small, uprights can provide some degrees of ductility, intended as the ratio between maximum and the yielding displacements, developing various failure modes according to the frame level of overstrength [see 67, 90]. A ductility factor of two was achieved when the braces failed while developing a bearing mechanism in the brace-column single-bolted connections.

It is believed, however, that relying on the failure of brace instability to provide inelastic dissipation would not be a safe approach for structures with a near-zero degree of overdetermination. Petrone et al. [45] provides for the first time clear indications on the design of upright frames while using standardized design procedure. Experimental and numerical investigations conclude that designing base-plate connections able to yield can promote dissipative mechanisms for seismic design of storage racks in the cross-aisle direction. Along the same research line, Maguire et al. proposed an analytical procedure for the design of racks equipped with yielding uplifting connections, which cause the structure to rock and thus benefiting from an increase in the fundamental periods of vibration [92]. Further research proved that stomping loads are not relevant for rocking-promoting connections [66]. It may be important to remember that although some investigations have been carried out to ascertain the stiffness and strength of the base plate of steel storage racks [43, 93], this research has only taken into account the down-aisle base-connection performance, and the literature about the post-elasting performance permitted by rocking-promoting base connections remains limited.

4.1 Energy dissipation devices for racking systems

Other strategies for the seismic design and retrofit of rack systems, when considering upright frames, can be put into practice. If the structures are provided with supplemental *energy dissipation devices*, two main cases can be distinguished:

1. the devices are inserted within the same structure, being connected to points of it, that during motion undergo on relative displacements and speeds; the most typical case is the well-known dissipative bracing, wherein the devices are inserted in bracing systems and dissipate energy in the relative displacement between two successive floors of a framed structure;

2. the devices are inserted between contiguous (adjacent) structures, or structurally independent parts of the same structure, and they dissipate energy in relative motion; this assumes that the two independent parts have different dynamic characteristics, in order to vibrate differently.

Researchers have tested and applied both solutions to steel storage rack frames.

4.1.1 Sliding friction base-plate

The use of friction dampers is on the rise for mitigating earthquake-induced effects on buildings, within the passive control framework. Friction-based devices can provide energy-dissipation by means of wide and stable loops, with a negligible hardening phenomenon and experiencing no damage. For seismic resistant structures, such devices are commonly embedded into braces [84], beam-to-column joints [86, 94, 95] or into column-base joints [85].

A novel dissipation joint was proposed by Tang et al. [162] for pallet racking systems. The low-cost method proposed in this paper is based on the insertion of a steel sliding friction base-plate connected to all the uprights (Figure 4.1(a)), developed for low and medium-rise racks. The proposed system has been compared with the most commonly used yielding base-plate [45]. The device [96] (Figure 4.1(d)) is able to dissipate energy thanks to the friction instead of forming yielding zones at the base connections, which generally has to be replaced after the earthquake. Friction is introduced via a controlled clamping force between the upright and a stub welded to the base-plate. Of course, each grade of tightness of the bolts produces a different base response.
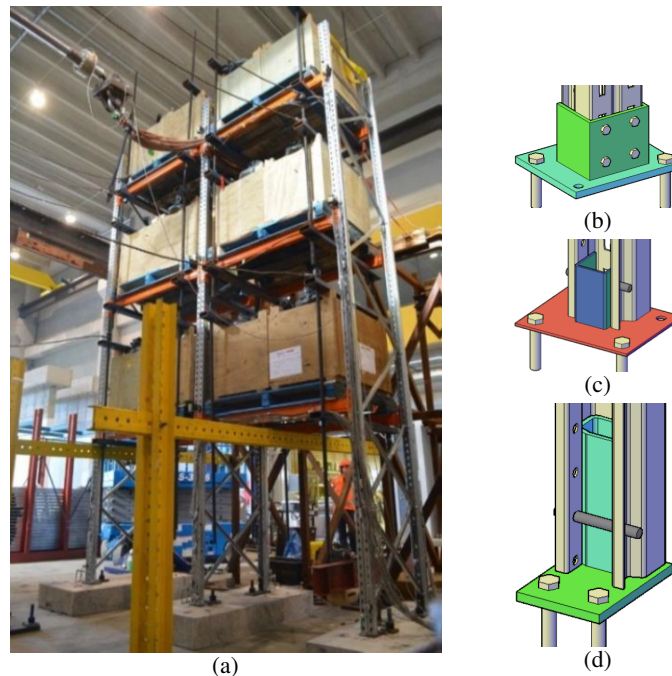
Figure 4.1: Test setup of the fully loaded frame (a); sketches of the three connections compared: (b) rigid base-plate, (c) yielding base-plate and (d) friction base-plate (reproduced from [162]).

Full scale snap-back tests were performed considering four different base-plate joints, which are installed at the base of a one-bay three-deck pallet racking system. The connection typologies involved in this campaign are (Figure 4.1): i) rigid or fixed base-plate (FB) Figure 4.1(b); ii) yielding base-plate (YB) Figure 4.1(c); iii) Friction base-plate with bolt tightening (DB) Figure 4.1(d); iv) Friction base-plate without bolt tightening (WB) Figure 4.1(d). The initial displacement was imposed at the third deck of the structure and equals 100 mm along the cross-aisle direction, which, as it has been stressed before, presents more lateral stiffness. The reason for only one direction is fairly clear. Though the sliding friction device can work in both directions, it needs the upright engaged into tension to be activated.

Figure 4.2 shows the test results. Permanent local deformations have been observed in FB frames that cause a large residual drift (dashed blue line), which is around 30 mm (tail of the dashed blue line), and it must be the one imposed by the actuator. It can be seen that most of the kinetic energy is dissipated within the first cycle. In all the other cases, no damage, apart from the base-plates themselves, has been observed and the initial residual displacements were recovered even if
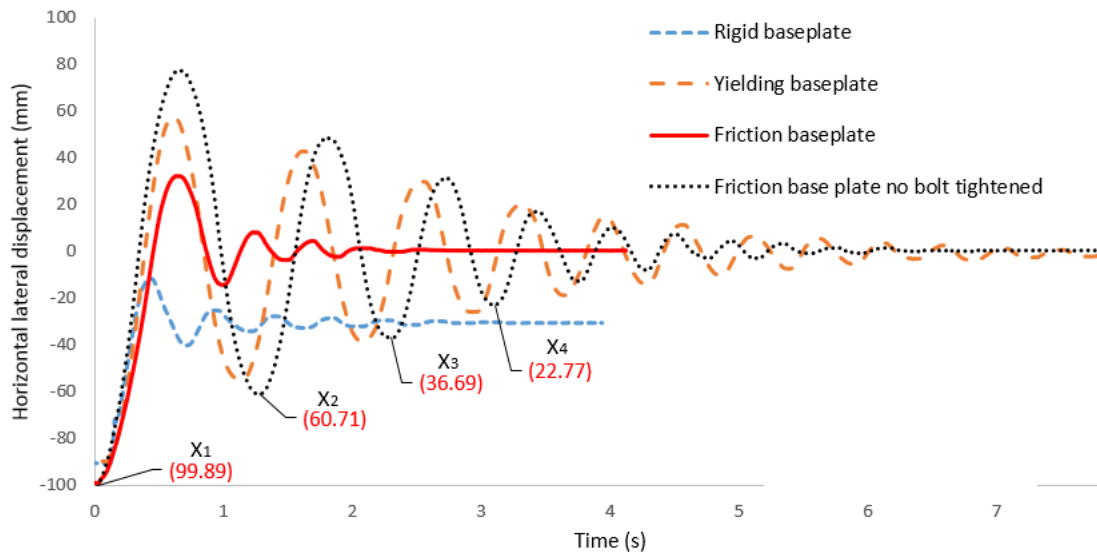
Figure 4.2: Time-history of horizontal displacements of the middle upright frame with the four base-plate configurations (reproduced from [162]).

the tests were started with the same imposed displacements. Rocking was observed for the frames fitted with YB (dashed orange line), DB (dotted black line) and WB (solid red line). Additionally, a first attempt to calculate the equivalent damping ratio from the free-vibration responses has been made by the Authors by using the logarithmic decrements method upon the first three cycles. The calculations reveal that the ratio is equal to 16.3% for FB frame (that is quite large) and 20% for WB frame, whereas for YB and DB is equal to almost 7%. Finally, the oscillation of internal axial force on the uprights has been recorded by using strain gauges. It has been shown that uprights of both DB and WB frames had smaller force demand compared to YB one. The amount of the compression force on the FB is 1.5 times greater than the other cases.

By comparing the performance of the devices, it is not immediate to pinpoint the outperformer. From the results outstandingly exposed in this paper, the friction sliding devices behave better than the yielding base-plate and far better than the fixed base-plate. According to the Authors, the bolt-tightened one gives more seismic resilience and is capable of reducing the force demand. However, it must be kept in mind that the tests are performed considering a dynamic framework not a *seismic* one. The structure equipped with the YBs proves to be as stiff as the one with the FBs, while the structures with DBs and WBs exhibit periods that are almost twice the FB's. This is indeed an advantage, for the structure does benefit from a period shift.

4.1.2 A practical solution for warehouses

Takeuchi and Suzuki [163] studied a high-rise automatic steel rack warehouse (height 52m) replacing side base chords (Figure 4.3) of the center truss, by buckling resisting columns (BRC).

The collapse mechanism of the entire structure is hence affected by the BRC: during an earthquake, the side trusses are kept elastic while BRCs are going into plastic and pull back the structure from residual deformations. The BRCs are composed of steel core-plates restrained with a concrete-filled tube. The restrain keeps the core-plate away from buckling and therefore its behavior is symmetric, showing a very excellent energy dissipation behavior. The performance of the structures against large earthquakes is greatly improved if compared to the same warehouse without BRCs: replacing only two columns out of 13 with BRCs makes the maximum shear force reduced by 25%, while replacing six, reduced to 45%.
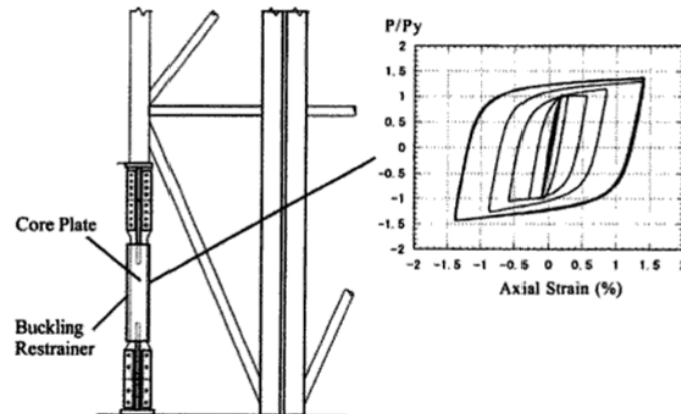
Figure 4.3: BRC system and its hysteretic force-strain relationship (reproduced from [163]).

4.1.3 Drive-in racks

Drive-in and Drive-through racks are special typologies of steel storage systems developed to maximize the storage density [see 10]. In the drive-through, as suggested by the name, operators can go through the structure in the aisle-direction, from both sides, while in the drive-in type, one side is for the forklift operation (refer to Figure 4.4). The principal difference between drive-in and pallet racks is that in the former no inter-storey beams are installed, making the structure more susceptible to instability phenomena. Global stability is therefore obtained mainly through stiffness supplied by base-plate connections and top beams. At the top of the structure, a bracing plane is realized and acts as a rigid diaphragm, distributing the lateral actions across the whole system. The pallets contribute to the frame stability, as demonstrated in [97].
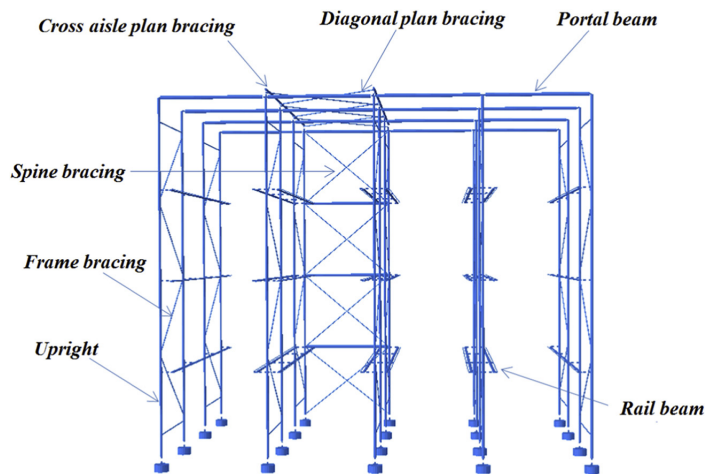
Figure 4.4: Framing systems for storage racks in the down-aisle and cross-aisle directions for a drive-in rack (reproduced from: [98]).

At the Sydney University, Australia, the first world-wide seismic full-scale shake table tests on drive-in frames (Figure 4.4) were performed [98]). The objectives of the study were to determine the natural frequencies and damping ratios from full-scale shake table tests as well as the inelastic responses of drive-in rack frames. Modes of vibration, base shear, and damage propagation have been investigated. In the first paper [98], two different framing systems have been considered: one fully braced in the cross-aisle direction with the diagonal braces extending from top to bottom; the second one relying mainly on a portal frame type and bending capacity of uprights in resisting earthquake-induced actions. The interesting results showed how plasticity is propagated along these particular structures before the structure collapses, identifying all the damages spread on braces

and uprights.

To improve the seismic reliability, special steel dissipation devices could be mounted to an external spine bracing system [164]. The device is a special steel plate that permits to mitigate the seismic actions while preserving the structural integrity of the principal components. A new bracing mechanism has been developed to improve the seismic behavior of steel storage racks using friction-damped seismic fuses. The same authors proposed a new bracing system with integrated seismic fuses; full-scale shake table tests of complete three-bay drive-in racks, including tests of the components of the fuses, are presented, clearly indicating the performance gain that the proposed brace can entail [88].

4.1.4 An out-of-the-box case: Parmigiano cheese rack structures

(a)   (b)

Figure 4.5: Typical storage system for Parmigiano cheese (a) and a collapsed one after something (b) (credits: Marco Simoncelli).

The great number of collapses caused by the *2012 Emilia-Romagna earthquake* (Italy) [99] showed the low reliability of the seismic zoning map for design which was in-force before 2003. The majority of the economic losses was experienced by the business sector [22], due to the collapse of many industrial buildings [100]. The poor performance of these structures, which had not been designed to withstand lateral actions, led many researchers to concentrate their attention on new recommendations for retrofitting the existing ones [101]. This seismic event also underlined the need for seismic provisions to be applied to non-structural elements [22] (Figure 4.5(b)). Theoretical research is also in progress in the field of the steel structures for the storage of the Parmigiano cheese (Figure 4.5(a)), a very important Italian product.

Generally, Parmigiano cheese is stored in structures made by composed steel tubular columns (two tubes of 50×50 mm with thickness of 3 or 4 mm and a global height from 7.0 to 9.0 m) having 1.5m of span (Figure 4.6). Along the cross aisle direction, each bay is connected by means of wooden panels, on which the cheese wheels rely, and via a continuous tubular steel on the top. Global length can vary from 18 to 40 m. When the steel rack is connected to the concrete wall (cases $S2$ and $S3$ in Figure 4.6(a)), it is only simply supported on the floor. On the other hand, when it is anchored to the floor, it is not connected to counter walls (case $S1$ in Figure 4.6(a)). Bracings are always present only in the down-aisle direction. Therefore, the structural scheme is quite close to the one of the Drive-in (ref. [10]), previously discussed, but in this case the stored products (Parmigiano wheels) do not help increase the transverse stability. A great number of these structures have been designed more than 20 years ago, considering only vertical forces (with no seismic actions) and therefore they are generally in an unsafe condition. For this reason, Franco, Massimiani, and Royer-Carfagni [102] proposed a complete study on the dynamic behaviour of these racks, focusing the attention on the seismic improvements techniques. The cases $S1$ and $S2$ exposed in Figure 4.6(a) are representative of the way this structures are often built. A proposed solution by the Authors is to use a passive-control system: viscous dampers are connected between
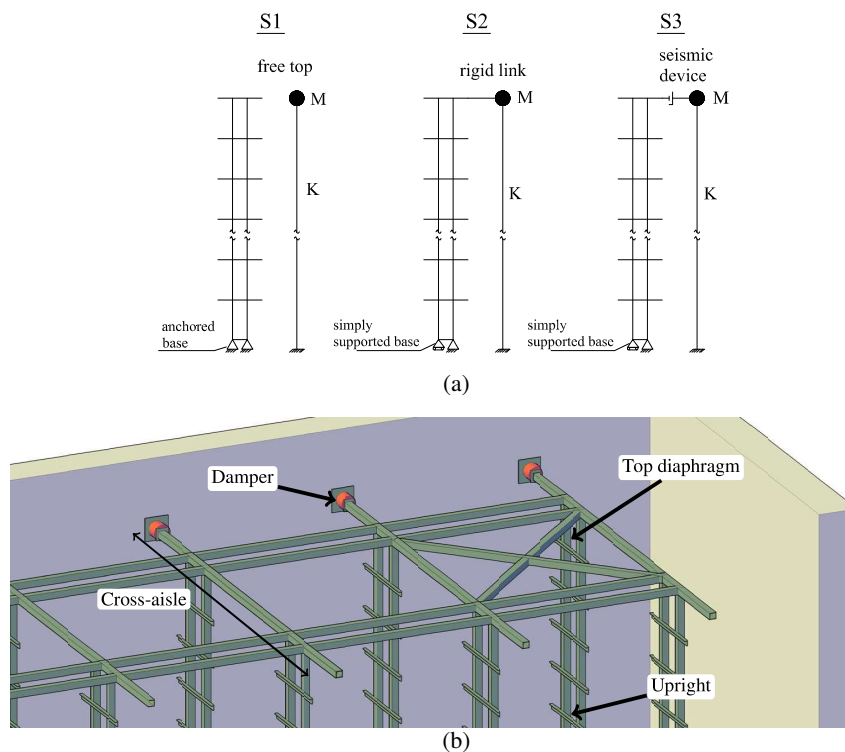
Figure 4.6: Three structural models to simulate *scalere* steel structures in the cross-aisle direction (a). Render view of case *S*3, which shows in red the damper devices (b)(sketch realized after Franco et al [102]).

the top of the storage racks and the surrounding concrete structures (*S*3 in Figure 4.6(a)).

The time-history analyses of the proposed configurations have shown that the use of dampers presents noteworthy advantages for all cases in which the constraint degrees of the racks are augmented and, consequently, their stiffness is increased. The advantages are in terms of stress reduction in the rack elements, and of reactive forces transmitted to the surrounding support structures. A sensitivity analysis has also been conducted to assess the optimal damping factor for the viscous coupling. An optimal damping condition is the one in which the bending moments in the longitudinal and transverse directions are comparable and, at the same time, the forces transmitted to the surrounding support structures are contained. A passive-control system, which provides the viscous coupling of the existing racks with a surrounding support structure, increases the seismic performance in terms of both stress and displacements. This countermeasure is simple and economical, because the refurbishment can be made without moving the cheese wheels, thus eliminating the cost for retaining the warehouse. On the minus side, this strategy requests to modify the dynamic behavior of the adjacent structure, which will need in turn to be checked against the forces transmitted by the devices.

Recently, a new investigation by Bernuzzi and Simoncelli [16] has put forward the use of cold-formed profiles for the realization of cheese racks, providing a detailed procedure for the numerical prediction of their performance under seismic events.

II
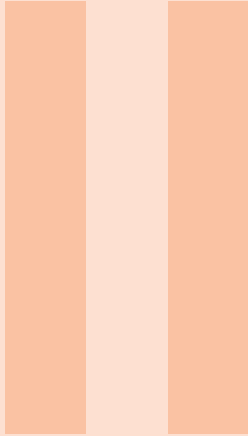
Seismic Isolation

5. Shake table testing for the CSS bearing device

A full-scale rack structure mounted on an isolation system that consists of two IsolGOODS® isolators, which has been presented in Subsection 3.2.2, is tested via uniaxial real-time shake table tests.

5.1 Test program and equipment

The seismic response of structures does depend on the accuracy of specimens and analysis procedures as well. To date, behavior of structures can be easily reproduced via computer software, even though a certain degree of approximation must be accepted. However, shaking table tests represent a method of investigating the dynamic properties of building structures; they are able to capture non-linearities which are inherently present in nature phenomena. In order to check the performance of an isolated rack structure by means of CSS devices, shaking table tests have been performed: critical for assessing the seismic response under earthquakes for innovative systems [103, 104].

5.1.1 Steel storage pallet racking structure

The specimen to be tested onto the shake table was selected among commercial proposal not designed against lateral actions, which may come from either earthquake or wind stresses, so to be representative of a wide class of structures in place on European countries [e.g. 18]. The selected structure is actually for indoor use and must lie on a concrete floor slab with a certain degree of flatness and guarantee bearing resistance as well. The 1200x800 Europallet is the reference unit-load, even if it can be used for loose goods, the *Instruction manual* suggests users stack everything on pallets by standard loading procedure involving forklift. As far as the structural performance is concerned, the layout of the pallet rack in use complies with the UNI EN 15512 [134].

The full-scale structure is a one-bay four-load-level rack, whose geometry is depicted in Figure 5.1. The upright frame is composed of two *C* lipped profiles truss-braced with a *D* scheme. The stability of the structure along the down-aisle is guaranteed by 4 pairs of square hollow cross-section beams, which are connected to the uprights by means of boltless three-tab connectors, which are further equipped with beam stoppers. The elements consist of steel grade S350GD. Connections of such kind provide enough stiffness to the down-aisle frame against global buckling [62]. The

---

The picture reported above shows a render view of the IsolGOODS® device developed and patented by FIP Industriale.
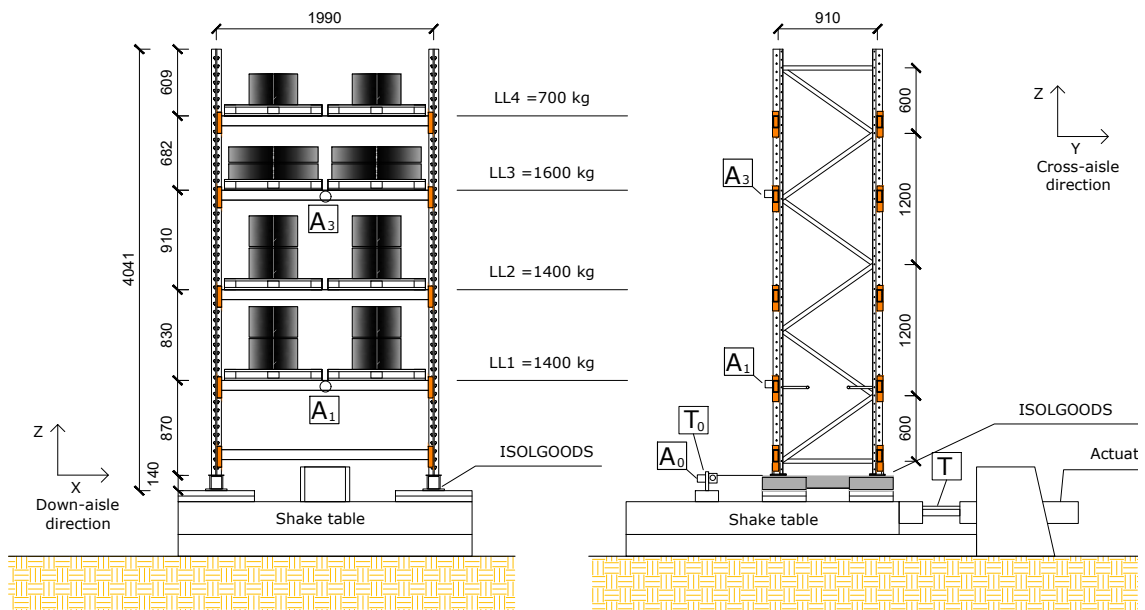
Figure 5.1: Test setup (all dimensions in mm): a) Elevation view; b) Side view

beams span over the length of the bay that is 2.00 m while the load-levels are not evenly interposed, to fit the different requirements that the unit-loads pose. At the first load-level (LL1), an *X* braced diaphragm was installed with two tubes with a circular hollow section, which was intended to avoid differential displacements between the 2 frames. The base-connection consists of a stub welded to a base-plate which is accommodated on the IsolGOODS® by means of 4 bolts. The stub is provided

with a hole that allows it to pin it to the first screw hole of the upright. The *Instruction manual* provides additionally the maximum permissible upright frame load and the maximum permissible (per pair of) beam load, 137 kN and 27 kN, respectively. As for the unit-load involved in this experimental campaign, it is necessary to underline that the rubber blocks are stiff enough to avoid spurious vibrations and hence prevent noise on the floor-acceleration time histories.

5.1.2 Shake table and instrumentation

Shaking table tests were conducted in the laboratory of FIP MEC (Italy) on the structure above described. The earthquake simulator consists of a rigid steel plate of 2 m x 2 m, which was constrained to move only in the y-direction by a set of rollers. The degree of freedom was set into motion by an hydraulic actuator which had a maximum stroke of ± 200 *mm* and a maximum velocity of 400 *mm/s*. The platform motion was controlled by the FlexTest 60 controller hardware, which used a valve driver to adjust the oil flux into the jack. The motion feedback was guaranteed by a Temposonics (MTS sensor)(T_0 in Figure 5.1) magnetostrictive, linear-position sensor whose sampling rate was set to 2400 Hz. The relative displacement of the device was measured with wire transducer (T_1 in Figure 5.1) whereas accelerations were measured with low-current triaxial accelerometers (A_1 and A_3 in Figure 5.1). The table acceleration was measured by means of a mono-axial accelerometer (A_0 in Figure 5.1).

The bases of the 2 devices, which constitute the base isolation system, were bolted directly to threaded holes into the platform of the shake table. Each device was also equipped with 4 threaded holes per side to accommodate the base-plate connectors by means of bolts. Also as a safeguard measure for the overturning of the rack, a loose chain was tethered to the laboratory's gantry crane.

As said, the accelerometers are installed either onto the shake table, 1st and 3rd deck. In order to provide a complete picture of the rack's performance, the accelerometer time series has been numerically inferred to get the deck accelerations for the 2nd and 4th. Based on the hypothesis of elastic behavior, the numerical model was built and run using a Matlab [166] code for extrapolating the sought time series. Though the structure was rocking, essential elastic deformations took place throughout it. In order to account for them, it has been assumed that the structure was oscillating according to the first mode shape.

5.1.3 Ground motions for seismic tests

Three seismic events were considered to assess the performance of the specimen with the base isolation system. The six ground motion records, whose main features are collected in Table 5.1, are used to impose the movement of the shake table. Additionally the elastic response spectra are depicted in Figure 5.2, which are obtained considering a damping ratio $\xi = 0.05$.

Table 5.1: Input motion for dynamic tests (* are retrieved from font: ITACA ItacaNet_30)

Test	Record	Date	Station	M_W	Mechanism	R_{min}	Soil	DIR	PGA [g]	PGV [m/s]	PGD [m]
#1 ——	Norcia*	2016-10-30	NRC	6.5	Normal	4.6	B	HNN	0.37	0.41	0.08
#2 ——								HNE	0.48	-0.48	-0.18
#3 ——	Emilia*	2012-05-29	MRN	6.0	Thrust	4.1	C	HGN	-0.29	0.58	-0.14
#4 ——								HGE	-0.22	0.28	-0.09
#5 ——	Roma		Spectrum-compatible				D		0.30	-	-
#6 ——									0.35	-	-

5.1.3.1 Norcia 2016

The first two ground motion records in Table 5.1 refer to the infamous 2016-2017 sequence that hit Central Italy for months. The fault system that generated the first shock in Amatrice in August was again activated on October the 30th, 2016 thus provoking the largest shock with a moment magnitude equal to $M_W = 6.5$, and epicenter close to Norcia. The records used in this work were registered in one of the stations located in Norcia, named NRC, and are characterized by very
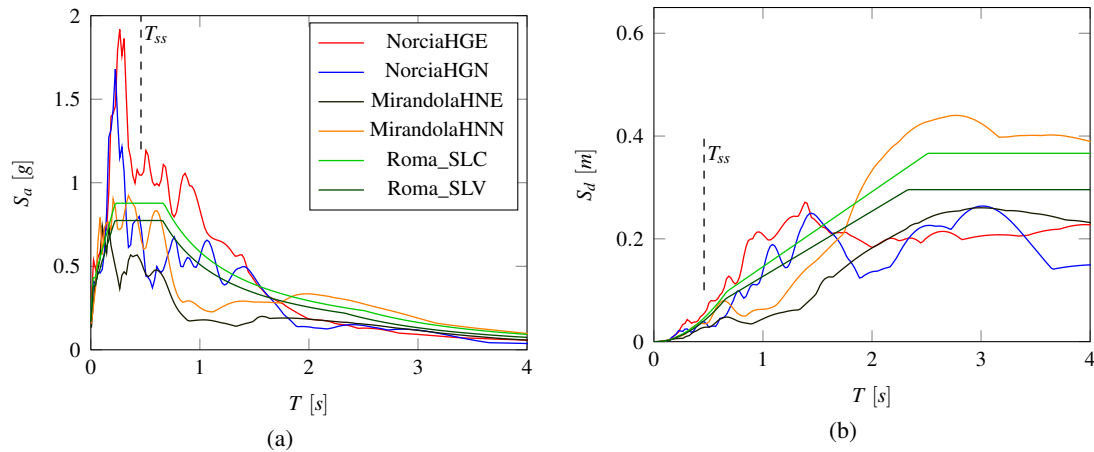
Figure 5.2: Input motion for dynamic tests. Elastic pseudo-acceleration response spectra (a) and Elastic displacement response spectra (b) obtained with a damping ratio $\xi = 0.05$. T_{ss} is the period of vibration of the superstructure.

large peak ground accelerations *(PGAs)*. The earthquake distribution analyzed by Michele et al [105] shows the activation of a *normal fault* system with a main SW-dipping fault extending for a total length of 40 km. The last mentioned work, however, does not explicitly refer to the largest shock, which occurred after the investigation had been carried out. A more complete description of this event can be found in Valerio et al [106]. In the aftermath of the seismic sequence, many researchers assessed the performance of structural and non-structural elements [15, 107]. Among these, Perrone et al [15] concludes that the vast majority of the experienced economic losses are due to the collapse of non-structural elements.

5.1.3.2 Roma

The second subset of accelerograms, namely #3 and #4, are synthetic spectrum-compatible accelerograms, compatible with target spectra generated according to the Italian seismic code provisions for an ordinary building, so that the reference life V_r of 50 years is accepted. The site response spectrum is built starting from the national seismic hazard map. A village nearby Rome (L 12.4473, N 42.1056) is taken into account, lying on type D soil. Herein the two *ultimate limit states* introduced by the Italian building code are considered. The *limit state for the safeguard of human life* (SLV)(#3), which corresponds to a satisfactory residual safety margin; the *limit state for collapse prevention* (SLC)(#4), which corresponds to the maximum considered earthquake with no-collapse requirement and residual, though small, safety margin. Respectively, their *exceedance probability* within the reference period V_r are 10% and 5%.

5.1.3.3 Emilia 2012

Ground motions #5 and #6 refer to the *Emilia 2012* event, which struck Northern Italy during May 2012. The time series corresponds to the second *aftershock* that occurred near Mirandola (IT-MRN), which recorded a peak ground acceleration of 0.29 g [108]. This seismic event was disruptive for the nearby industrial districts, where a huge percentage of the industrial buildings suffered severe damage, because they had been built without any seismic design. As a matter of fact, the area was not declared seismic by law until a few years before the earthquake. Along with the failure of prefabricated RC structures [21, 109], lots of steel storage structures gave rise to considerable losses computed in terms of stored goods shedding [22]. Within the interest of this work, this seismic event is deemed to be critical for the structure under-study. The recording station was quite close to the epicenter therefore the strong motions can be classified as a near-fault, with a *pulse-like behavior*. This class of records are well-known for posing a major risk to isolated structures, with particular reference to highly damped ones [110]. This is essentially due to a high energy content

for higher frequencies. As a last remark, the higher demand in terms of displacements can be noticed from the elastic response spectra shown in Figure 5.2(b).

5.2   Results of shake table tests

5.2.1   Sinusoidal test results

Prior to assessing the global behavior of the base isolated rack, an initial test was performed assuming a monochromatic input signal for the shake table. The wave is characterized by a frequency of $f_0 = 0.50Hz$ and an amplitude of $d_0 = 70\ mm$; 5 complete cycles were imposed, the first of which was with a smoothed ramp. For this signal is focused on a particular period, namely $2.00s$, at this value the displacement demand is consistently higher, which triggers the response of the isolated structure close to the isolated period. The test is also important to set up all the instrumentations in place, as well as to check whether the seismic tests can be safely performed.
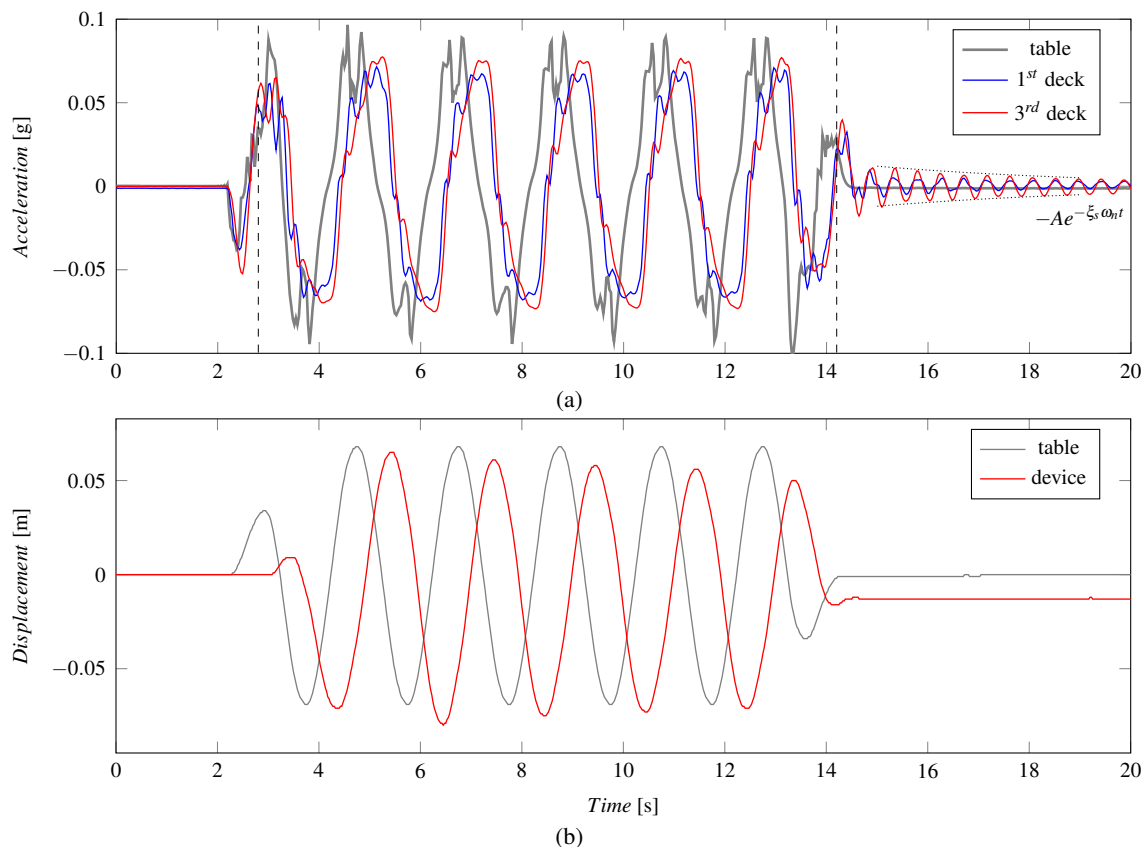
Figure 5.3: Time series for sine test: (a)acceleration time histories for the shake table, 1st and 3rd deck. The dashed gray lines mark the sliding range (b)

Figure 5.3(a) collects the acceleration time series which come from the accelerometers in place at the shake table (A_0), 1st (A_1) and 3rd deck (A_3). The peak ground acceleration induced on the shaking table equals to $pga \approx 0.1g$. For the devices that do not start sliding at unison with the movement of the table, the first peak shows an increasing trend along the height of the structure for the recorded accelerations, which is expected. However, as long as the static friction is exceeded, the devices become effective and hence the recorded floor accelerations are lower than the one recorded at table level. It can be noted that the magnitudes of the two series are quite close which underlines that the structure is rocking like a rigid body. Nevertheless, a slight difference in phase between the two signals reveals a certain elasticity in the structural response.

Figure 5.3(b) reports the displacement time histories for the table and the device. As it can be seen, the sinusoidal shape for the table displacement fits almost perfectly a theoretical one with the same period and amplitude, namely $d(t) = d_0 sin(2\pi f_0 t)$, where t is the time. The result is also confirmed by Figure 5.4, which compares the power density spectra for the signal as recorded in

this test and the theoretical counterpart. It is apparent that the facility is able to convey the expected power density in the range of interest. However, the physical system introduces some spurious components for high frequencies, which have little power.
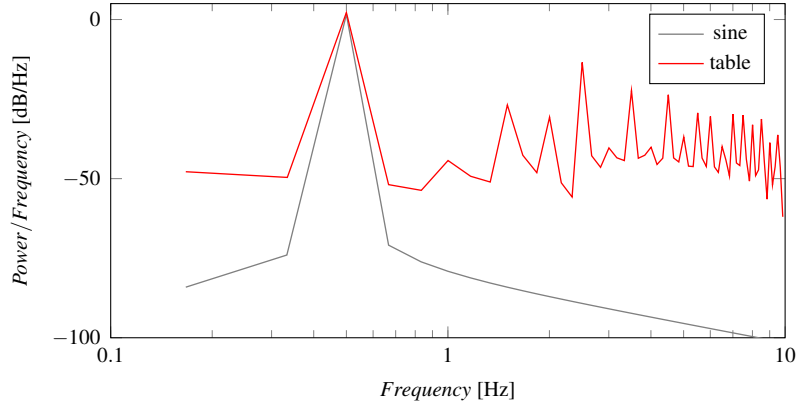
Figure 5.4: Power spectral density estimate for the theoretical signal sine input (red line) and the table acceleration (gray line), as considered during the 3 periods.

Additionally, the fundamental vibration period for the pallet rack is calculated from the free vibration response towards the end of the time series depicted in Figure Figure 5.3(a), starting from around 15s. In order to estimate the natural period of the superstructure T_s, the solution for the equation of motion is considered. The transient term, for under-damped systems, preserves its exponential form if written in terms of acceleration, which is $A(-\xi\omega_s t)$, where A is a certain constant, ξ is the damping, ω_s is the circular frequency of vibration of the super-structure, t is the time. Two curves, coming from the above introduced transient term, are introduced upon the free vibration of the structure (densely dotted line). The values that best fit are $A = 0.012$, $T_s = 0.47s$ and $\xi = 0.016$. The period was double-checked with a spectral analysis based on the Fourier transform, which confirmed the obtained value.
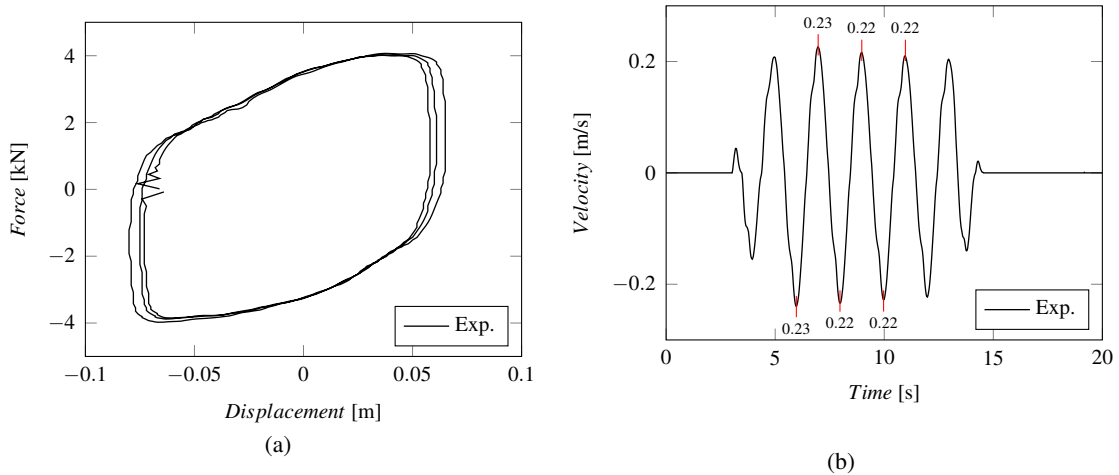
Figure 5.5: Experimental force-displacement hysteresis loops (a) and velocity time history (b) for the sinusoidal test.

The sine test is used to assess the friction coefficient of the CSS devices as in place. The dynamic friction coefficient can be evaluated by the energy dissipation that the isolation system provides. The procedure herein used can be found in European standard EN 15129 [143], which prescribes:

$$\mu_{dyn} = \frac{1}{3}\sum_{i=1}^{n}\frac{A_i}{4N_s d} \tag{5.1}$$

where A_i is the area enclosed in the ith hysteresis loop, N is the vertical load, d is maximum displacement. In fact, EN15129 considers the mean value of the μ_{dyn} over three cycles. Figure 5.5(a) shows the hysteresis loops related to the sinusoidal signal test. It refers to the first three periods starting from the end of the first ramp period (around $5s$). The corresponding dynamic friction coefficient equals 0.047 which matches with a peak velocity about 0.22 ms^{-1}, as can ascertained by the value exposed in Figure 5.5(b).

5.2.2 Seismic test results

The isolated structure was tested under earthquake-like excitation through real-time shake-table tests which make use of either real earthquake records and synthetic generated ones. The motion was imposed to the shake table via an oil-dynamic actuator, which was moving according to a displacement feedback system, as mentioned in Subsection 5.1.2.
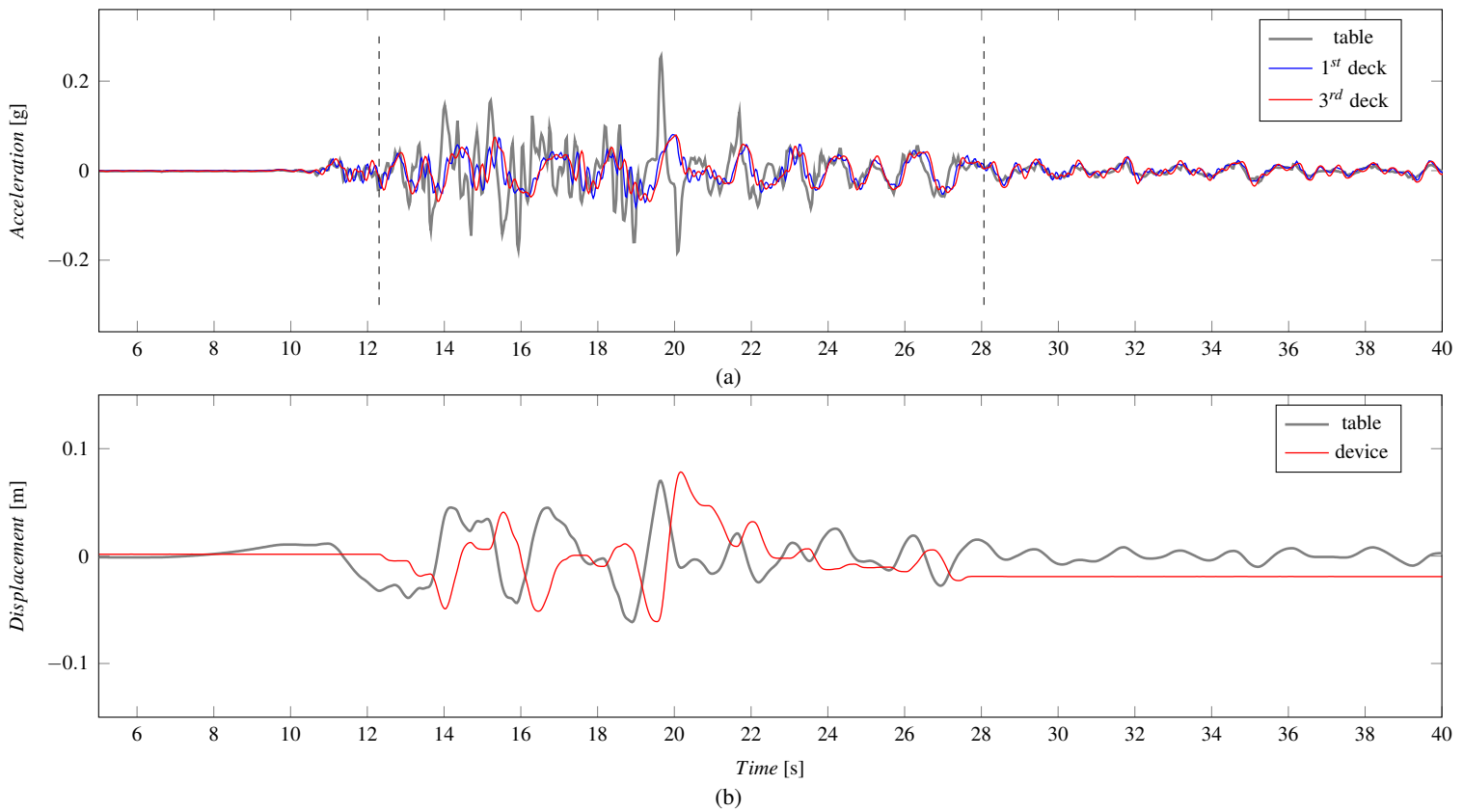
Figure 5.6: *Norcia HGN* #1 - Acceleration time histories for the shake table (A_0), 1st (A_1) and 3rd (A_3) deck. (a). Displacement time histories for the shake table (T_0) and the device (T_1) (b)

Figure 5.6 and Figure 5.7 report the acceleration and displacement time histories of the first two ground motions in Table 5.1, which refer to the *Norcia 2016* event. The two physical tests are reproduced at the same intensities.

Figure 5.6(a) and Figure 5.7(a) depict the acceleration time series as recorded by the three accelerometers in place. As soon as the simulations start and there is no sliding, the deck accelerations show to be almost of the same magnitude of the table one. However, when the isolation system is activated, noticeable differences in the magnitude of the accelerations take place. The peak ground accelerations for both are around 0.25 g, which is nevertheless shrunk by the base isolation system to a value around 0.07 g on the third load-level. In addition, the superstructure does not experience any magnification effect due to the different heights of its levels. In Figures 5.6(b) and 5.7(b) can be observed that the sliding time window covers most of the earthquake input
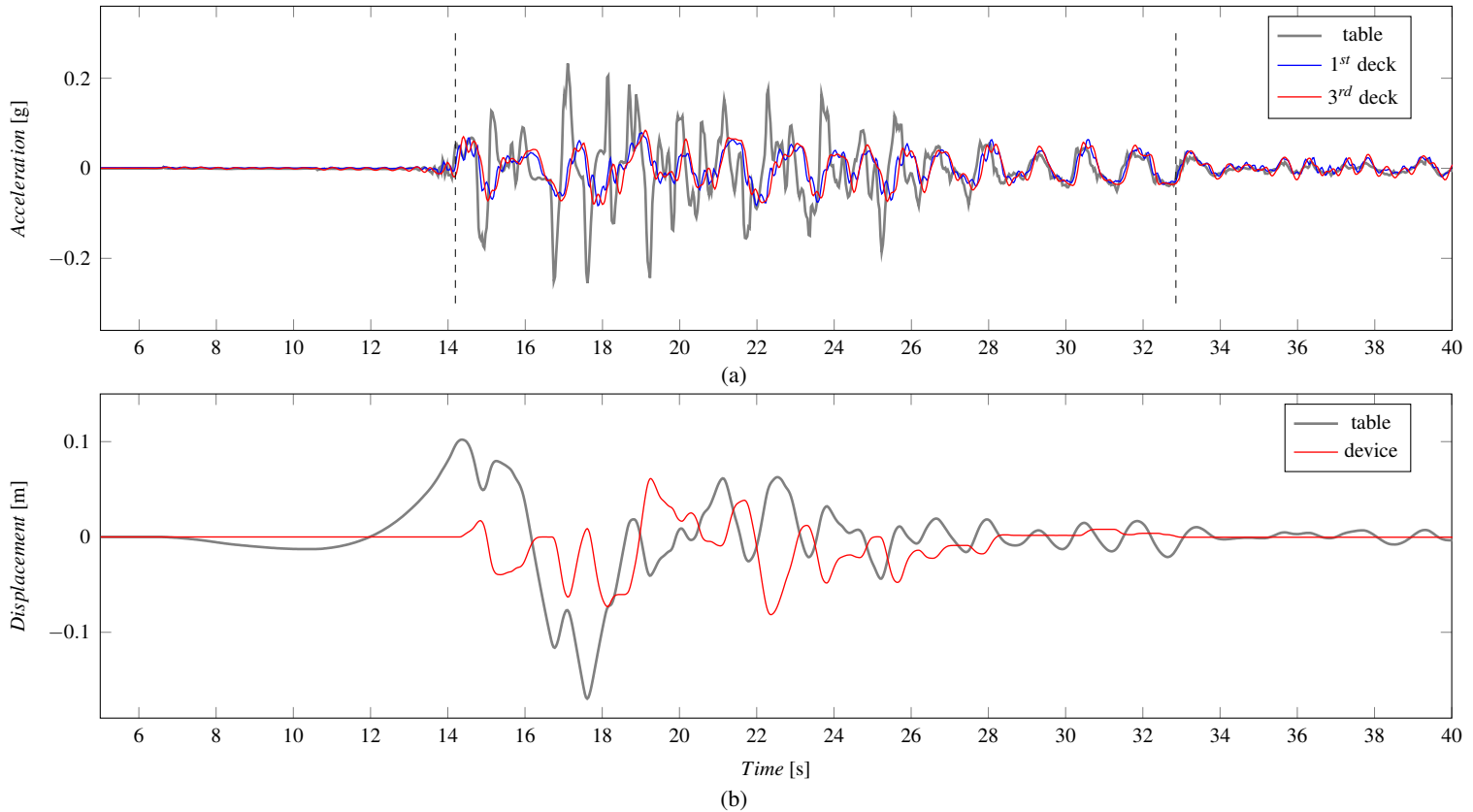
Figure 5.7: *Norcia HGE* #2 - Acceleration time histories for the shake table (A_0), 1st (A_1) and 3rd (A_3) deck. (a). Displacement time histories for the shake table (T_0) and the device (T_1) (b)

for these two cases and this makes evident the much longer period of the structures.

Figure 5.8 shows the fidelity of the shaking table to reproduce the input ground motion. As it has been previously explained, the system feedback worked on displacements thus making the table displacement time series perfectly coincident with the target ones. Therefore, the performance of the shake table is considered in terms of power density spectrum (PDS). For the two ground motions *Nocia 2016*, the facility is considered to reproduce with enough accuracy the frequency range of interest $F \in [0.3, 3.0]$ Hz.

Figure 5.9 reports the acceleration time histories of the other 4 ground motions, whose main features are depicted in Table 5.1. The first two panels (a) and (b) depict the result for the *Emilia 2012* event. The isolation system is activated for short time-windows, which correspond to the most energetic parts of the strong motions. Unlike what was seen for the previous cases, the acceleration time histories exhibit higher values with respect to the ground acceleration, when the isolation system is not working. Figures 5.9(c) and 5.9(d) depicts the result for the test #5 and #6. The accelerograms are characterized by a long sequence of peaks, which are not so common for on-field record ground motions. The system demonstrates to perform as expected, preventing most of the seismic-input energy content from being transmitted to the super-structure. In terms of maximum floor accelerations, the responses for the last two tests are comparable with the first two. Considering the acceleration time series which account for the 1st and 3rd deck, it clearly appears the super-structure behaves like a rigid body, with slight differences on the values of the deck acceleration.

5.2.2.1 Spectrum-compatible *Roma*

Figures 5.9(c) and 5.9(d) depicts the results for the test #3 and #4. The accelerograms are characterized by a long sequence of peaks, which is quite typical for synthetic spectrum-compatible signals.
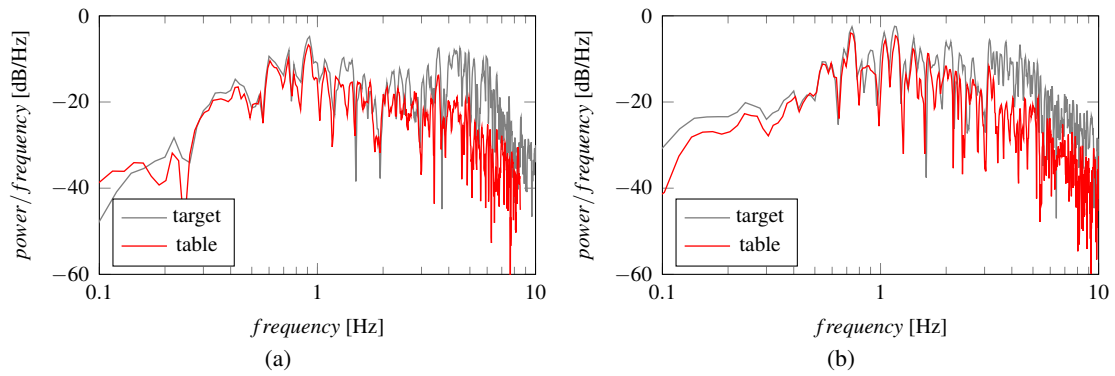
Figure 5.8: Power spectral density estimate for target input and the table acceleration recorded for *Norcia HGN* #1 (a) and *Norcia HGE* #2 (b).

The SI system performs as expected, preventing most of the seismic-input energy content from being transmitted to the super-structure. In terms of maximum floor accelerations, the responses for the last two tests are comparable with the first two. Considering the acceleration time series which account for the 1st and 3rd deck, it clearly appears the super-structure behaves like a rigid body, with slight differences over the values of the deck acceleration. The reduction of acceleration's magnitude is confirmed also for these two samples: from a PGA of around 0.25 g to maximum deck accelerations of around 0.08 g.
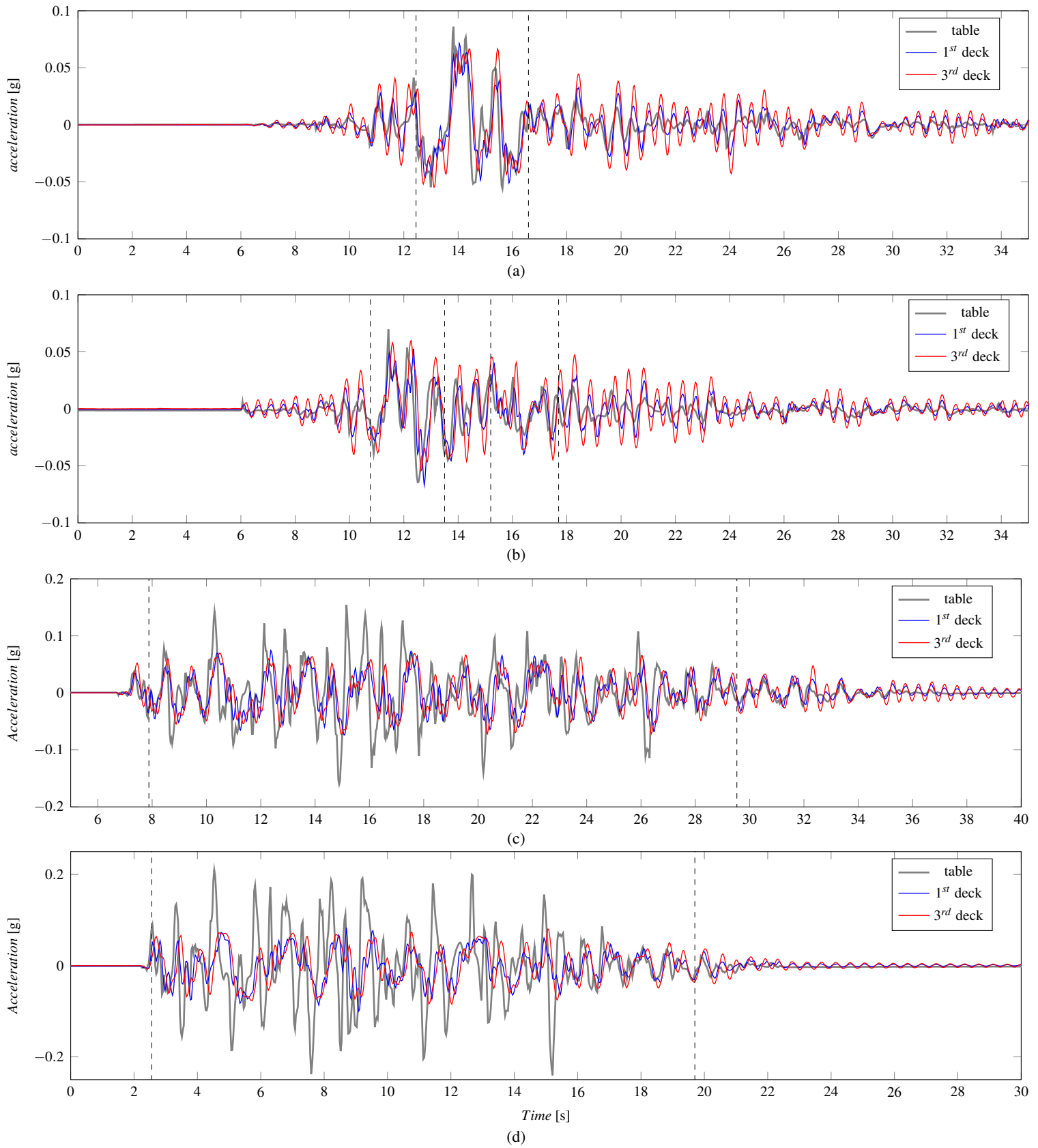
Figure 5.9: Acceleration time histories for the shake table (A_0), 1st (A_1) and 3rd (A_3) deck - *Roma SLV* (c); Roma SLC (d). The dashed gray lines mark the sliding range.

5.2.3 Results discussion

Overall, the performance of the isolation system has allowed the pallet rack to overcome all the tests with no damage. This has been confirmed by either a visual survey, which has underlined the presence of no residual deformation, and numerical simulations, whose results are shown in the next Section.

In order to have a more comprehensive view of the results of the shaking table tests, the maximum accelerations at every load-level are depicted in Figure 5.10. The data as generated using the procedure introduced in Section 5.1.2 are used. The panel depicts the acceleration patterns along the height of the frame and each line reports the maximum floor accelerations recorded when the isolated structure undergoes the ground motions in Table 5.1. The values at $\bar{h} = 0$ correspond to the maximum shake table accelerations, whereas the values along the height represent the maximum floor accelerations. For low intensity earthquakes, the isolation system slides only when there is a strong sequence, so that the structure feels the ground motion almost as it is. This is expected for it depends on the break-away friction coefficient that characterizes the devices, whose value is around 5%. Therefore, a value of the floor acceleration around 1/20 of the acceleration of gravity is reasonable. For instance, considering the time series in 5.9(b), though the devices are activated throughout a short time window (namely, from 12-17 s), the superstructure is alleviated by most of the seismic effects. For ground motions with higher values of peak ground acceleration, the effectiveness of the isolation system can be immediately caught – please refer to the events *Norcia 2016* and *Roma*.
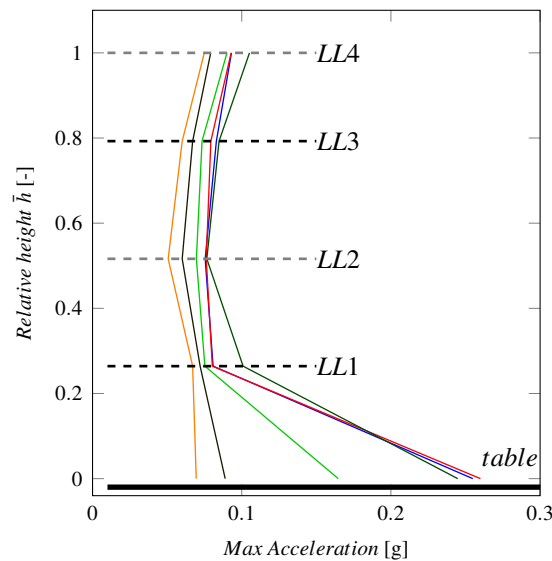
Figure 5.10: Comparison of the peak ground accelerations with the maximum deck accelerations for the six records considered in this study.

6. Numerical modeling of CSS isolated racks

6.1 Numerical modeling of the base-isolated structure

6.1.1 The isolator

The results of the experimental tests have been herein used to validate a numerical model of the base-isolated structure. The OpenSEES [111] (Open System for Earthquake Engineering Simulation) framework is used to numerically reproduce the physical tests. To begin with, a sinusoidal test has been reproduced to set up the fundamental parameters that are needed to simulate the IsolGOODS® device. The *singleFPBearing*[1] element is deployed to reproduce the CSS isolator features; it is a concave sliding surface device with a spherical joint. For the aim of this work, however, the sliding surface collapses into a line, whereas the joint collapses from spherical to cylindrical. The friction model, used for the analyses carried out for these numerical settings, is:

$$\mu(V) = \mu_{fast} - (\mu_{fast} - \mu_{slow})e^{-a|V|} \tag{6.1}$$

where V is the sliding velocity, μ_{slow} and μ_{fast} are the kinetic coefficients of friction at low and high velocity, respectively; a [sm^{-1}] is the rate parameter that gives shape to the relationship. The above-mentioned parameters are calibrated upon the sine test outlined in Section 5.2.1: they are $\mu_{slow} = 2.88\%$, $\mu_{fast} = 5.40\%$, and $a = 7.15$ [sm^{-1}]. The friction model was first proposed by Constantinou et al. (1990) [112] for sliding bearings with friction coefficients that provide a good description of Teflon-polished steel systems. It is commonly used by many commercial computer programs, such as SAP2000[2] and MIDAS[3] software, to model pendulum isolators.

To reproduce the seismic isolation system in place, each IsolGOODS® isolator is modeled by means of two *singleFPBearing* elements, linked by a rigid beam. The numerical model used for the bearings additionally requires setting up the initial stiffness k_1, which corresponds to the pre-sliding phase. The first studies on this matter [151] suggested choosing this value as proportional to the restoring stiffness k_2. In the wake of this, many authors agreed on a value of the initial stiffness in the range $50 - 100 \, k_2$ [37, 113], though [114] proposed the use of values ranging within $500 - 1000$. For the model herein considered, in light of the results of previous characterisation tests on the devices, the initial stiffness is set to $k_1 = \mu_{fast}N_{sd}/\delta_{slip}$ by means of the pre-slip deformation

---

[1]Single_Friction_Pendulum_Bearing_Element
[2]SAP2000
[3]MIDAS
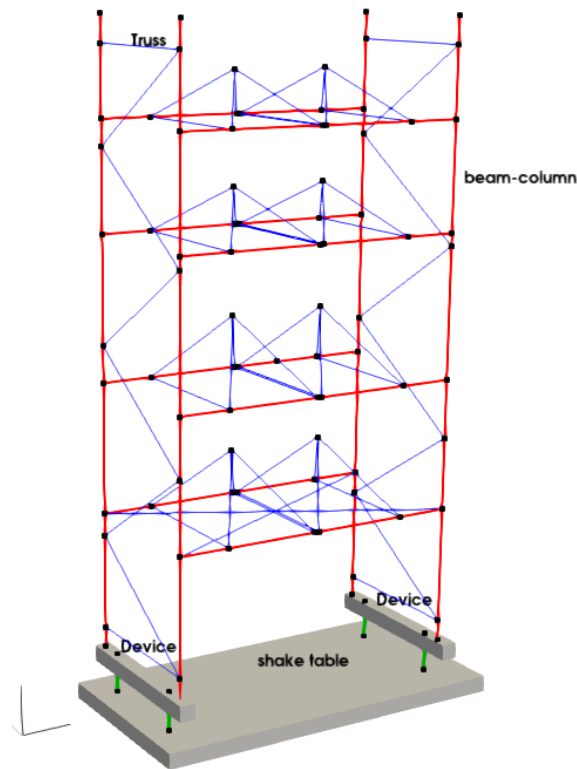
Figure 6.1: 3D view of the numerical model as built in the OpenSEES environment.

$\delta_{slip} = 1$ mm; this equals 6.65 kNm^{-1}, considering the static vertical load on each device given by the gravitational load alone (N_{sd}).

6.1.2 The superstructure

The superstructure is introduced into the numerical model. Its members are reproduced considering beams and columns as *ForceBeamColumn3d* elements (red elements in Figure 6.1), with cross-section properties given by the fiber-section model. The cross-section properties are automatically computed by the code from the given geometries, which correspond to those described in Section 5.1.2. The braces are introduced as *corotTruss* elements (blue elements in Figure 6.1) that are pinned to the columns. It must be emphasized that the beams are modeled as elastic elements that are rigidly connected to the uprights, for these elements are not stressed by the load condition imposed. With the structure modeled into a 3-D framework, the torsional degree of freedom of each node is prevented with elastic elements, to which only torsional stiffness is assigned. As for the masses, the elastomeric isolators and expansion joints, in place during the tests, are reproduced as lumped masses located at the center of mass of each block. This last detail is implemented to correctly achieve the fundamental frequencies of vibration; this method is described in EN 16681 as well. An auxiliary system of trusses is used to link these last nodes to the pallet-beams, as is shown in Figure 6.1.

6.1.3 Numerical model setup

The boundary conditions are such that the bottom column-ends are pinned to an auxiliary rigid body, which is part of the isolation system. This last statement complies with neglecting the base-connection rotational stiffness, which is a fair assumption. The devices are in turn fixed to the ground; its motion is imposed according to the applied record. The transient analyses are performed

by employing the implicit Hilber-Hughes-Taylor (HHT) time integrator with an α coefficient equal to -0.05 [115] and a time step equal to $dt = 0.01$ s. The numerical damping is necessary to cancel out the spurious effects of higher modes of vibration, which may affect the structural response in terms of accelerations, while preserving second order accuracy. The structural damping is implemented as stiffness-proportional damping where the damping coefficients are computed from the frequency of the base-isolated structure [see 116, 117], with a damping ratio of $\xi = 0.04\%$.

Once the super-structure has been modeled, its fundamental period is assessed by means of an eigenvalue analysis. The first period of vibration (T_1) corresponds to 0.45 s, which is consistent with the one that was evaluated from the decay test (0.47 s) performed on the real structure (Section 5.2.1). The eigenvalue analysis is repeated after introducing the isolation system; the value used for parameter k_1 (initial stiffness of the isolator) induces a small change in the fundamental period of the global system that equals 0.51 s.

6.1.4 Validation

Eventually, the numerical model is validated against the data provided during the physical test campaign. Figure 6.2 reports four panels that compare both experimental and numerical results obtained for entry #1 in Table 5.1. Panels 6.2(a) and 6.2(b) directly compare data acquired from the tests with the numerical prediction. On the other hand, Panels 6.2(c) and 6.2(d) compare data that have been processed.
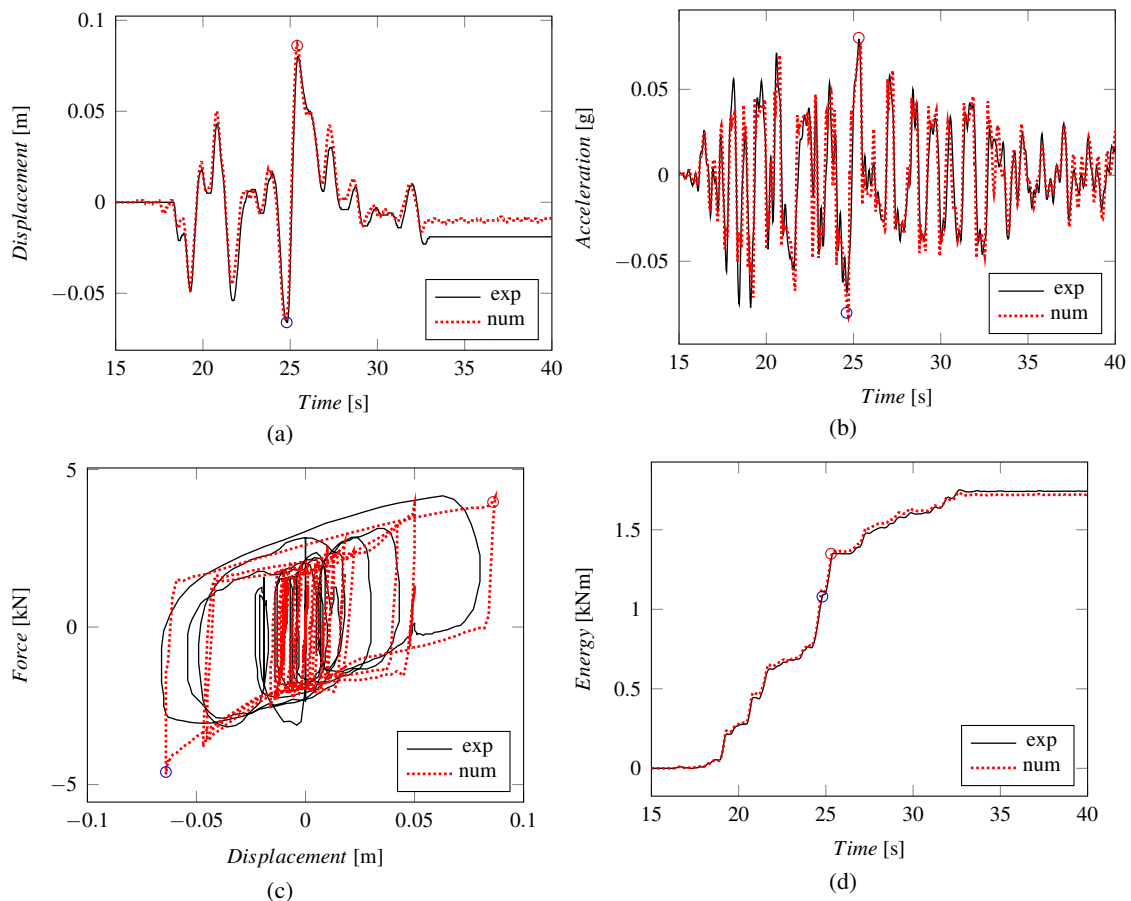
Figure 6.2: Experimental versus numerical response for the ground motion #1 in Table 5.1 (NORCIA-HNN): (a) displacement time histories; (b) acceleration time histories at level 3; (c) hysteretic force-displacement curves; (d) seismic input energy time histories.

Figure 6.2(a) compares the sliding displacements measured at isolator level, which show good agreement considering that the numerical model can hit the main peaks recorded during the test
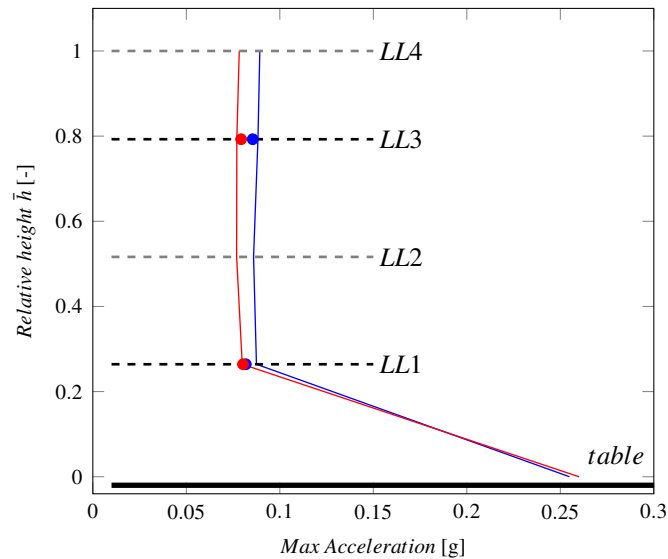
Figure 6.3: Experimental versus numerical response for the ground motions #1 and #2 in Table 5.1

with satisfactory accuracy. The numerical model starts to experience small sliding fluctuations at the very beginning of the simulation. Nevertheless, the accelerations, which are shown in Panel 6.2(b), start almost in unison with the experimental ones. As mentioned before, the main peaks, which are highlighted in the figures by means of ○ and ○, are correctly estimated. The response in terms of accelerations (Panel 6.2(b)) shows an overall good agreement as well. The numerical model predicts most of the time series correctly. There are small differences in the first peaks (through $\approx t = 20$ s) that may be due to a static friction coefficient not fully compliant with the physical one. This is also apparent from Panel 6.2(c), which depicts the hysteretic force-displacement curves for the isolation system. The main features of the physical curve are fairly represented by the numerical model. Despite a conspicuous bias on the initial value of the breakaway friction coefficient, most of the mid-loops are well captured. Also, the branch that can be retracted from ○ → ○ shows that the model is able to capture the increase of coefficient of friction due to higher sliding velocity. Finally, Panel 6.2(d) compares the seismic input energy time histories, which overlap almost completely.

Overall, the model herein set up and employed has proved capable of accurately reproducing the dynamic response of the isolated structure. The main features are reproduced with a satisfactory degree of accuracy. As a result, it is possible to assume that the superstructure has been correctly modeled.

6.1.5 Incremental dynamic analyses

The results collected from the experimental campaign described above show that a non-seismic designed structure, when seismically isolated with a system like the one under study, can withstand many strong seismic events without experiencing any damage and without pallet sliding. To broaden the range of applicability of the proposed isolation system, the validated numerical model is employed to perform incremental dynamic analyses [118]. For the following simulations, the four events considered for the tests are once again considered. In addition, two records of the *2012 Emilia* event are considered, namely entries #5 and #6 in Table 5.1, for a grand total of six earthquakes. This event is introduced, along with the previous ones, because it represents a class of quakes that are considered extremely dangerous for base-isolated structures. The reasons for that can be quickly deduced from the response spectra depicted in Figure 5.2, and are given in the following sub-section.

Table 6.1: Result from IDAs on the fixed structure (^{x} marks the quantity that brings the structure to fail)

Test	Record	Direction/SL	failure [PGA [g]]	maxAcceleration [g]	minAxialUpright [kN]	minAxialBrace [kN]
#1	Norcia	HNN ●	0.037	0.150	-4.45	-4.99^x
#2		HNE ●	0.030	0.160	-3.59	-4.99^x
#3	Roma	SLV ●	0.035	0.170	-3.99	-4.99^x
#5	Emilia	HGN ●	0.037	0.060	-2.48	-4.99^x
#6		HGE ●	0.039	0.160	-4.13	-4.99^x

6.1.5.1 Fixed structure

Prior to putting forward the results of IDAs, it is important to assess the performance of the fixed structure under earthquake actions. This task is accomplished numerically. The structural model, as described in Section 6.1, is tested considering the six accelerograms as described above (Tables 5.1). However, the boundary conditions are slightly different since the column bases are considered pinned to the ground. In the same fashion as with the tests, the ground motions are applied along the cross-aisle direction only, which is the most critical for such a typology of structures. Several response quantities have been monitored, such as the maximum floor acceleration (*maxAcceleration*) for the four decks, and the maximum axial loads for uprights (*maxAxialColumn*) and braces (*minAxialBrace*).

The maximum values that the monitored quantities can assume are evaluated as follows. The *maxAcceleration* is bounded by the friction coefficient between the wooden pallet and the metal that makes up the beams. This value is, in practical terms, pertinent to the coating layer that covers the outer surfaces of the pallet beams. According to Adamakos et al. (2018) [65], a fair value for the pallet-to-beam friction coefficient is $\mu_s = 0.20$, which complies also with the lower bound proposed by EN 16681 [129]. Accordingly, the maximum value acceptable for *maxAcceleration*= 0.20 g. As for the axial load in columns, it is imposed that the base-plate connection can bear a maximum tension force $T = 14$ kN, which corresponds to the shear resistance of the one-bolt connection. Lastly, maximum axial compression in the braces is monitored. Presently, the braces are bolted to the uprights by means of one-bolt connection with M8 class 8.8 and are assumed to be made up of steel grade S350GD. The most severe load case for the braces, which have a structural scheme that resembles simply supported beams, is when they are engaged in compression, with an ultimate buckling load evaluated as 4.99 kN.

To find the breaking point corresponding to each record, nonlinear time history analyses are performed on the fixed structure. The intensity of the seismic input follows a linear pattern (i.e. PGA with steps of +0.001 g). Table 6.1 reports the results of such analyses in terms of maximum supported PGA values at the failure points. The ^{x} symbol highlights the quantities that lead to failure. The structure meets crisis in 100% of the cases for buckling phenomenon occurring in the lowermost diagonal brace, with quite low intensities of ground motions. When brace instability precedes any other mechanisms, the structures fail within the elastic range regardless. Hence, any plastic resource of the structure cannot be exploited. The performance of the structure is quite poor since collapse is achieved with a mean failure PGA of around 0.035 g. This outcome coincides with what many past seismic events have highlighted: structures fail even under low-intensity earthquakes. The PGA reached in the shaking table tests on the isolated rack is seven, eight, and seven times higher than the PGA associated with failure in the non-isolated rack, respectively for Norcia HNN, Norcia HNE, and Roma inputs. It is important to provide additional knowledge with respect to the results explored in this and the following paragraph. Being the structure asymmetric along the cross-aisle, the ground motions have been applied in two opposed directions, and the data shown relates to the most stringent ones.

6.1.5.2 Isolated structure

Figure 6.4 shows the results of the analyses performed on the isolated structure, organized in terms of IDA curves. Just as has been done for the fixed structure, the *maxAcceleration* (Figure 6.4(a)) among all 4 decks and the maximum axial loads for columns (*maxAxialColumn*) (Figure 6.4(b)) and braces (*minAxialBrace*) (Figure 6.4(c)) are now intended as engineering demand parameters (EDPs). Unlike the fixed structure, the maximum displacement of the devices (*maxDisplacement*) is checked (Figure 6.4(d)), thereby functioning as another EDP corresponding to the maximum design displacement of the device. Of course, the design displacement could be increased, but in this case the value corresponding to the tested isolators is considered. The selected intensity measure (IM) is again the PGA that is reported on the y-axes of the 4 panels. For the sake of comparison, the points at which the fixed structure fails (filled dots ●), as described above, are also reported in the charts.
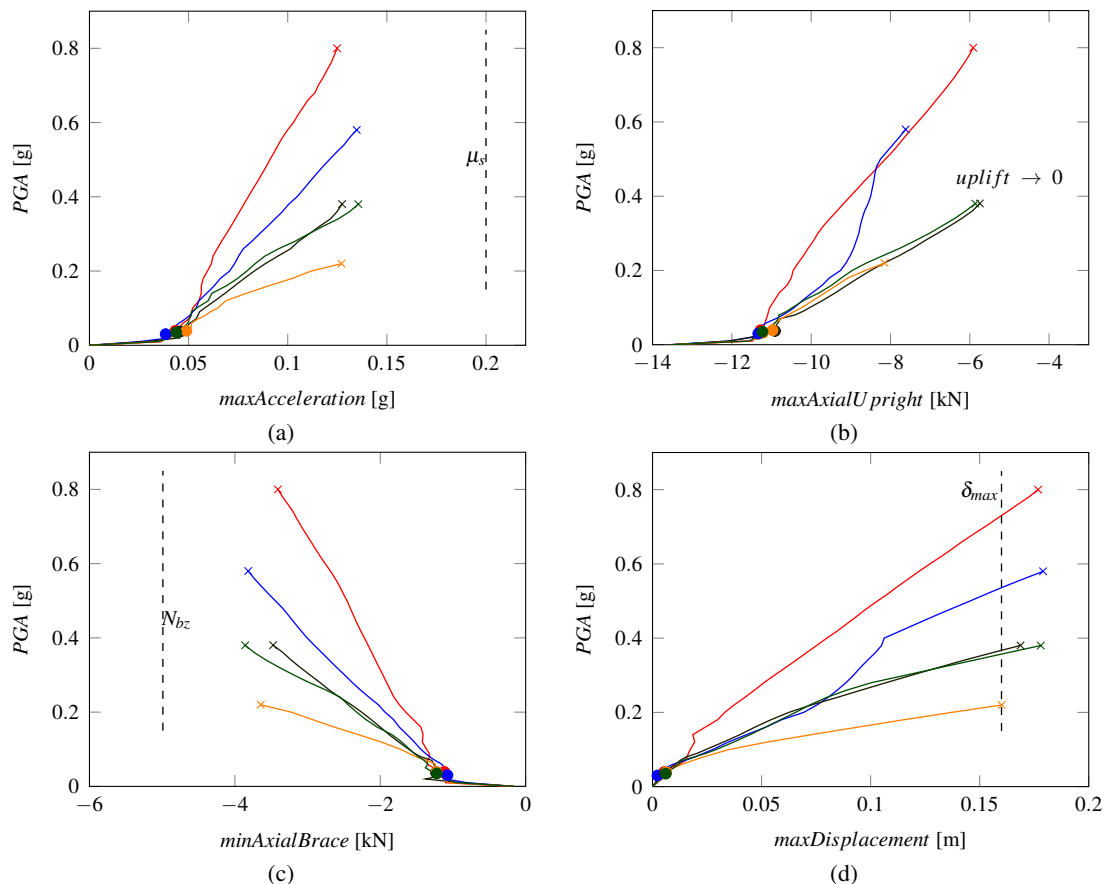
Figure 6.4: Incremental dynamic analysis curves for the maximum deck acceleration ((a)), maximum axial force in uprights ((b)), minimum axial force in braces ((c)), maximum displacement for the isolation system ((d)). The solid dots represent the value of PGAs that correspond to failure for the fixed structure

The results of the incremental analyses presented in Figure 6.4 show that the structure can bear much more intense seismic events when an isolation system is put in place. From Panel 6.4(a) it is easy to understand that the SI is able to drastically reduce the deck acceleration at any level (vertical dashed line μ_s). The low level of acceleration transmitted to the superstructure is reflected in the low internal actions throughout the members. This last insight is confirmed by what Panels 6.4(b) and 6.4(c) depict. The base connections are engaged in compression in all the simulations performed for the five time series, so the columns' up-lift is always prevented. The axial compression in the braces, which proved to be a weak spot of the structure, hardly reaches 4 kN, so the buckling phenomena for such members is avoided (vertical dashed line N_{bz}). Nevertheless, the lateral displacements in the isolation system become critical. Panel 6.4(d) demonstrates the

IDA curves in terms of maximum (unsigned) device displacement, where the failure conditions for the isolated structure can be identified. It is quite obvious that the isolators properties, the friction coefficient and design displacement are commonly selected for a specific earthquake intensity and design spectrum; when the intensity increases, at a certain point, the isolation system reaches its maximum capacity. In this case, the isolation system is designed for medium-seismicity areas, and consequently its displacement capacity is not very high.

It can be seen that the results exposed in this panel (d) resemble the displacement demand that can be observed in Figure 5.2(b). The most severe condition is represented by the pulse-like *Emilia HGN* record, which displayed failure at 0.17 *g*. It is worth highlighting that the choice of PGA as IM comes from the need for comparison.

6.2 Discussion

The novel curved surface sliding isolator IsolGOODS® has been presented. The device is purposely developed by FIP MEC for steel storage racks, and is particularly apt for single- and double-entry adjustable pallet racking systems. The device has been designed to provide seismic isolation along the cross-aisle. In contrast with what is now available on the market, the IsolGOODS® isolator belongs to the pendulum isolator class, which can exploit outstanding features according to the rather peculiar rack structures' characteristics. The isolation period achieved by means of pendulum isolators is almost independent of the superstructure mass. This indeed unquestionably poses a point of strength, for the rack masses present a high degree of uncertainty. Additionally, such devices can provide the structure with considerable energy dissipation capabilities.

The IsolGOODS® bearing effectiveness is proved by means of shake-table tests. The isolation system is applied to a rack structure that does not comply with any seismic code provisions. Several tests are performed employing a suit of records with a variety of characteristics. By reviewing the result time series, proposed in terms of accelerations, it is evident that the isolation system transmits little deck accelerations to the superstructure, which has a response that demonstrates a phase lag of a few degrees. By way of inference, low internal forces are expected, since the structure almost behaves like a rigid body. The most intense record in terms of ground acceleration (Norcia HGN $PGA = 0.26$ *g*), reveals that the system can cut down the deck acceleration by about 40%. Finally, the steel storage rack underwent meticulous inspection that sought out damage, yet it proved to have remained pristine.

III

Dissipative device

7. Base-plate Connection

The overall lateral resistance of the upright frames is greatly affected by the flexural behavior of the base-plate connections. For the special configuration that often characterizes the slenderness and the way upright frames are arranged, base connections may be the only place to safely locate plastic deformation without involving mechanisms within the upright elements. The high lateral stiffness of upright frames is also cause of concern for the happenstance of excessive accelerations at decks level. It is safe to say that the sliding of pallets on the supporting beams can be the most serious threat to the shedding of goods, which can either endanger the health of workers/customers or even damage some structural parts thus leading to cascading effects. In the cross-aisle direction, the fundamental period is generally short, ranging from 0.50s to 1.00s [see 2, 45, 67, 91, 162] depending on the structure slenderness ratio.

7.1 Design procedure for racks in seismic zones

7.1.1 Design procedure

The structure under study is a single-depth adjustable pallet rack with four load levels, each of which can accommodate three unit-loads (UL) per bay, as it is shown in Figure 7.1 for inner bays. Furthermore, Figure 7.1 proposes a side view of the upright frame, where the load levels (LL) are pointed out. The four levels are equally inter-spaced at 2.00 m; the reason for a small discrepancy in the height of the first level is due to the presence of the base-plate connections, considered here 10 mm; the weight of each UL equals 800 kg. Therefore, the mass which is used at each LL for both the definition of the vertical forces and the *seismic mass* is 2400 kg. On this account, [129] defines the design weight of a unit load as:

$$W_{E.UL} = R_F \cdot E_{D2} \cdot Q_{P.rated} = 23.54 kN, \tag{7.1}$$

where R_F is the rack filling grade reduction factor, which is assumed to be equal to 1.00 in the cross-aisle direction; E_{D2} is the load weight modification factor assumed equal to 1.00; $Q_{P.rated}$ is the specified value of the weight of the ULs for the compartment. Note that this procedure slightly deviates from the reference EC8 provisions, in which the structure seismic weight and seismic mass differ. The value considered for this last quantity corresponds to an area of influence of the upright frame equal to the beam span. The weight of the seismic mass is hence identified by:

$$W_E = W_{E.G} + W_{E.UL}, \tag{7.2}$$

The picture reported above shows the designed base-plate connection tested in the Laboratory of Steel Structures, NTUA (Athens, Greece).

where $W_{E.G}$ is the permanent load. For the safety verification at the Ultimate Limit States (ULSs), the characteristic values of the permanent and the variable actions for UL are taken with both combination factors equal to 1.00. Their effects are combined with the design value of the seismic action $A_{E.d}$ for the reference return period. The reference value for the friction coefficient is assumed $\mu_s = 0.37$, which inherently assumes normal working conditions in the warehouse. This value is standard for coated surfaces of the beams which are in contact with wooden pallets.
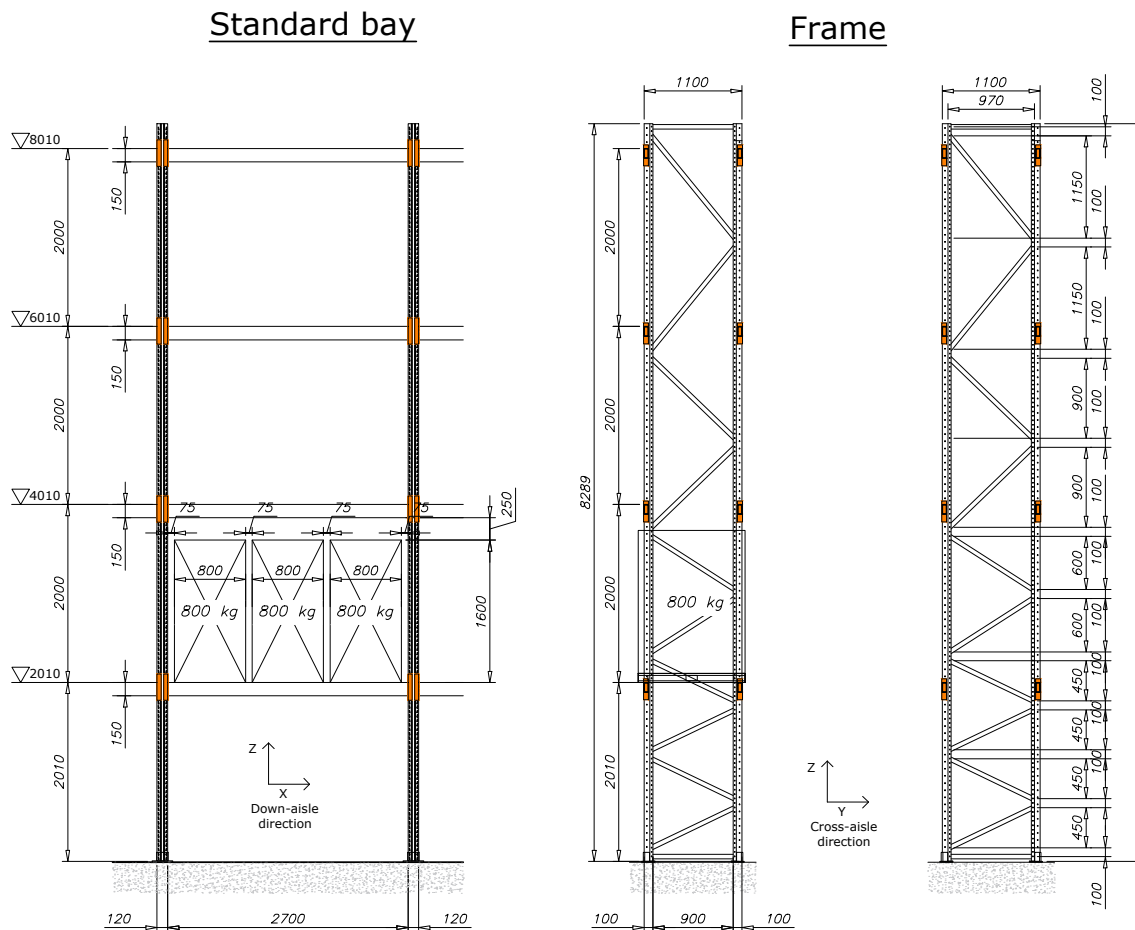
Figure 7.1: Front and side views, and frame arrangement for the structure under study. Courtesy of NEDCON B.V.

The design concept employed for upright frames as earthquake resistant systems complies with the so-called *low dissipative structural behavior*, as defined by code specifications. For this occurrence, the effects of the seismic action can be determined by means of elastic global analyses, and the nonlinear behavior of the material is not directly taken into account. EN 16681 allows using behavior factors $q \leq 2.00$. Standing on the structural regularity assumption, which is fulfilled by the proposed configuration, it is permitted to model the 3D structure layout by means of sub-systems (ref. to Figure 7.1). This is exploited when the upright frame is alone analyzed as a 2D lateral force-resisting system.

7.1.2 Seismic action

As stated in EN 16681, the first instance of the reference *elastic response spectrum*, S_e, is defined according to EN 1998-1 (EC8) [137]. Only the horizontal component of the seismic action is

considered. The parameters that qualify the spectrum are given in Table 7.1. Note that the viscous damping for the unloaded structure is assumed to be 3%. It also herein defined the *Importance factor*, γ_1, of the structure. The shape of the elastic ground-acceleration response spectrum is depicted in Figure 7.2 (blue line).

Table 7.1: Values of the parameters for $Type1$-elastic response spectrum as defined in EC8

Ground type	S	$T_B[s]$	$T_C[s]$	$T_D[s]$	$a_{gR}[g]$	γ_1	ξ [%]	β	q_{ca}
C	1.15	0.20	0.60	2.00	0.25	0.84	0.03	0.20	1.50
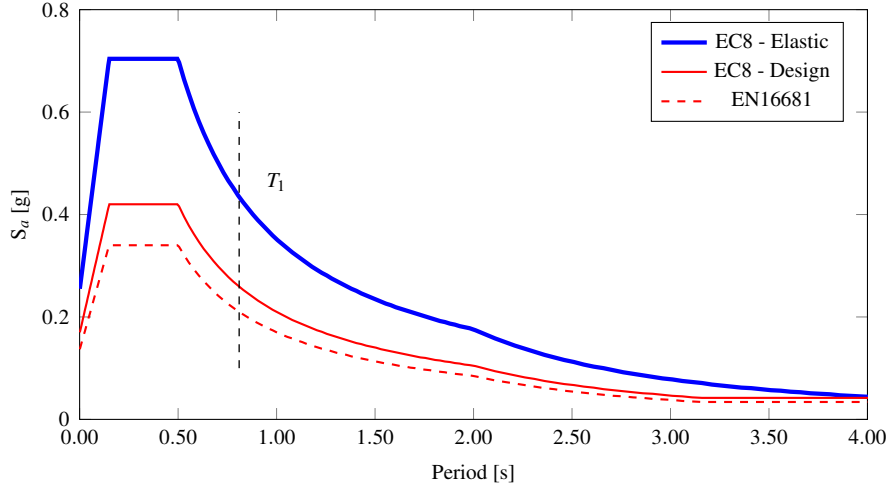
Figure 7.2: Elastic response spectrum (solid blue line) and the design spectra according to EC8 (solid red line). The modified response spectrum as obtained through the procedure defined in EN16681 is reported as well (dashed red line).

The nominal life of the structure is assumed to be 30 years, which corresponds to a default value for conventional warehouse racks; the *Importance Class* is as well defined as Class *II*. Hence, $\gamma_1 = 0.84$, which corresponds to a 10% exceedance probability of the seismic action during the nominal life. Following the provisions given by [129], the *modified design spectrum* is introduced as:

$$S_{d.mod} = K_D \cdot S_d(T) = \left(1 - \frac{P_{E.prod}}{P_E}(1 - E_{D1} \cdot E_{D3})\right) S_d(T), \tag{7.3}$$

where S_d is the *design spectrum* the parameters of which are given in Table 7.1, according to its definition in EC8; $P_{E.prod}$ is the total weight stored on the rack whereas P_E is the total weight of the rack in the seismic design situation; E_{D1} and E_{D3} are the design spectrum modification factors and are used to *adapt* the ordinates of the design spectrum.

The parameter E_{D1} is defined as:

$$E_{D1} = max(0.4; \frac{g\mu_s}{S_e(T_1)} + 0.20) \leq 1.00, \tag{7.4}$$

where T_1 is the fundamental period of vibration. As it may be evident from its formulation, E_{D1} takes into account the possibility of activating the beam-pallet sliding mechanism, which can provide the structure with extra energy dissipation. If reference is made to the ratio in (7.4), its magnitude depends on the likelihood of the pallet-sliding mechanism to be activated. As detailed in the EN 16681, the structure dynamic characteristics play a paramount role for activating these mechanisms, being the pseudo-acceleration $S_E(T_1)$ a direct, albeit not unique, cause of this phenomenon. Note

that EN 16681 suggests using $E_{D1} = 1.00$ if pallets are impeded from sliding. Regarding E_{D3}, the code introduces this value to account for *dissipative phenomena* which are typical for the dynamics of racking structures, not directly included in the spectrum proposed by EC8, however recognized during past studies. The value is given in the form of $E_{D3} = 0.80$, and it may be caused by viscous damping of about 10% for the loaded structure.

Table 7.2: Members' parameters used into the numerical model. Partial safety factors involved in the safety checks performed using the formulas in [134].

$\gamma_{m0} = 1.10$	$\gamma_{m1} = 1.10$	$\gamma_{m2} = 1.25$									
		$A_{eff}[mm^2]$	$A_{gross}[mm^2]$	t [mm]	$f_{y.k}[MPa]$	$I_{yy}[mm^4]$	$I_{zz}[mm^4]$	$W_{yy}[mm^3]$	$W_{zz}[mm^3]$	$W_{eff.yy}[mm^3]$	$W_{eff.zz}[mm^3]$
Upright	$125 \times 83 \times 30$	656	800	2.50	355	1 114 848	651 276	22 058	12 453	18 003	14 503
Brace	$50 \times 40 \times 20$	270	274	2.00	355	113 722	57 327	-	-	0	2 297

To completely define the modified design spectrum in accordance with the EN16681, a behavior factor q must be assigned to the structure. The code gives various instructions on how to set this value up and, as mentioned before, it has to be lower than 2.00 on account when a low-dissipative resisting mechanic is expected. The eccentric D-shaped diagonal pattern, in which members are engaged either in tension and in compression, also affects this process. A value of $q = 1.50$ is eventually assumed, following the recommendations in [129].
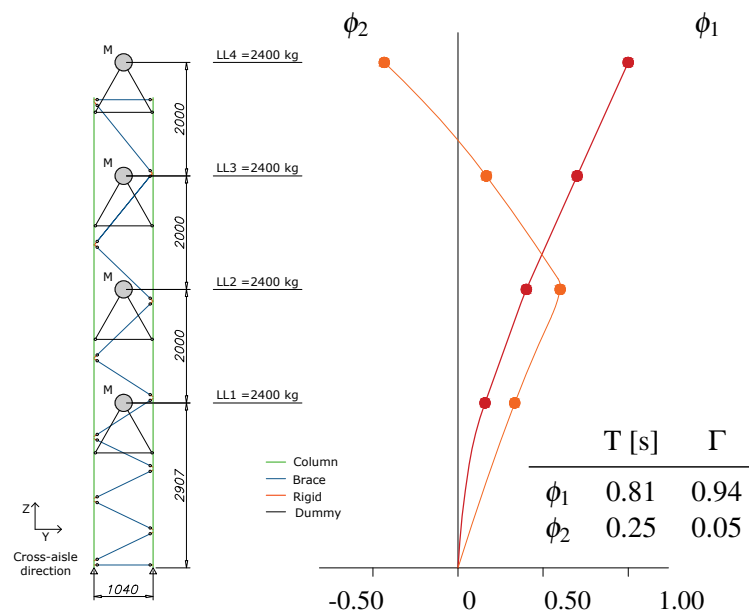
Figure 7.3: Structural scheme for the cross-aisle frame, and first and second modes of vibration.

The final assessment of the modified design spectrum through various parameters, as identified before, leads to a shape that is depicted in Figure 7.2. The solid red line shapes the design spectrum S_d whereas the dashed red one, the modified design spectrum $S_{d.mod}$, in which $K_d = 0.81$ is assumed by following Eq. (7.3).

7.2 Design procedure for ductile base-plate connection

The control of the maximum compression action in an upright can be obtained by controlling the maximum tensile force in the other upright. For instance, it can be achieved via a special design of the base-plate connection that promotes a dissipative mechanism. Due to its narrowness, the seismic behavior of an upright frame is very likely to exhibit complete uplift of one of the two uprights. This circumstance can be exploited by designing the base-plate-upright connection to fail according to *mode-1* as defined in (EC3 [132]). The base-plate in bending is a quite ductile

mechanism (see, equivalent cantilever model in [149]), which can also leverage the deformability of the anchors bolts. However, the proposed application deals with a tee-stub with short anchor bolts, which are indeed limited in their length by the slab-thickness, which rarely exceeds 20cm.

Considering the scheme in Figure 7.3, it is possible to define the maximum compression action C and the maximum tensile action T in the two columns of the upright for the gravity and seismic load combination. It is hypothesized that only a first order analysis, the two force can be evaluated as:

$$C = \frac{4m \cdot g}{2} + \frac{F_b}{p} \boldsymbol{\phi}^T \cdot \boldsymbol{z}; \tag{7.5}$$

$$T = \frac{4m \cdot g}{2} - \frac{F_b}{p} \boldsymbol{\phi}^T \cdot \boldsymbol{z}, \tag{7.6}$$

where m is the mass at each deck, F_b is the lateral shear force, p is the width of the upright, $\boldsymbol{\phi}$ is the first mode shape computed using a modal analysis [142], and $\boldsymbol{z}$ is the vector that collects the absolute deck heights.
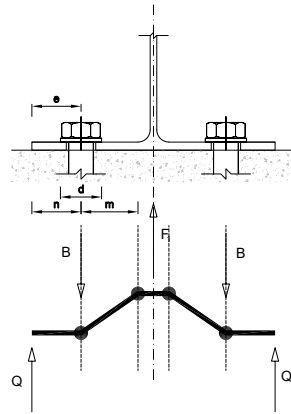
Figure 7.4: T-stub geometrical properties and *Mode-1* failure for a t-stub with short anchor bolts.

Once the *mode 1* failure is guaranteed, the yielding force of the T-stub is defined as:

$$F_1 = \frac{4M_{pl}}{m}; \tag{7.7}$$

$$M_{pl} = \frac{1}{4} \sum l_{eff} t^2 f_y / \gamma_{m0}. \tag{7.8}$$

The effective length l_{eff} can be evaluated according to EC3 (see Table 6.6). Reference can be made to bolts in end bolt-row, which corresponds to the commonest case with two bolts per row. For *mode 1* and for a *non-circular* pattern of yielding lines, the value can be computed as:

$$l_{eff} = 4m + 1.25e, \tag{7.9}$$

where m, and e correspond to the dimensions indicated in Figure 7.4.

The procedure described above has been used to design a base-plate connection node for an upright profile provided by NEDCON B.V. It was imposed a maximum load in compression corresponding to 130 kN, thus giving a maximum tensile force of 30 kN. The bolt arrangement has been decided according to the compressive load. The thickness of the plate t and the lever arm m have been defined to guarantee the selected maximum tensile force in the other upright.

7.2.1 Specimen

A base-plate connection for adjustable pallet racking systems was conceived to provide structures with energy-dissipation capacity. The behavior of this type of connection shares some of the main

features of T-stub mechanisms. mainly subjected to axial load, which is generally used to model the top and bottom Tee of beam-to-column connections; in such situations, the working principles are well-understood and the performance under cyclic loads have proven to be quite remarkable [79, 94, 119, 120] in terms of dissipated energy and ductile displacements. Figure 7.5 depicts the layout to perform the experimental testing campaign for the proposed specimen, which was preliminarily discussed in [154].

The base-plate connection was tested under monotonic and cyclic loads in the Laboratory of Steel Structures, NTUA (Athens, Greece). In Figure 7.5, the experimental setup is shown, where the testing machinery and the specimen are indicated. The static actuator has a stroke of ± 150 mm and can reach up to 300 kN; the accuracy of measuring equipment belongs to the first class of accuracy, thus giving an expected error on the measurement of ± 1.5 kN. Aiming at assessing the performance of the specimen when a vertical displacement is imposed, the degree of freedom activated by the actuator is along the axis of the column stub (vertical), and limited to positive direction. The piston is initially positioned in the middle of its stroke capabilities as such to guarantee reasonable clearance for the maximum imposed displacement. The motion feedback system that controls the force-positioning of the piston is a servo-hydraulic actuator made by MTS testing industries; the control point for the definition of the displacement is located on top of the load cell, monitored by a Temposonics (MTS sensor) magnetostrictive, linear-position sensor with a sampling rate of $2400 Hz$.
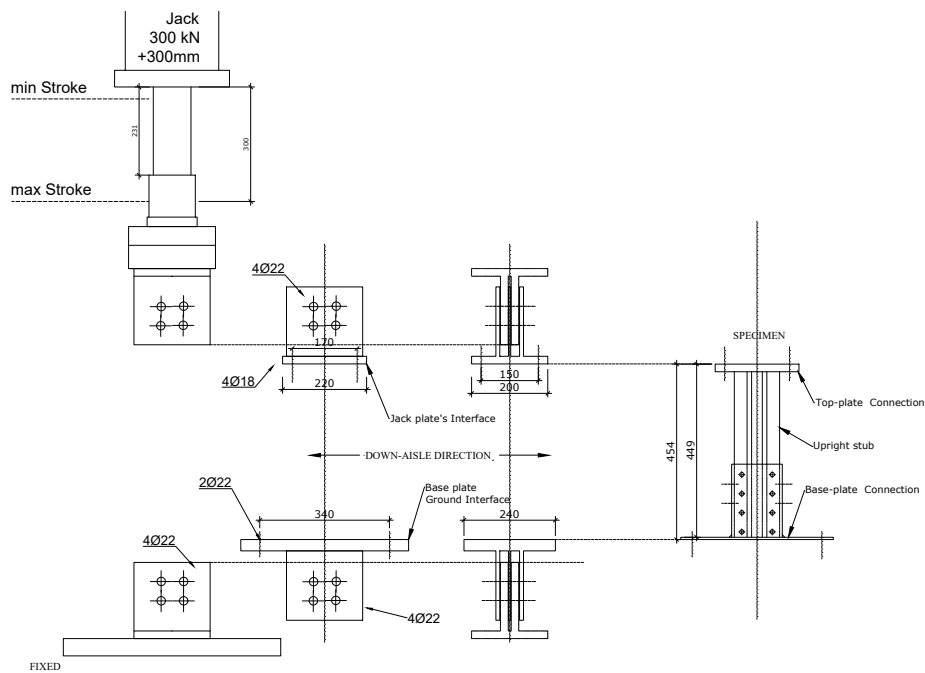
Figure 7.5: Schematic of the laboratory test setup (all dimensions in mm)

In the schematic proposed in Figure 7.5 the two interfaces that are necessary to connect the whole specimen into the testing machinery are identified as the jack plate and the base-plate ground interfaces. They were designed to provide negligible deformation when transferring the piston load onto the specimen. The specimen, which is schematically depicted in Figure 7.5 (right), comprises a 20mm-thick top-plate, welded to the upright stub profile, and connected to the piston mobile head using four M20 bolts made of 8.8 class high strength steel [137]. Note that the load cell is located between the piston head and the upper plate. Upright stubs were supplied by NEDCON B.V. (The Netherlands), with an overall depth of 120 mm and an overall width of 94 mm, and made of steel S350GD [150].

The specimen comprises two main parts: the horizontal surface virtually in contact with the
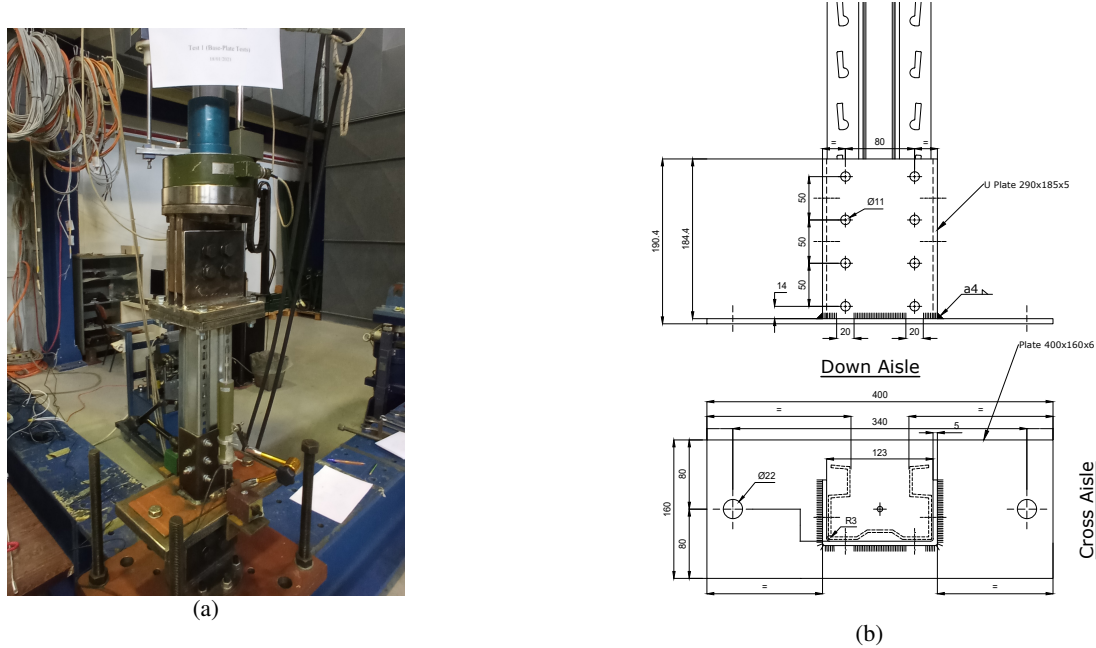
Figure 7.6: Perspective photographic view of the specimen mounted into the testing machinery (a). Lateral and top views of the base-plate connection (b) (all dimensions in mm).

concrete floor (plate 6 mm thick), and the bracket (plate 5 mm thick), which will host the holes that allow the finished piece to be connected to the upright column stub. The bracket is made out of one piece of steel 5 mm thick, which was bent to deliver its final shape. Young's modulus E (GPa) Yield stress $f_y = 235$ MPa Ultimate strength $f_u = 415$ MPa made of S235 ($f_y = 235$ MPa and $f_u = 415$ MPa) steel fastened through the flanges by means of two has been assembled by welding steel plates, is connected to the bracket by means of ten M8 bolts 8.8 class. The photographic image and the schematic view representing the test specimen are given in Figure 7.6. In order to guarantee an optimal stress distribution in the profile, the upright was cut 425 mm long ($\approx$ four times its depth).

7.2.2 Results

The monotonic test has been performed by applying a displacement time history from $0 - 42$ mm, with a constant velocity equal to $v = 0.015$ mm/s and a total elapsed time of 2800 s. The cyclic protocol has been defined in accordance with the AISC Seismic Provisions [133], which provides a test sequence given as a function of the peak deformation δ_y, with a decreasing number of cycles as the load step increases (Figure 7.7). The value δ_y that is used to build the loading path is determined from the monotonic test performed beforehand. A series of asymmetric lateral displacement cycles is imposed to the specimens, which resulted in vertical displacement equal to 0.375 (6), 0.50 (6), 0.75 (6), 1.0 (4), 1.5 (2), 2.0 (2), 2.5 (2), 3.0 (2), and 4.0% (2 cycles). The imposed loading displacement function is reported in Figure 7.7 by the black solid curve. As a matter of course, the load velocity is set to a reasonably low rate ($v = 0.100$ mm/s) to guarantee pseudo-static loading conditions. The specimens are instrumented with two linear variable displacement transducers (LVDTs) located on both sides of the base plate to measure the uplift displacement, monitoring the actual vertical displacement at the base plate.

The results of the tests are reported in Figure 7.8. The two tests show an overall good agreement in terms of overall behavior, providing good performance accounting for the cyclic consistency of the loops. The sampling frequency was set to 1 Hz, and the line that represents the force-displacement hysteretic behavior is obtained by averaging the response of the specimen repeated twice. By comparing the two curves reported in Figure 7.8, it can be noted that the specimen performance is hardly affected by the number of cycles when the displacement does not exceed
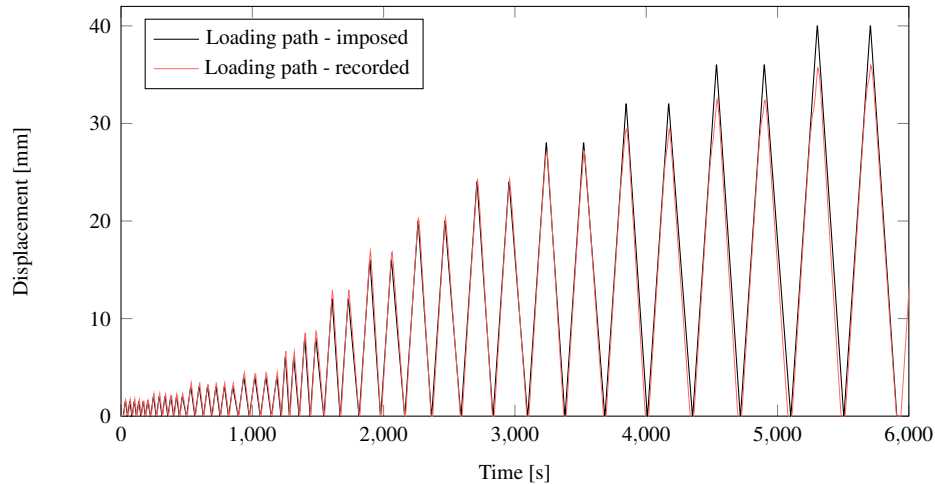
Figure 7.7: Cyclic loading protocol definition according to the AISC Seismic Provisions [133] (black line) and measured vertical displacement by LDVTs (red line).

20 mm. At this specific vertical displacement, the stiffness of the connection increases due to activation of the resistance of the plate flange in tension. Further cycles, in fact, start amassing damage on the contact surface between plate and bolts.
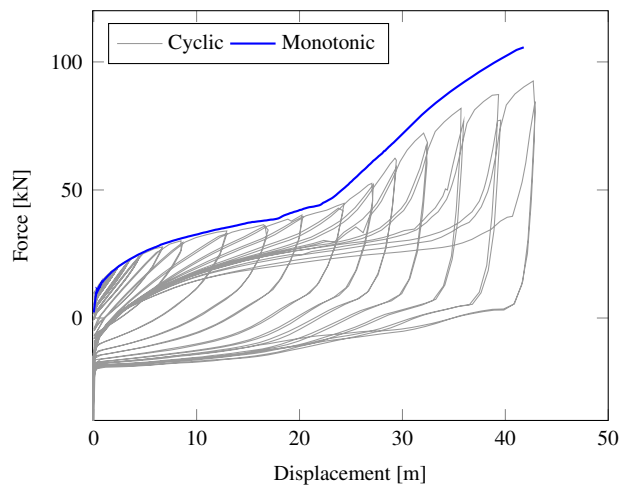
Figure 7.8: Experimental results of the monotonic and the cyclic tests.

The post-elastic performance of the tested specimen arises from the exploitation of the dissi-pative failure mechanism (Type 1 mechanism [132]), which is promoted by design, guaranteeing the strong-bolt weak-flange resistance relationship. It is characterized by the formation of a plastic hinge in the T-stub flanges, plus a circular pattern around the bolts' axis (ref. Figure 7.9). As it can be noticed, the shape of the cycles can be related to similar experimental results, in which the performance of T-stub connections was studied, accounting for energy dissipation capacity and stiffness degradation for the pinching of the hysteresis loops [79, 121].
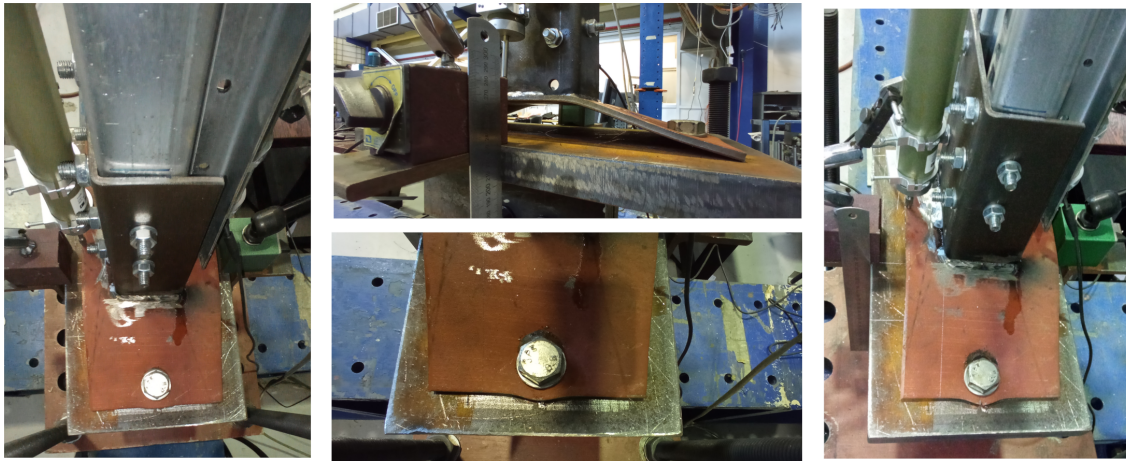
Figure 7.9: Photographic report of the specimen in the testing machine. Different instances of the monotonic test are framed, in which the displacement was around 30 mm.

8. Numerical modeling of base-plate connections

8.1 Base-plate connection

The performance of the proposed base-plate connection arrangement has been studied numerically considering a 2D framework. Figure 8.1 presents the two numerical model setups that have been designed following different tiers of detail, delivering different levels of accuracy and computational effort. Model $A1$ can be considered to perform high-fidelity simulations in a beam-based numerical model, allowing for detailing the base-plate connections and thus accounting for coupling effects that might occur during the simulations. On the other hand, Model $A2$ leverages aggregated information on the final behavior of the system being modeled; hence, the model is less flexible than the first one, but it is definitely lighter to be numerically solved.
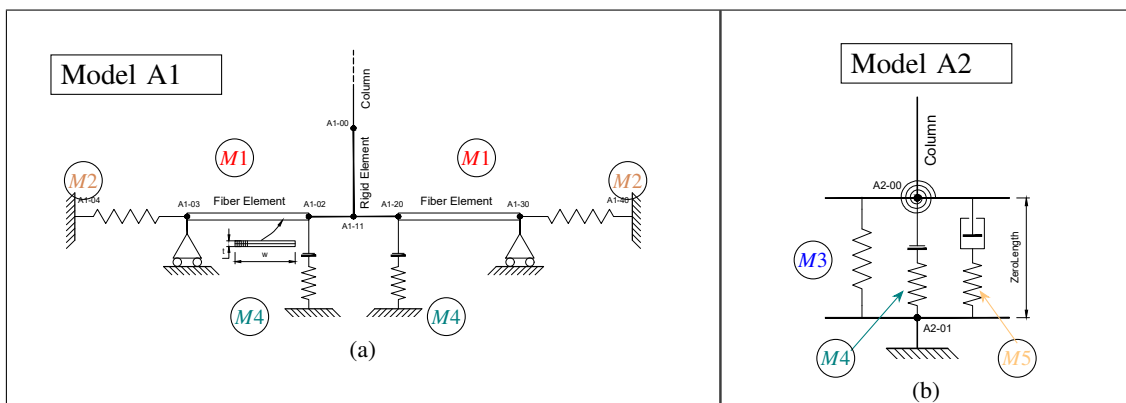
Figure 8.1: Proposed numerical model approaches for the base plate; (a) and (b) report a schematic representation of model $A1$ and model $A2$, respectively.

8.1.1 Model $A1$

Model $A1$ is a faithful geometric reproduction of the base-plate connection, in which the position of the nodes follow from the layout presented in Figure 7.6. To begin with, deformation along the height of the bracket is considered to be negligible as well as its in-plane deformation. As such, the bracket is modeled by a compound of *rigid elements* (nodes 00-11,11-02, and 11-20). The end

The picture reported above shows the designed base-plate connection under cyclic loading path test (Laboratory of Steel Structures, NTUA Athens, Greece).

nodes of these elements are connected to a *fiber element* that mimics the elastic-plastic behavior of the plate through using diffused plasticity; fiber elements shown in Figure 8.1(a) have a rectangular cross section defined such that:

$$h = t, \text{ and } w = l_{eff},\tag{8.1}$$

to which an elastic-plastic material is applied (that is, $M1$ in Figure 8.2). To model the bolts' effect on the dynamics of the base plate in tension, nodes 03 and 30 are constrained to have only the x DOF activated. At these very nodes, two extra links elements (one per each side) are connected, which simulate the contribution of the plate in bearing ($M2$), which is activated when the uplift of the base connection becomes relevant. Within the numerical framework, this mechanism is captured by using the P-Δ effects within the simulated framework, thus triggering a relative horizontal motion between the connected nodes.

The modeling of the connection is completed by the kinematic restrictions that are imposed by the plate-to-slab contacts. For introducing the unilateral nature of this restriction, a material with the capability of offering stiffness in one direction only, i.e., *NoTension material M*4, is assigned to a link vertically oriented. Two such elements connect nodes 02 and 20 to designated fixed positions, providing the base-plate with almost no deformation in compression. Note that the material $M4$ is applied with half the stiffness that is computed for charting Figure 8.4.
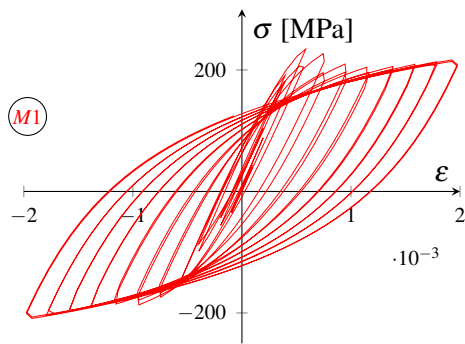
Figure 8.2: Steel04 material - plate material
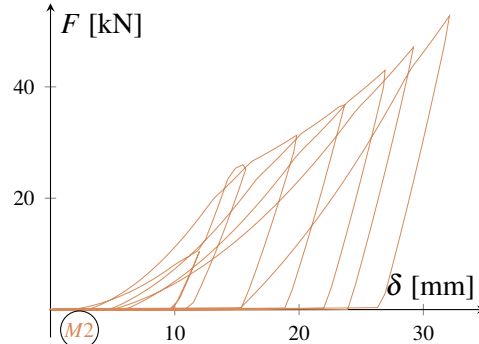
Figure 8.3: Hysteretic material - plate in bearing

The *uniaxialMaterial Steel4*[1] ($M1$ in Figure 8.2) is applied to each fiber of the plate cross sections, and is defined by using the outcome of a coupon test (Young's modulus $E = 203$ GPa; yield stress $f_y = 268$ MPa; and ultimate strength $f_u = 455$ MPa). The tensile resistance test was performed on a stripe of steel taken from one of the specimens that was afterwards tested. The material setup is completed by defining kinematic hardening according to the Menegotto-Pinto model [122] (as modified by [123]), with an hardening ratio $E_k/E_0 = 0.01$, and using the recommended parameters to provide smooth transitions and multiple slopes. The ultimate parameters are defined by setting the ultimate strength (f_u), and controlling the exponential transition with a radius $R_u = 5$. The constitutive model $\sigma - \varepsilon$ is reported in Figure 8.2 - (Steel 04 - plate material).

The bearing mechanisms that develops when the plate holes come in contact with the bolts is modeled by considering a bilinear Hysteretic material[2], the relationship of which is characterized three points on the F-δ curve. Due to the bolt-plate clearance, the first point, $F_1 - \delta_1$, is given as (0,0). The second point, $F_2 - \delta_2$, is defined as the threshold that activates bearing:

$$F_2 = f_y dt, \quad \text{and} \quad \delta_2 = f_y/E_s.\tag{8.2}$$

The third point needed to complete this material's setup is given by considering the ultimate resistance of the bearing mechanism as [124]:

$$F_3 = 1.5 f_u dt, \quad \text{and} \quad \delta_3 = 4\delta_2.\tag{8.3}$$

---

[1]Steel4_Material
[2]Hysteretic_Material

The resulting relationship is reported in Figure 8.3 ($M2$). Note that the negative part of the F-δ curve is defined such that the mechanism resistance becomes irrelevant when the cycle inverts; this is accomplished by introducing the negative parameters reduced by $1/200$.

The elastic modulus of the NoTension material[3] $M3$ is defined considering the stiffness of concrete slab in contact with the base plate. Following the approach shown in EN 15512, Young's modulus of the concrete is chosen as $E_s/10$. The $F - \delta$ curve of the material is shown in Fig. 8.4. The proposed definition is convenient because it is useful to considering the mono-lateral nature of the concrete-slab interactions, where the use of computationally expensive contact materials.
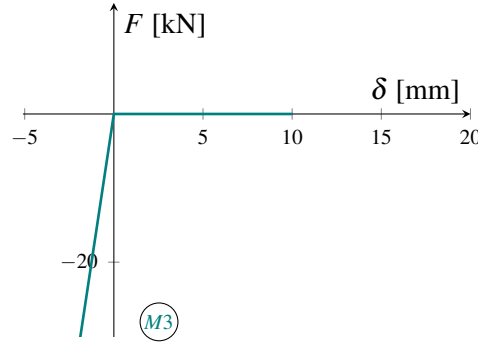
Figure 8.4: No Tension material - plate-concrete contact

8.1.2 Model $A2$

Model $A2$ deals with a pure mechanical representation of the base-plate connection behavior. Its schematic is given in Figure 8.1(b), from which can be seen that the model comprises three zero-length links working in parallel, and only two nodes. The mechanical properties of these links are defined in Figure 8.5, Figure 8.4, and Figure 8.6 (i.e., $M3$, $M4$, and $M5$). Differently from the previous model, a gap material ($M5$) is here used to take into account the increased stiffness and resistance that occurs for big vertical displacements. The column joins into the upper node 00, through an elastic hinge that accounts for the bending moment transmission due to the bolted connection. Its rotational stiffness is determined according to the procedure proposed in EC3. Note that the rotational spring here reported will have no effects on the following validation test, but it is defined for its use into the simulations performed in Section 8.2. Note that $M3$ that is used for Model $A2$ is consistent with the definitions given above, but for the values of stiffness that is doubled.

The hysteretic material $M4$ describes the behavior of the plate during the first phases of the test, when the plate bearing mechanism is not activated yet. By considering that the plate behaves like a double-clamped beam, the first point to form the $F - \delta$ relationship is given by:

$$\delta_1 = 1/3 f_y b^2/(E_s t), \qquad \text{and} \qquad F_1 = \delta_1 E_s t^3 L_{eff} f_y dt/b^3. \tag{8.4}$$

The second point is defined in accordance with the formulation proposed in [125], that is:

$$F_2 = \frac{(2 - \phi_0/L_{eff})L_{eff} f_y t^2}{(2b)}, \qquad \text{and} \qquad \delta_2 = \frac{F_2 b^3}{(E_s L_{eff} t^3)}, \tag{8.5}$$

where $b = m - \phi_0/2$. Note that the stiffness of the T-stub flange in bending is derived using the analytical model originally proposed in EC3. The final point for this model is obtained by considering that there is a hardening ratio of 0.14, yielding a force of:

$$F_3 = 1.84 F_2, \qquad \text{when} \qquad \delta_3 = 7\delta_2. \tag{8.6}$$
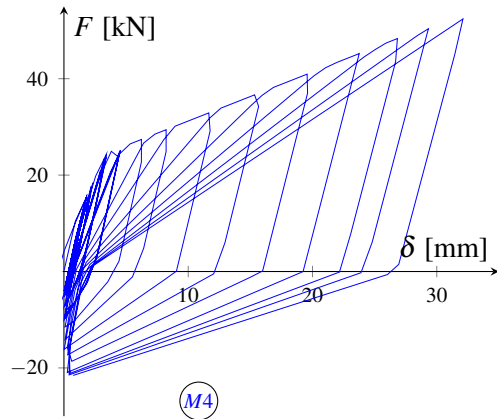
Figure 8.5: Hysteretic material - base-plate connection.
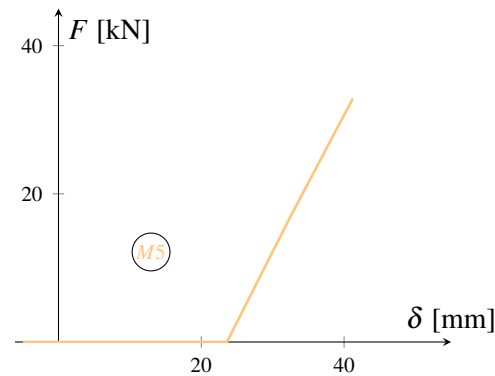
Figure 8.6: Gap material - plate in tension.

The Gap material $M5$, which accounts for the contribution of the plate when engaged in tension, is activated by the threshold *gap* given by the parameter δ_3 of $M4$. Due to its elastic nature, the material is further completed by an elastic modulus and an elastic threshold, both of which are identified in $M2$. The $F - \delta$ curve of the material is shown in Figure 8.6, which comprises the initial gap that accounts for the initial displacement needed to reduce the bolt-hole clearance, thus activating the plate tension resistance.

8.1.3 Validation

The two proposed numerical models that are proposed to reproduce the response of the base-plate connection designed in section 7.2 are validated in the following contrasting with the experimental data given in 7.2.1. The OpenSEES framework is used for such validation, as the various elements that compose each configuration were defined using description from the specific OpenSEES library. Nevertheless, the procedural description that provides the parameters estimation allows using other commercial software for the same purpose.

Figure 8.7 reports on the validation of the two models beforehand introduced under cyclic test. The response of the models is contrasted against the experimental data that refers to the cyclic loading protocol in Figure 7.7. Both models yield good agreement, capturing the main characteristics of the reference behavior. Model $A1$ offers a smoother shape in comparison with Model $A2$, due to the presence of the *steel04* material, which allows seamless transitions from linear to non-linear phases. In contrast, $A2$ combines a simpler relationship for the definition of the linear transition; in terms of energy per cycle, Model $A1$ shows better performance during the time evolution, in spite of exhibiting similar overall dissipation. Owing to sharing the same elements that provide compressive stiffness for mimicking the plate-to-slab contact, the two models show similar features. Note that the real loading protocol that is used for the validation is slightly different from its pure definition, andone shown in Figure 7.7.

The comparisons proposed Figure 8.7 uses the numerical prediction that is provided by the open-source OpenSEES software [111] (version 3.2.2 64-bit running on Windows system). The code is set up to statistically solve imposed displacements in the same fashion of the experimental, by following a static procedure to predict the response of the model. By and large, this is an implicit assumption that comes directly from the way tests are performed to deliver specimen behavior void of any dynamic effects. The peak displacements defined by the protol are imposed to the upper node 00 by means of smaller increments given as a function of each peak displacement: this configures a displacement-controlled algorithm for which a Newton solver is used.

---

[3]Elastic-No_Tension_Material
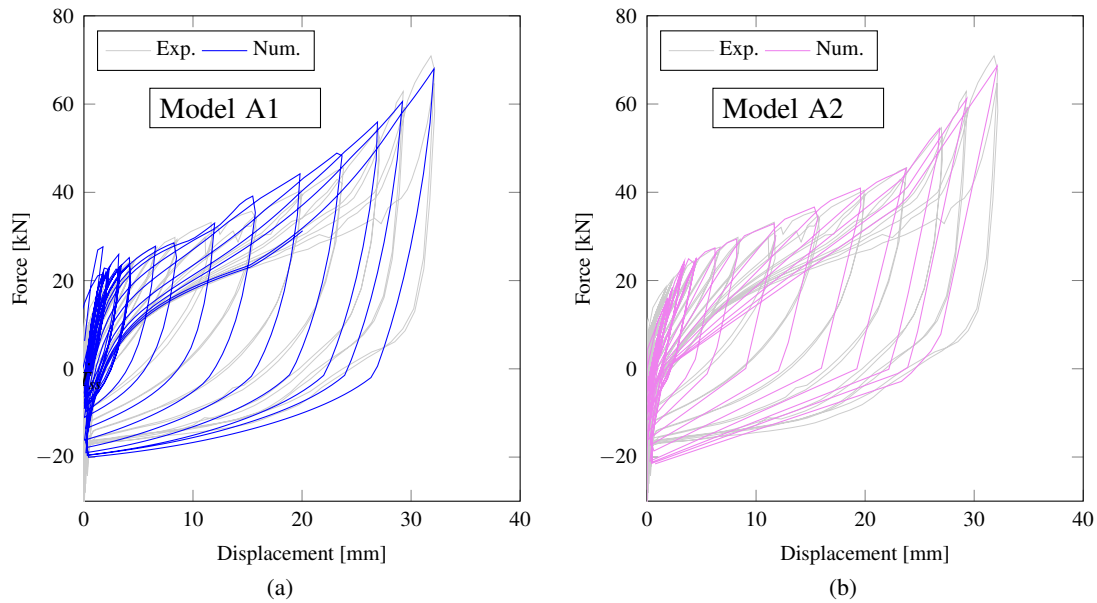
Figure 8.7: Comparison between tested moment-rotation hysteretic curves of connection A1 (a) and A2 (b).

8.2 Numerical investigation

8.2.1 Structure Modeling

The same software version defined above is used to model the structure response: a 2D concentrated plasticity model of the rack shown in Figure 8.8 is constructed using the validated setup that has been presented in section 6.1 and published in [2].

The structure members are reproduced considering columns as *ForceBeamColumn2d* elements (blue elements in Figure 8.8, with cross-section properties given by fibre-section model. The code computes the mechanical properties starting from the assigned geometries, which correspond to those described in Table 7.2, for which approximated outer shape layouts are given in Figure 8.8 to avoid disclosing sensitive information. The braces are simulated by composing nonlinear beam-column elements (red elements in Figure 8.8) that are pinned to the point where the one-bolt connections occur. As it is shown in Figure 8.8, a bow-type imperfection model is used to geometrically include an initial deflection of $L/150$; the internal five nodes are placed at interval and following a sinusoidal shape. The two rotational springs connect the two end-nodes to the upright frame, to which a relatively low rotational stiffness is applied. Pallet mass is reproduced by lumping the total mass at each deck to the center of mass of each block. This last detail is implemented, as well in accordance with the layout described in EN 16681, to correctly achieve the fundamental frequencies of vibration. An auxiliary system of relatively stiff trusses (green elements in Figure 8.8) is used to link these last nodes to the uprights, as is shown in Figure 8.8.

The boundary conditions differ within the two approaches to model the base plate. Being the model included in a 2D framework, the out of plane behavior DOFs are already frozen, and the motion restrictions offered by the base connection shown in Figure 8.1 are sufficient to ensure a well-defined global stiffness matrix. Once the super-structure has been modeled and joined to the base connections, the two possible configurations give rise to two fundamental periods, computed by means of an eigenvalue analysis [142]. When Model $A1$ is used, the first period of vibration (T_1) corresponds to 0.85 s, whereas for Model $A2$, 0.83 s is obtained. In both models, the first mode of vibration mobilizes almost the same equivalent mass, around 83%. The eigenvalue analysis, the results of which are reported in Figure 7.3, for the pinned model outputs $T_{1.pinned} = 0.81$ s, yet smaller than the ones produced by the analyses performed for this model.
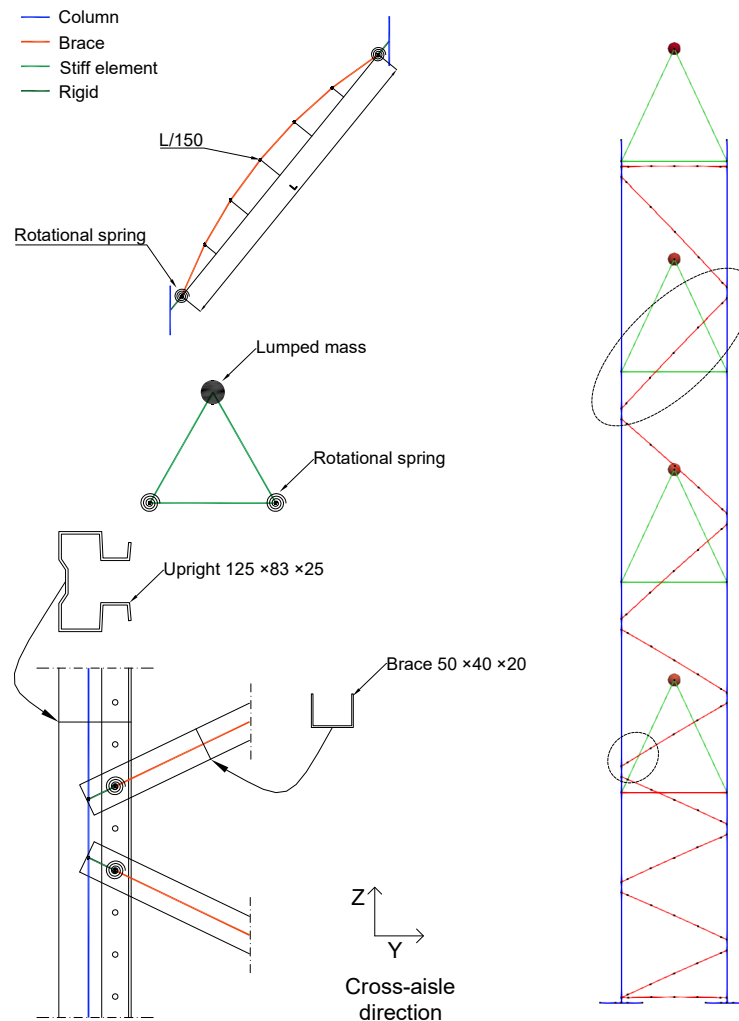
Figure 8.8: Numerical model for the upright frame used for nonlinear dynamic analyses including dissipative base-plate connections.

The slightly changed, increased, periods of vibration obtained when base plates are modeled could be due to weaker connections, which provoke longer oscillation periods when the structure is fully elastic. Nevertheless, being the reported discrepancies lower than a few percent and consistent with expectations, the model can be utilized to quantify the gain, if any, offered by the proposed connections.

8.2.2 Dynamic model

Transient non-linear dynamic analysis are performed by employing the implicit Hilber-Hughes-Taylor (HHT) time integrator with an α coefficient equal to -0.05 [115] and a timestep equal to $dt = 0.01$ s. The numerical damping is necessary to cancel out the spurious effects of higher modes of vibration, which may affect the structural response in terms of accelerations, while preserving second order accuracy. To account for global geometric nonlinearity effects, the P-Δ formulation is used for all beam-column elements, including the subsets of elements that are used to simulate the

loss of stiffness in the brace in compression. A linear formulation, instead, describes the geometric transformation of the stiff elements that locate the masses in the right positions. As a result of the introduced geometric nonlinearity, convergence of the displacement vector is achieved using a Newton-Krylov method, which is notoriously much faster than the modified Newton algorithm.

Some information on the computational cost of solving the full system can be relevant for providing a global picture on the applicability of the proposed procedure for evaluating the performance of upright frames using time-integrated analysis method. The four load-level structure requires an assembly of 149 nodes (447 DOFs) and 117 beam elements. When the numerical model comprises either a pinned-type base connection or a model such as Model $A2$ to implement the base footing system, elements and nodes quantitatively stay the same, whereas the implementation of Model $A1$ requires to introduce 22 more nodes and 6 more elements. The increase in the size of the system to be solved does not heavily affect the simulation runtime, since the system matrix size remains within the cache size of the CPU system. Nevertheless, the computational time does increase due to use of fiber elements with elastic-plastic material, which causes an increase in the number of iterations for each timestep to achieve convergence.

8.2.3 Ground motion selection

For the objective of the following analyses is to investigate the seismic performance of cross-aisle upright frame with the conceived base-connections, nonlinear dynamic analyses appear to be the most suitable tool. Particularly, presented in [118], Incremental Dynamic analyses (IDAs) consist in defining a parametric seismic demand that is therefore used to calibrate the intensity of the accelerogram(s) (or ground displacement(s)) that imitates the seismic threat and it is able to statistically represent the chosen area.

An automated procedure for record selection has been purposely implemented into the MatLab computer code [167] and it has been distributed as open-source software under an LGPL license. The repository that contains the computer program (Pseudocode 1), and a database of seismic events, is available at the following link GitHub:makeItCompatible. The database was built using processed acceleration series [152] downloaded from the Italian Strong Motion Network (RAN) ITACA 3.2 website [168]; 167 events with moment magnitude, M_W, higher than 5.0 were selected, giving 8529 records from 2843 stations.

Algorithm 1: Pseudocode for the selection procedure for the definition of the ground motion suits.

Data: *Target Spectrum* (S_{EC8}), *Soil*, R_{min}, M_W, *Duration*, *Direction*;
for ($e = 1$: *each earthquake* $\in$ *Database*)
    Data: *Accelerogram data*;
    0 check *Data compatibility*;
    1 initialize $RSS = \infty$ (logical assignment);
    2 initialize $S_e = Spectrum(e)$;
    do
        3 define RSS (residual sum of squares) as:

$$RSS = \sum_{i=1}^{n} (S_{EC8.i} - k \cdot S_{e.i})^2; \tag{8.7}$$

        4 minimize Eq. (8.7) operating on k;
    Result: *Spectrum(e)*
    while $RSS > tol$;
end

The main structure of the code is described in Pseudocode 1, including only the fundamental features that are of interest for its use with the given database; nevertheless, the reader can find other scripts in the same folder to create a structured database from any other suite of accelerograms. First, it is important to highlight that ITACA provides ground motions along width their spectrum already compiled; regardless, for the given target spectrum is defined with damping ratio of 3%, and being the predefined ones defined at 5%, for each of the 8529 series, the acceleration time series were reprocessed, and included in the archive available in the repository. The first phase of the selection procedure foresees the definition of input data for narrowing the range of admitted records. When looping over the spectrum database (S_e), and when the earthquake record is compatible with the given properties, a fitting test is defined in Eq. (8.7) by using the residual sum of squares (*RSS*) between the target and the analyzed spectrum (step 3 in algorithm 1). The *RSS* definition contains a scaling factor, *k*, that functions as an automated tuned parameter, allowing to set a Newton's algorithm to minimize it. Finally, the *while-do* loop is broken either when the *RSS* magnitude is less than a certain tolerance (*tol* in algorithm 1), or when the algorithm stagnates over the same scaling factor for a few cycles.
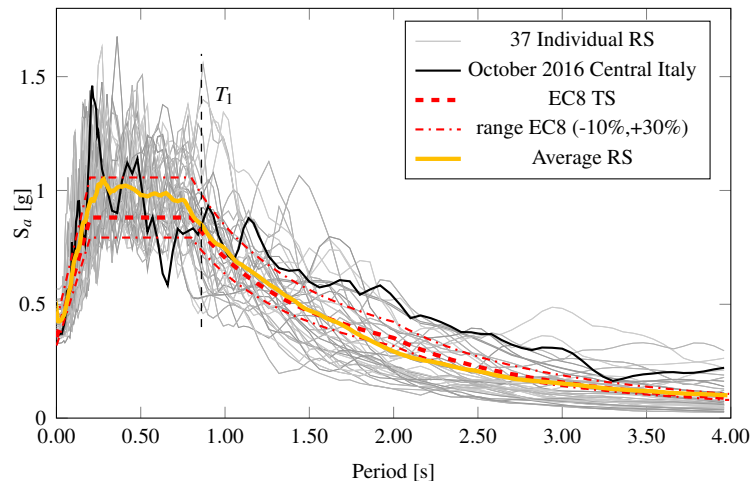
Figure 8.9: Seismic demand definition for the incremental dynamic analyses. The chart reports: the target elastic target spectrum (EC8 TS); the accepted range for spectral compatibility (range EC8); the average elastic response spectrum; and the raw elastic response spectra (gray lines + 1 black line), which are selected through the proposed software.

A suite of 38 natural records is obtained for performing response history analyses. The main constraints imposed on the code are, apart from the EC8 spectrum and a tolerance of 0.15 (compatible with the definition of compatibility in EC8), focal distance $R_{min} < 50$ km, and, of course, all directions but *Z*. The set is selected to be consistent with hazard at an intensity level corresponding to a 10% exceedance probability over the nominal life of 30 years in high-seismicity European sites. Namely, the elastic spectrum defined in Figure 7.2 is the target reference shape for the selection of spectrum-compatible events. Figure 8.9 shows the scaled spectra, and the average line for all the 38 ones, which is well confined within the red dashed lines reporting the admitted EC8 range. The fundamental vibration period of the frame is reported, and can be used as a reference to check the spectral dispersion across this part of the mean spectrum.

8.2.4 A Simulation result analysis

Following the earthquake suite identification, a first numerical simulation is performed to appreciate the dynamic behavior of the upright frame in detail, and to clarify the contribution of different connections to the overall system response. The ground motion representation for this test case is chosen from the suite presented in Figure 8.9; its spectrum is given in solid black line and it was

recorded during the seismic event on the 26th October, Central Italy Earthquake (Visso in Macerata province, $M_W = 6.10$)[4]; an in-depth description of the seismic sequence that struck Central Italy in 2016, with two main shocks 3 months apart, is given in [126]. This event record has been selected from two main reasons: its scaled spectrum matches the seismic demand defined by EC8 with a small *RSS*; and its acceleration time history, shown in Figure 8.10(a), can be easily split into two sub-portions, each of which clearly carries a specific dominant frequency. Figure 8.10(a), in fact, provides two spectrum comparisons which correspond to the adjacent boxed time windows: the black line represents the FT of the whole signal (duration 180 s), whereas each gray line refers to the boxed portion of signal. The two comparisons highlight what the reader might notice at a glance: the first part has a much more high-frequency energy content, provided by the much faster P-waves (pressure) and some of the PP-waves seems to be present at the end of it. The second part, the much wider oscillations exhibited by the main peaks suggest that they result from S-waves (shear) propagation.

The data used for the discussion in this section corresponds to the results of one time-domain analysis performed with an input acceleration factor to provide 0.080 m as maximum displacement for the pinned configuration. This procedure follows from considering the maximum demand at the PGA, and this may be important for understanding some of the features of the proposed charts in Figure 8.10. It additionally reports two more panels that show the upright frame time evolution model response in terms of top displacement (b) and axial upright force in the most stressed cross section (c), respectively. Each colored line in the two panels correspond to a different base-plate connection model, as indicated in the companion legend. Note that the frame that makes use of the *Pinned* connection comprises a rotational hinge with small rotational stiffness and two DOFs suppression in the *x* and *z* direction, respectively. Due to the close agreement between the responses of the frame with Models *A*1 and *A*2, in the following only *A*1 is described.

The displacement and force time evolution reveals that the response of the frame to the seismic loads does change significantly when the base connection has non-linear behavior as the one provided by the proposed one. During the first parts of the simulations, the models show similar responses since the features of the plate are not activated yet. However, when the ground motion is strong enough, the activation of the yielding lines into the plate causes the lateral stiffness of the system to drop as demonstrated by the increase in lateral displacements. Likewise, the maximum axial force in the lowermost stub remains limited in both minima and maxima that it assumes throughout. Maximum values (tension) rarely exceed the F_U threshold that indicates the yielding load in tension of the base plate; compression forces are limited too, with peaks around 100 kN.

Both charts (b) and (c) show that the frame response is greatly affected by the record frequency energy content as defined and classified in (a): the first boxed signal, with high-frequency energy content, induces comparable displacement, whereas axial forces are much higher for the pinned configuration. Particularly, the red and the blue lines give a close understanding of the system response period, showing longer periods of vibrations for the frame equipped with Model *A*1, in contrast with the period of the pinned frame; the ground motion here is able to transmit much more energy in the pinned structure due to its fundamental period that, as shown before, is close to 0.80 s. The much longer period (around 1.30 s) that the rack has when the base yields allows it to escape much of the energy which is filtered out to a great extent. This mirrors, however, into an increased displacement demand. Conversely, the pinned system is less stressed by the seismic conditions provoked by the second part of the accelerogram: the top displacement is smoother in comparison, and the displacement amplitude is smaller. Axial forces are greatly reduced too but still higher than the one experienced by the configuration *A*1, which instead is greatly challenged by the frequency content that characterizes this part of the ground motion.

Figure 8.11 depicts the geometric layout of the upright frame in two instances of the simulation and for the three considered base configurations. Left and right panel elements coloring indicates

---

[4]ITACA database event ID: EMSC-20161026_0000095
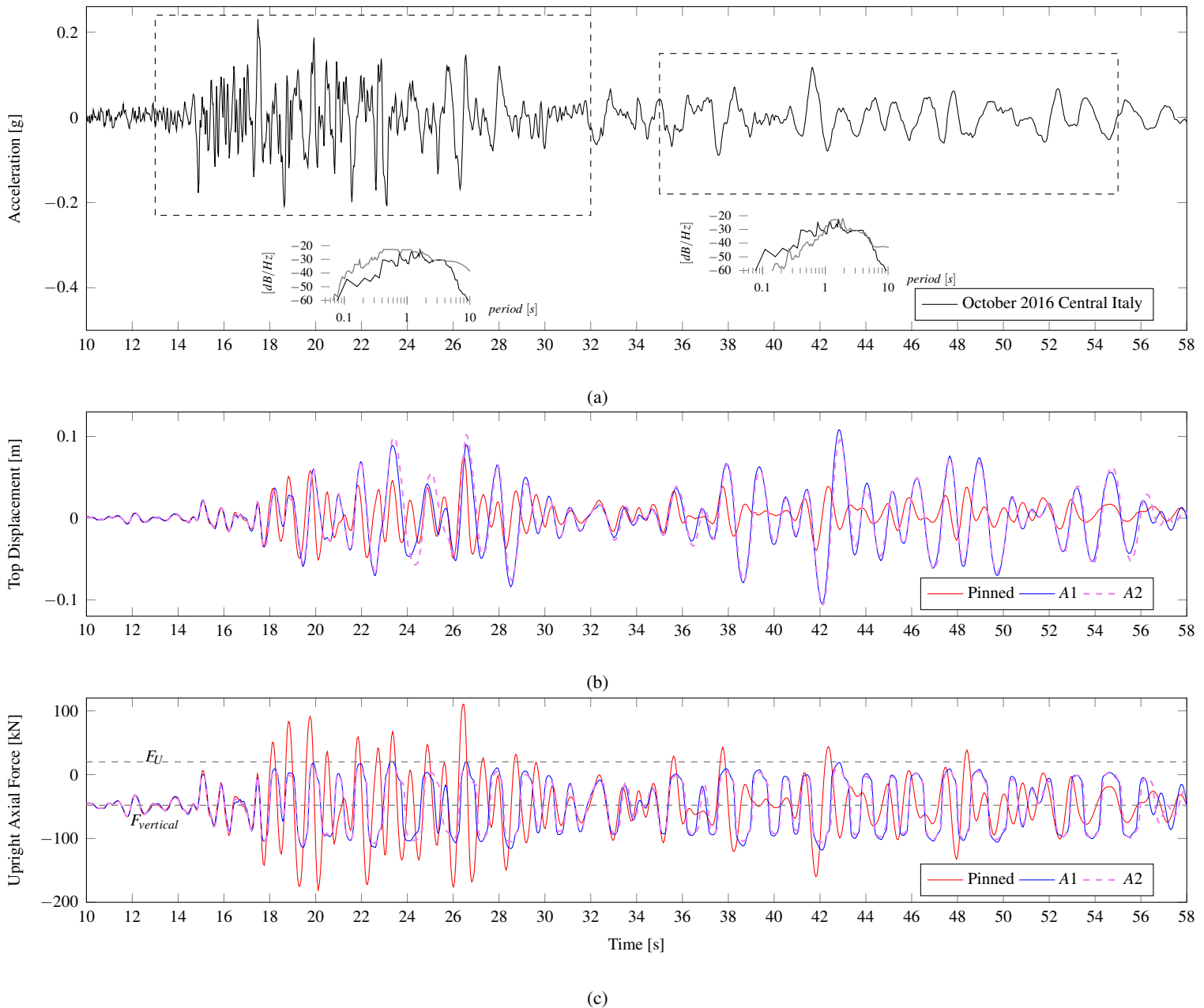
Figure 8.10: Acceleration record for October 2016 Central Italy event (station Castelnuovo di Assisi - CSA); the dashed lines box the time windows used for the local spectral analyses shown immediately below them (a). Displacement (b) and force (c) time evolution numerical model response for difference base-plate connection models.

the axial force and the bending moment, respectively. The timeframe is chosen to provide insights on the way the internal stress components diffuse into the beam elements. The first row shows the structure positions at 20.10 s, when the frame response peaks for the pinned configuration, whereas the second, the positions at 42.20 s, when the frame lateral displacement of $A1$ does. The four panels conclude that using the proposed base-plate connections is extremely beneficial not only in terms of reducing the force amplitude, but also provides better bending moment distribution.
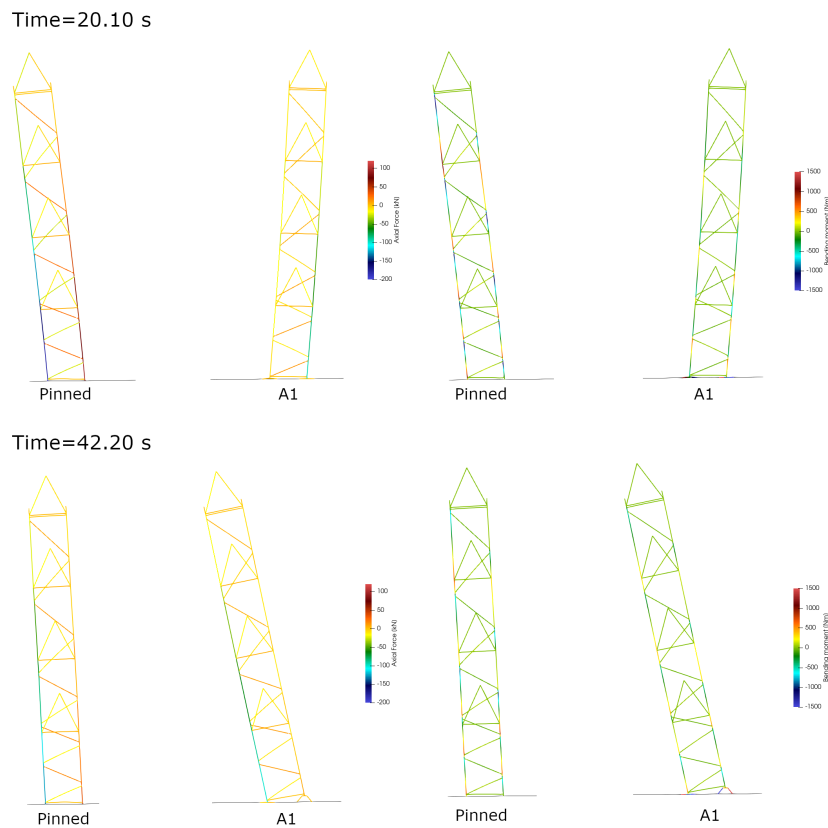
Figure 8.11: Screenshots of the numerical model taken during two instants of the simulation. The three upright frames in each panel differ for the base plate connections, as indicated below each panel. The coloring of the first column indicates the axial force, whereas the coloring of the second, indicates the bending moment (node positions are magnified by a factor of 20).

8.2.5 Incremental dynamic analysis

Figure 8.12 reports the results of the analyses performed on the upright frame with two base-plate connection models and the data is organized in terms of IDA curves. As a result of the previous analysis, only the *pinned* and the *A*1 model will be considered for the following investigation. A fundamental step for performing IDAs comprises the computation of an increment vector that provides the scaling factors that define the seismic intensity for each time history. The process starts with a target displacement vector $\Delta = [0,\ 0.005,\ 0.01 : 0.010 : 0.100]$ m, therefore transformed into acceleration scaling factors using three baseline simulations at three imposed maximum displacements, namely 0.01, 0.05, and 0.12 m. Said scaling factors for these three displacements are computed using an iterative procedure that corrects the applied scaling factor according to the system response until a satisfactory agreement is achieved between two consecutive scaling factors. From the definition of Δ it comes that 103 multipliers are used, for a grand total of 3 914 nonlinear dynamic analyses. The simulations are carried out on a computer with a Intel(R) Core(TM) i9-10900K CPU (operating at 4.9 GHz), 64 GB of RAM, sped-up by running each IDA in three batches of 32 parallel virtual processors.

Post-processing data is used to build the IDA curves shown in Figure 8.12. The selected intensity measure (IM) is the PGA and it is reported on the y-axis of the chart. PGA has demonstrated to be the best choice when structure systems that may dynamically involve state-dependent modes of vibration in the seismic process. The *Axial load*) in the upright columns is now intended as engineering demand parameters (EDPs), particularly, throughout each record minimum and maximum values are evaluated. They hence are arranged to form curves depicting raw data (light
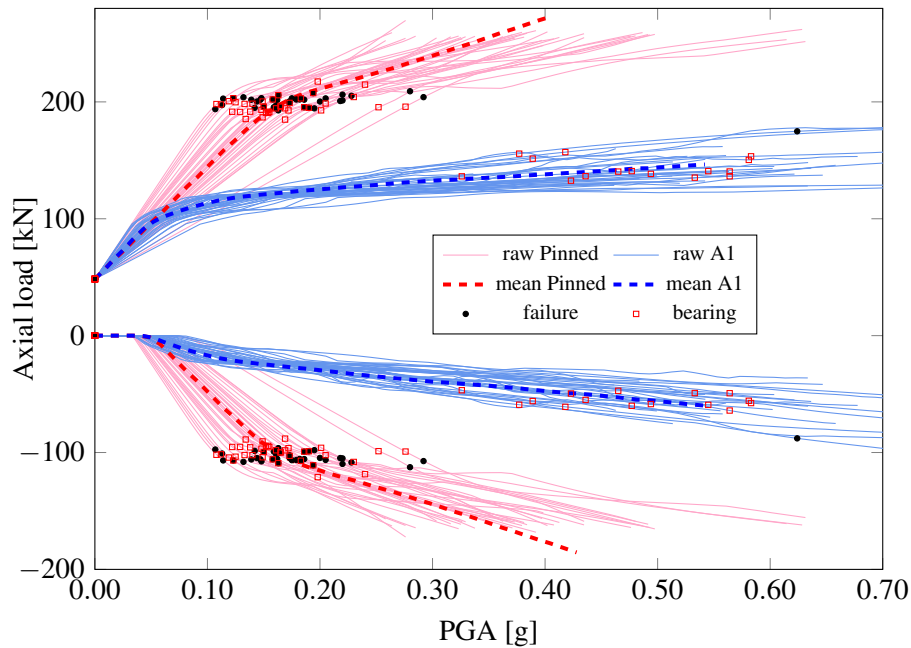
Figure 8.12: IDA functions for the minimum (tension) and maximum (compression) axial load read into the upright elements, for the 38 accelerograms in the defined set. For each IDA line, the failure point may be reported by a filled dot, and the bearing activation point in the brace-upright connections as well (empty square).

colored curves) for the two examined structures (i.e., *pinned* and *A*1); mean lines are also drawn for the four uniform sets of data. In addition, for each IDA the failure point may be reported (filled dots ●), which is evaluated performing resistance and stability checks as indicated in [134], and the bearing activation point in the brace to upright connections (empty square □).

The results of the incremental analyses presented in Figure 8.12 show that the structure can bear much more intense seismic events when yielding connections are utilized. For PGA<0.08 g, the two systems yield similar performance due to substantial agreement in the static schemes since the gravity loads are still sufficient to engage both uprights in compression. For increased values of PGAs, the response of the *pinned* system is closely linear, for both axial components, and it remains so until the bearing resisting mechanism in the brace-upright connections is activated. However, as it is clear from the chart, the frame fails almost for all the 38 accelerograms when the compression load is about 200 kN. The upright frame equipped with pinned footings fails at mean PGA of 0.19 g. When, instead, the response of the upright frame equipped with base-plate connections is analyzed, it can be concluded that once plate yielding lines form, the axial load reveals a much smaller increase rate and overall the structure can withstand greater PGAs.

8.3 Discussion

The proposed base-plate connection has proved useful for structures designed in seismic zones for which seismic acceleration can be identified as medium intensity. The increase in performance for the case presented has been obtained by following an analytical procedure that uses as a starting point a predefined rack configuration designed for a seismic zone of given intensity. For vertical cross-aisle frames, the location of the plastic deformation at the base level appears to be fairly obvious and for this reason many researchers have provided useful configurations to carry this concept forward. The proposed base connection design procedure can be applied for the design of different seismic conditions and vertical frame configurations.

IV Conclusions

9. Conclusions

9.1 Summary

The major seismic codes used for the rack design, EN16618 and FEMA460, provide recommendations to increase the seismic safety of rack structures but, unfortunately, do not give any provision about the use of isolation systems, which could increase their use if it were codified. If overturning of stored goods is of concern, there are only two ways reported for the improvement of the safety of racks in seismic zones: *rack netting* and *structural strengthening*. The rack netting is a steel netting installed on all sides of the rack, covering the bay openings from top to bottom. Though effective, the method is also very impractical for several reasons. As regards the latter provision, it can be noted that it allows structures to meet code requirements but increases the lateral stiffness and, at the same time, adding rigidity and introducing higher accelerations throughout the system. The product shedding prevention must be always considered in the design process, being the total cost of stored goods generally much higher than the cost of the structural components. According to the expected seismic intensity, *dissipative devices* and *seismic isolation* seem to be very useful and effective solutions.

Seismic isolation strategies are undoubtedly effective in reducing the seismic risk for civil and industrial structures, and the purpose of the reviewed applications in this work is to highlight it. An application of a *standardly* designed isolation system to a high rack structure is taken as an example, in which the rack was treated on a par with a classical building. Regarding the seismic isolation of selective storage pallet racks, the RIGID-U-RAK system (Pellegrino®) and the FIP MEC System (IsolGOODS®) can bring many advantages, such as the reduction of accelerations along the cross-aisle direction, the reduction of the inter-storey drifts and the prevention of the overturning of the stored goods. Another important aspect is related to the energy dissipation during earthquakes. In fact, normally the energy dissipation is concentrated only on the beam-column joints that are subjected to great damage during the earthquake. The use of dissipative devices or base isolation systems increases the energy dissipation reducing the plastic rotation in the joints and consequently the structural damage, guaranteeing a safe in-service use also after the seismic events.

The novel IsolGOODS® isolator has been presented and its performance investigated for the first time. The physical testing campaign is preliminarily used for validation through the shaking table test results, which has allowed to validate a numerical model dynamically. The validation outcomes showed that the open-source-code-based model can reproduce the physics with sufficient degree of accuracy. IDAs are performed considering the same records used physically but with increased intensities and by monitoring several EDPs. The results show that the isolation system alleviates

much of the superstructure workload: both internal forces and deck accelerations are always below the maximum values that the members can sustain. On the other hand, the failure mechanism takes place at isolator level, where the maximum displacement is exceeded. As expected, the structure performance tracks quite closely with the elastic response spectra, and indeed, the system records failure at $PGA = 0.57$ g, on average. For real applications, the displacement capacity as well as the friction coefficient of the isolation system can be tuned to the specific earthquake demand.

In spite of their uncommon features, isolation systems and purposely provided devices to a code-compliant structure, whose seismic response is modified by them, have to comply with the body of laws in the Country where the structure is erected. For instance, throughout the European countries, the seismic devices are built and installed in accordance with the European Standard on *Anti-seismic devices* [143], which identifies functionalities, design rules and conformity requirements for the devices to be used: IsolGOODS® is such one device.

Finally, the use of energy dissipating devices is discussed. As the applications examined suggest, the use of special dissipative devices capable of dynamically altering the response of the system represents an effective and economical solution to improve the seismic resilience of the racks both in the transverse direction and in the longitudinal one. As such, the routine use of moment resisting frames as lateral resisting systems for buildings has translated well into accounting for the behavior of aisle frames; regarding the cross aisle, this work explores the performance of a T-stub-based-link that can be used for pallet racking systems, with the aim of increasing the energy dissipation capacity of upright frames. The proposed concept for devising new base-plate connections has been shown to perform similarly to standard T-stubs, which are widely used to model the overall 3D behavior of beam-to-column connections of steel structures. This type of connection can be used for the construction of new strong lateral structures, as well as for the retrofit of existing ones, where lateral loads are a problem.

9.2 Outlook

This thesis work provides two important legacies for future investigations.

The fact that seismic isolation system can be used to enhance the performance of racks when operated in seismic zone with demand that can be defined as to be from moderate to high implies that further research would be necessary to establish simplified procedure for the design of the isolation systems, and to precisely pinpoint the various pros and cons of using such hardware for special structures. The advantage of curved surface sliders over rubber bearings stands clear in their capability of releasing the isolation period from the system mass, which has a high dispersion in case of pallet racks, but, more generally, for storage systems. Researchers are nowadays studying and trying to develop innovative and more efficient devices for racks. However, the main conclusion that this work provides is that seismic isolation technique is effective if *skilfully designed*.

In this work a limited number of structural tests and configurations have been considered, and the numerical procedure for evaluating the variation in performance of a rack system equipped with special anti-seismic devices, albeit expensive in terms of computational costs, is described in a detailed way, and taken to completion without the use of any commercial software. The use of similar tools may guarantee setup repeatability, which can be useful for future researchers taking on this subject. Nevertheless, the main result remains the practical feasibility and relatively low costs involved in the design and manufacturing process, which would require small deviations from what is now the standard routine for welding and bolting systems for base plate connections currently in use.

Future work that stems from this proposed design procedure may lead to the quantification of a behavior factor for similar structure schemes and thus proposing simple and clear standardized procedures devoted to make the seismic design of racks in seismic zones economically feasible.

References

Articles

[1]   B. Tagliafierro, R. Montuori, and I. Vayas. "A hybrid modeling procedure for base-plate connections for pallet racking systems in seismic areas based on experimental tests and nonlinear numerical analyses." In: *Under review In: Thin-Walled Structures* (2022) (cit. on p. 8).

[2]   B. Tagliafierro, R. Montuori, and M. G. Castellano. "Shake table testing and numerical modelling of a steel pallet racking structure with a seismic isolation system." In: *Thin-Walled Structures* 164 (2021), p. 107924. ISSN: 0263-8231. DOI: https://doi.org/10.1016/j.tws.2021.107924 (cit. on pp. 8, 68, 81).

[3]   M. Simoncelli, B. Tagliafierro, and R. Montuori. "Recent development on the seismic devices for steel storage structures." In: *Thin-Walled Structures* 155 (2020), p. 106827. ISSN: 0263-8231. DOI: https://doi.org/10.1016/j.tws.2020.106827 (cit. on pp. 8, 21, 40).

[4]   R. Montuori, E. Nastri, and B. Tagliafierro. "Residual displacements for non-degrading bilinear oscillators under seismic actions." In: *Mechanics Research Communications* 111 (2021), p. 103651. ISSN: 0093-6413. DOI: https://doi.org/10.1016/j.mechrescom.2020.103651 (cit. on p. 8).

[5]   R. Montuori, E. Nastri, and B. Tagliafierro. "An Optimal Seismic Force Pattern for Uniform Drift Distribution." In: *Buildings* 9(11) (2019), p. 231. DOI: https://doi.org/10.3390/buildings9110231 (cit. on p. 8).

[6]   F. Yener and H. R. Yazgan. "Optimal warehouse design: Literature review and case study application." In: *Computers & Industrial Engineering* 129 (2019), pp. 1–13. ISSN: 0360-8352. DOI: https://doi.org/10.1016/j.cie.2019.01.006 (cit. on p. 17).

[7]   O. Tunca et al. "Structural features of cold-formed steel profiles." In: *Challenge Journal of Structural Mechanics* 4 (June 2018), p. 77. DOI: 10.20528/cjsmec.2018.02.005 (cit. on p. 17).

[8]   F. Markazi, R. Beale, and M. Godley. "Experimental analysis of semi-rigid boltless connectors." In: *Thin-Walled Structures* 28.1 (1997), pp. 57–87. ISSN: 0263-8231. DOI: https://doi.org/10.1016/S0263-8231(97)00003-7 (cit. on p. 17).

[9]   K. Tilburgs. "Those peculiar structures in cold-formed steel: "Racking & Shelving"." In: *Steel Construction* 6.2 (2013), pp. 95–106. DOI: 10.1002/stco.201310016 (cit. on p. 17).

[10]   D. Tsarpalis et al. "Macro-characteristics and taxonomy of steel racking systems for seismic vulnerability assessment." In: *Bulletin of Earthquake Engineering* (2022). DOI: 10.1007/s10518-022-01326-x (cit. on pp. 17, 44, 45).

[11]   D. K. Miller. "Lessons learned from the Northridge earthquake." In: *Engineering Structures* 20.4 (1998). Innovations in Stability Concepts and Methods for Seismic Design in Structural Steel, pp. 249–260. ISSN: 0141-0296. DOI: https://doi.org/10.1016/S0141-0296(97)00031-X (cit. on p. 18).

[12] A. Suppasri et al. "Improvement of Tsunami Countermeasures Based on Lessons from The 2011 Great East Japan Earthquake and Tsunami — Situation After Five Years." In: *Coastal Engineering Journal* 58.4 (2016), pp. 1640011-1-1640011–30. DOI: `10.1142/S0578563416400118`. eprint: `https://doi.org/10.1142/S0578563416400118` (cit. on p. 18).

[13] J. Takagi and A. Wada. "Recent earthquakes and the need for a new philosophy for earthquake-resistant design." In: *Soil Dynamics and Earthquake Engineering* 119 (2019), pp. 499–507. ISSN: 0267-7261. DOI: `https://doi.org/10.1016/j.soildyn.2017.11.024` (cit. on pp. 18, 22, 25).

[14] S. Uma and G. Beattie. "Observed performance of industrial pallet rack storage systems in the Canterbury earthquakes." In: *Bulletin of the New Zealand Society for Earthquake Engineering* 44 (Dec. 2011). DOI: `10.5459/bnzsee.44.4.388-393` (cit. on pp. 18, 19).

[15] D. Perrone et al. "Seismic performance of non-structural elements during the 2016 Central Italy earthquake." In: *Bull Earthquake Eng* 17 (2016), pp. 5655–5677 (cit. on pp. 18, 19, 51).

[16] C. Bernuzzi and M. Simoncelli. "Seismic Design of Grana Cheese Cold-Formed Steel Racks." In: *Buildings* 10.12 (2020). ISSN: 2075-5309. DOI: `10.3390/buildings10120246` (cit. on pp. 18, 25, 46).

[17] R. Becker. "Fundamentals of performance-based building design." In: *Building Simulation* 1 (Dec. 2008), pp. 356–371. DOI: `10.1007/s12273-008-8527-8` (cit. on p. 18).

[18] S. Avgerinou et al. "Full-scale tests on used steel storage racks." In: *Steel Construction* 12.3 (2019), pp. 231–242. DOI: `10.1002/stco.201900009` (cit. on pp. 18, 28, 48).

[19] D. Dubina, I. Marginean, and F. Dinu. "Impact modelling for progressive collapse assessment of selective rack systems." In: *Thin-Walled Structures* 143 (2019), p. 106201. ISSN: 0263-8231. DOI: `https://doi.org/10.1016/j.tws.2019.106201` (cit. on p. 18).

[20] J. Crosier, M. Hannah, and D. Mukai. "Damage to steel storage racks in industrial buildings in the Darfield earthquake." In: *Bulletin of the New Zealand Society for Earthquake Engineering* 43 (Dec. 2010). DOI: `10.5459/bnzsee.43.4.425-428` (cit. on pp. 18, 19).

[21] L. Liberatore et al. "Failure of industrial structures induced by the Emilia (Italy) 2012 earthquakes." In: *Engineering Failure Analysis* 34 (2013), pp. 629–647. ISSN: 1350-6307. DOI: `https://doi.org/10.1016/j.engfailanal.2013.02.009` (cit. on pp. 19, 51).

[22] L. Rossi, B. Holtschoppen, and C. Butenweg. "Official data on the economic consequences of the 2012 Emilia-Romagna earthquake: a first analysis of database SFINGE." In: *Bull Earthquake Eng* 17 (2019), pp. 4855–4884. DOI: `https://doi.org/10.1007/s10518-019-00655-8` (cit. on pp. 19, 45, 51).

[23] I. Connor. "Performance of steel storage racks in the Darfield Earthquake." In: *Bulletin of the New Zealand Society for Earthquake Engineering* 45 (June 2012), pp. 61–70. DOI: `10.5459/bnzsee.45.2.61-70` (cit. on p. 19).

[24] C. Bernuzzi and M. Simoncelli. "An advanced design procedure for the safe use of steel storage pallet racks in seismic zones." In: *Thin-Walled Structures* 109 (2016), pp. 73–87. ISSN: 0263-8231. DOI: `https://doi.org/10.1016/j.tws.2016.09.010` (cit. on pp. 19, 21, 22).

[25] E. Mirambell. "The convenient equilibrium between the development and updating of a normative code, research and engineering practice." In: *Steel Construction* 14.1 (2021), p. 1. ISSN: 18670520. DOI: `10.1002/stco.202170103` (cit. on p. 19).

[26] C. Castiglioni et al. "The "SEISRACKS2" EU-RFCS Research Project "Seismic Behaviour of Steel Storage Pallet Racking Systems"." In: *Costruzioni Metalliche* LXVII (Jan. 2015), pp. 37–48 (cit. on pp. 19, 27).

[27] C. Bernuzzi et al. "Unbraced pallet rack design in accordance with European practice-Part 1: Selection of the method of analysis." In: *Thin-Walled Structures* 86 (2015), pp. 185–207. ISSN: 0263-8231. DOI: https://doi.org/10.1016/j.tws.2014.06.015 (cit. on p. 20).

[28] C. Bernuzzi. "European and United States approaches for steel storage pallet rack design: Part 1: Discussions and general comparisons." In: *Thin-Walled Structures* 97 (2015), pp. 308–320. ISSN: 0263-8231. DOI: https://doi.org/10.1016/j.tws.2015.08.012 (cit. on p. 20).

[29] C. Moen and B. Schafer. "Elastic buckling of cold-formed steel columns and beams with holes." In: *Engineering Structures* 31 (Dec. 2009), pp. 2812–2824. DOI: 10.1016/j.engstruct.2009.07.007 (cit. on p. 20).

[30] P. Prabha et al. "Evaluation of connection flexibility in cold formed steel racks." In: *Journal of Constructional Steel Research* 66.7 (2010), pp. 863–872. ISSN: 0143-974X. DOI: https://doi.org/10.1016/j.jcsr.2010.01.019 (cit. on p. 20).

[31] N. Baldassino et al. "An experimental investigation on solid and perforated steel storage racks uprights." In: *Journal of Constructional Steel Research* 155 (2019), pp. 409–425. ISSN: 0143-974X. DOI: https://doi.org/10.1016/j.jcsr.2019.01.008 (cit. on pp. 20, 22).

[32] F. Gusella, M. Orlando, and K. D. Peterman. "Influence of mechanical and geometric uncertainty on the seismic performance of cold-formed steel braces with additional holes." In: *Structures* 29 (2021), pp. 494–506. ISSN: 2352-0124. DOI: https://doi.org/10.1016/j.istruc.2020.11.054 (cit. on pp. 20, 22).

[33] C. Bernuzzi, A. Pieri, and V. Squadrito. "Warping influence on the static design of unbraced steel storage pallet racks." In: *Thin-Walled Structures* 79 (2014), pp. 71–82. ISSN: 0263-8231. DOI: https://doi.org/10.1016/j.tws.2014.01.024 (cit. on p. 20).

[34] V. Mohan et al. "Cold-formed steel pallet rack connection: an experimental study." In: *International Journal of Advance Structural Engineering* 7 (Feb. 2015). DOI: 10.1007/s40091-015-0082-9 (cit. on p. 21).

[35] A. Filiatrault, P. S. Higgins, and A. Wanitkorkul. "Experimental Stiffness and Seismic Response of Pallet-Type Steel Storage Rack Connectors." In: *Practice Periodical on Structural Design and Construction* 11.3 (2006), pp. 161–170. DOI: 10.1061/(ASCE)1084-0680(2006)11:3(161) (cit. on p. 21).

[36] A. Firouzianhaji et al. "Shake Table Testing of Standard Cold-Formed Steel Storage Rack." In: *Applied Sciences* 11.4 (2021). ISSN: 2076-3417. DOI: 10.3390/app11041821 (cit. on pp. 21, 30).

[37] F. Gusella, M. Orlando, and P. Spinelli. "Pinching in Steel Rack Joints: Numerical Modelling and Effects on Structural Response." In: *International Journal of Steel Structures* 19.1 (Feb. 2019), pp. 131–146. ISSN: 2093-6311. DOI: 10.1007/s13296-018-0095-x (cit. on pp. 21, 27, 40, 60).

[38] E. Jacobsen and R. Tremblay. "Shake-table testing and numerical modelling of inelastic seismic response of semi-rigid cold-formed rack moment frames." In: *Thin-Walled Structures* 119 (2017), pp. 190–210. ISSN: 0263-8231. DOI: https://doi.org/10.1016/j.tws.2017.05.024 (cit. on pp. 21, 27).

[39] C. Galeotti et al. "On the seismic response of steel storage pallet racks with selective addition of bolted joints." In: *Structures* 34 (2021), pp. 3806–3817. ISSN: 2352-0124. DOI: https://doi.org/10.1016/j.istruc.2021.10.001 (cit. on p. 21).

[40] C. Bernuzzi and C. A. Castiglioni. "Experimental analysis on the cyclic behaviour of beam-to-column joints in steel storage pallet racks." In: *Thin-Walled Structures* 39.10 (2001), pp. 841–859. ISSN: 0263-8231. DOI: https://doi.org/10.1016/S0263-8231(01)00034-9 (cit. on pp. 21, 40).

[41] O. Bové et al. "Ductility improvement of adjustable pallet rack speed-lock connections: Experimental study." In: *Journal of Constructional Steel Research* 188 (2022), p. 107015. ISSN: 0143-974X. DOI: https://doi.org/10.1016/j.jcsr.2021.107015 (cit. on p. 21).

[42] A. Kanyilmaz et al. "Assessment of the seismic behaviour of braced steel storage racking systems by means of full scale push over tests." In: *Thin-Walled Structures* 107 (2016), pp. 138–155. ISSN: 0263-8231. DOI: https://doi.org/10.1016/j.tws.2016.06.004 (cit. on pp. 21, 22).

[43] B. P. Gilbert and K. J. Rasmussen. "Determination of the base plate stiffness and strength of steel storage racks." In: *Journal of Constructional Steel Research* 67.6 (2011), pp. 1031–1041. ISSN: 0143-974X. DOI: https://doi.org/10.1016/j.jcsr.2011.01.006 (cit. on pp. 22, 41).

[44] S. Shah et al. "State-of-the-art review on the design and performance of steel pallet rack connections." In: *Engineering Failure Analysis* 66 (2016), pp. 240–258. ISSN: 1350-6307. DOI: https://doi.org/10.1016/j.engfailanal.2016.04.017 (cit. on p. 21).

[45] F. Petrone et al. "The cross-aisle seismic performance of storage rack base connections." In: *Journal of Constructional Steel Research* 122 (2016), pp. 520–531. ISSN: 0143-974X. DOI: https://doi.org/10.1016/j.jcsr.2016.04.014 (cit. on pp. 21, 27, 41, 42, 68).

[46] C. Chen, R. Scholl, and J. Blume. "Seismic Study of Industrial Storage Racks, Report Prepared for the National Science Foundation and for the Rack Manufacturers Institute and Automated Storage and Retrieval Systems (Sections of the Material Handling Institute)." In: (Jan. 1980), 569 pp (cit. on p. 21).

[47] C. Bernuzzi and M. Simoncelli. "Steel storage pallet racks in seismic zones: Advanced vs. standard design strategies." In: *Thin-Walled Structures* 116 (2017), pp. 291–306. ISSN: 0263-8231. DOI: https://doi.org/10.1016/j.tws.2017.03.002 (cit. on pp. 22, 27).

[48] C. Bernuzzi et al. "Pushover Analyses of Hand-Loaded Steel Storage Shelving Racks." In: *Journal of Earthquake Engineering* 21.8 (2017), pp. 1256–1282. DOI: 10.1080/13632469.2016.1210063 (cit. on p. 22).

[49] R. Montuori et al. "Rigid plastic analysis for the seismic performance evaluation of steel storage racks." In: *Steel and Composite Structures* 32.1 (July 2019), pp. 1–19 (cit. on pp. 22, 27).

[50] X. Zhang, K. J. Rasmussen, and H. Zhang. "Beam-element-based analysis of locally and/or distortionally buckled members: Application." In: *Thin-Walled Structures* 95 (2015), pp. 127–137. ISSN: 0263-8231. DOI: https://doi.org/10.1016/j.tws.2015.06.021 (cit. on p. 22).

[51] K. J. Rasmussen, X. Zhang, and H. Zhang. "Beam-element-based analysis of locally and/or distortionally buckled members: Theory." In: *Thin-Walled Structures* 98 (2016), pp. 285–292. ISSN: 0263-8231. DOI: https://doi.org/10.1016/j.tws.2015.06.020 (cit. on p. 22).

[52] N. Makris. "Seismic isolation: Early history." In: *Earthquake Engineering & Structural Dynamics* 48.2 (2019), pp. 269–283. DOI: 10.1002/eqe.3124 (cit. on p. 22).

[53] C. Fabrizio, A. M. de Leo, and A. D. Egidio. "Tuned Mass Damper and Base Isolation: A Unitary Approach for the Seismic Protection of Conventional Frame Structures." In: *Journal of Engineering Mechanics* 145.4 (2019), p. 04019011. DOI: 10.1061/(ASCE)EM.1943-7889.0001581 (cit. on p. 23).

[54] A. De Luca and L. G. Guidi. "State of art in the worldwide evolution of base isolation design." In: *Soil Dynamics and Earthquake Engineering* 125 (2019), p. 105722. ISSN: 0267-7261. DOI: https://doi.org/10.1016/j.soildyn.2019.105722 (cit. on pp. 23, 25, 26, 38).

[55] P. Clemente and A. Martelli. "Seismically isolated buildings in Italy: State-of-the-art review and applications." In: *Soil Dynamics and Earthquake Engineering* 119 (2019), pp. 471–487. ISSN: 0267-7261. DOI: https://doi.org/10.1016/j.soildyn.2017.12.029 (cit. on pp. 23, 25).

[56] G. Gesualdi, D. Cardone, and G. Rosa. "Finite element model updating of base-isolated buildings using experimental results of in-situ tests." In: *Soil Dynamics and Earthquake Engineering* 119 (2019), pp. 422–432. ISSN: 0267-7261. DOI: https://doi.org/10.1016/j.soildyn.2018.02.003 (cit. on p. 23).

[57] A. Longo, R. Montuori, and V. Piluso. "Theory of plastic mechanism control for MRF-CBF dual systems and its validation." In: *Bulletin of Earthquake Engineering* 12.6 (2014), pp. 2745–2775. DOI: 10.1007/s10518-014-9612-2 (cit. on p. 23).

[58] V. Piluso et al. "Probabilistic Theory of Plastic Mechanism Control for Steel Moment Resisting Frames." In: *Structural Safety* 76 (2019), pp. 95–107. ISSN: 0167-4730. DOI: https://doi.org/10.1016/j.strusafe.2018.08.003 (cit. on p. 23).

[59] M. N. Fardis. "Capacity design: Early history." In: *Earthquake Engineering & Structural Dynamics* 47.14 (2018), pp. 2887–2896. DOI: 10.1002/eqe.3110 (cit. on pp. 23, 40).

[60] K. Ghaedi et al. "Invited Review: Recent developments in vibration control of building and bridge structures." In: *Journal of Vibroengineering* 19 (Aug. 2017), pp. 3564–3580. DOI: 10.21595/jve.2017.18900 (cit. on p. 25).

[61] P. Pan et al. "Base-isolation design practice in Japan: introduction to te post-Kobe approach." In: *Journal of Earthquake Engineering* 9.1 (2005), pp. 147–171. DOI: 10.1080/13632460509350537 (cit. on pp. 25, 27).

[62] D. Jovanovic et al. "Hysteresis model for beam-to-column connections of steel storage racks." In: *Thin-Walled Structures* 142 (2019), pp. 189–204. ISSN: 0263-8231. DOI: https://doi.org/10.1016/j.tws.2019.04.056 (cit. on pp. 27, 48).

[63] G. Gabbianelli, F. Cavalieri, and R. Nascimbene. "Seismic vulnerability assessment of steel storage pallet racks." In: *Ingegneria Sismica* 37 (June 2020), pp. 18–40 (cit. on p. 27).

[64] Z. Lyu et al. "Assessment of the Dynamic Behavior of Beam-to-Column Connections in Steel Pallet Racks under Cyclic Load: Numerical Investigation." In: *Advances in Civil Engineering* 2018 (Nov. 2018), pp. 1–12. DOI: 10.1155/2018/9243216 (cit. on p. 27).

[65] K. Adamakos, S. Sesana, and I. Vayas. "Interaction Between Pallets and Pallet Beams of Steel Storage Racks in Seismic Areas." In: *International Journal of Steel Structures* 18 (Nov. 2018), pp. 1018–1034. DOI: 10.1007/s13296-018-0041-y (cit. on pp. 27, 64).

[66] J. R. Maguire et al. "Residual capacity of cold-formed steel rack uprights following stomping during rocking." In: *Journal of Constructional Steel Research* 159 (2019), pp. 189–197. ISSN: 0143-974X. DOI: https://doi.org/10.1016/j.jcsr.2019.04.039 (cit. on pp. 27, 41).

[67]   N. Talebian et al. "Factors contributing to the transverse shear stiffness of bolted cold-formed steel storage rack upright frames with channel bracing members." In: *Thin-Walled Structures* 136 (2019), pp. 50–63. ISSN: 0263-8231. DOI: https://doi.org/10.1016/j.tws.2018.12.001 (cit. on pp. 27, 41, 68).

[68]   A. Filiatrault et al. "Experimental Seismic Response of Base Isolated Pallet-Type Steel Storage Racks." In: *Earthquake Spectra - EARTHQ SPECTRA* 24 (Aug. 2008). DOI: 10.1193/1.2942375 (cit. on pp. 28, 33, 35–39).

[69]   G. P. Warn and K. L. Ryan. "A Review of Seismic Isolation for Buildings: Historical Development and Research Needs." In: *Buildings* 2.3 (Aug. 2012), pp. 300–325. ISSN: 2075-5309. DOI: 10.3390/buildings2030300 (cit. on p. 27).

[70]   P. C. Roussis. "Study on the Effect of Uplift-Restraint on the Seismic Response of Base-Isolated Structures." In: *Journal of Structural Engineering* 135.12 (2009), pp. 1462–1471. DOI: 10.1061/(ASCE)ST.1943-541X.0000070 (cit. on p. 28).

[71]   V. Kilar et al. "Seismic analysis of an asymmetric fixed base and base-isolated high-rack steel structure." In: *Engineering structures* 33 (2011), pp. 3471–3482 (cit. on pp. 30–33).

[72]   V. Kilar et al. "Cost viability of a Base isolation system for the seismic protection of a steel high-rack structure." In: *International Journal of Steel Structures* 13.2 (June 2013), pp. 253–263 (cit. on pp. 30, 32, 33).

[73]   S. Petrovčič and V. Kilar. "Effects of Horizontal and Vertical Mass-Asymmetric Distributions on the Seismic Response of a High-Rack Steel Structure." In: *Advances in Structural Engineering* 15 (Nov. 2012), pp. 1977–1988. DOI: 10.1260/1369-4332.15.11.1977 (cit. on p. 30).

[74]   CSI software. "Integrated Finite Element Analysis and Design of Structures Basic Analysis Reference Manual." In: *Computers and Structures Inc.* (2010), p. 430 (cit. on p. 31).

[75]   A. Bhuiyan et al. "A rheology model of high damping rubber bearings for seismic analysis: Identification of nonlinear viscosity." In: *International Journal of Solids and Structures* 46.7 (2009), pp. 1778–1792. ISSN: 0020-7683. DOI: https://doi.org/10.1016/j.ijsolstr.2009.01.005 (cit. on p. 38).

[76]   G. Candia, J. C. de la Llera, and J. L. Almazán. "A physical model for dynamic analysis of wine barrel stacks." In: *Earthquake Engineering & Structural Dynamics* 39.10 (2010), pp. 1063–1081. DOI: 10.1002/eqe.979 (cit. on p. 39).

[77]   M. Ferrari. "LOKIBASE: the device for seismic isolation of pallet racking systems." In: *Costruzioni Metalliche* 3.Maggio-Giugno (2019), pp. 82–91 (cit. on p. 39).

[78]   M. Ferrari. "LOKIBASE: the device for seismic isolation of pallet racking systems." In: *Costruzioni Metalliche* 4.Luglio-Agosto (2019), pp. 111–122 (cit. on p. 39).

[79]   V. Piluso and G. Rizzano. "Experimental analysis and modelling of bolted T-stubs under cyclic loads." In: *Journal of Constructional Steel Research* 64.6 (2008), pp. 655–669. ISSN: 0143-974X. DOI: https://doi.org/10.1016/j.jcsr.2007.12.009 (cit. on pp. 40, 73, 75).

[80]   S. Marras and K. T. Mandli. "Modeling and Simulation of Tsunami Impact: A Short Review of Recent Advances and Future Challenges." In: *Geosciences* 11.1 (2021). ISSN: 2076-3263. DOI: 10.3390/geosciences11010005 (cit. on p. 40).

[81]   I. Vayas, D. Vamvatsikos, and P. Thanopoulos. "Innovative systems for seismic resistance: The INNOSEIS Project." In: *ce/papers* 1 (Sept. 2017), pp. 3375–3384. DOI: 10.1002/cepa.392 (cit. on p. 40).

[82] M. D. Titirla et al. "On the mechanical modeling of an innovative energy dissipation device." In: *Ingegneria Sismica* 34 (June 2017) (cit. on p. 40).

[83] M. D. Titirla, P. K. Papadopoulos, and I. N. Doudoumis. "Finite element modelling of an innovative passive energy dissipation device for seismic hazard mitigation." In: *Engineering Structures* 168 (2018), pp. 218–228. ISSN: 0141-0296. DOI: https://doi.org/10.1016/j.engstruct.2018.04.081 (cit. on p. 40).

[84] V. Piluso et al. "Seismic response of MRF-CBF dual systems equipped with low damage friction connections." In: *Journal of Constructional Steel Research* 154 (2019), pp. 263–277. ISSN: 0143-974X. DOI: https://doi.org/10.1016/j.jcsr.2018.12.008 (cit. on pp. 40, 42).

[85] M. Latour et al. "Experimental response of a low-yielding, self-centering, rocking column base joint with friction dampers." In: *Soil Dynamics and Earthquake Engineering* 116 (2019), pp. 580–592. ISSN: 0267-7261. DOI: https://doi.org/10.1016/j.soildyn.2018.10.011 (cit. on pp. 40, 42).

[86] E. Nastri et al. "Seismic response of steel Moment Resisting Frames equipped with friction beam-to-column joints." In: *Soil Dynamics and Earthquake Engineering* 119 (2019), pp. 144–157. ISSN: 0267-7261. DOI: https://doi.org/10.1016/j.soildyn.2019.01.009 (cit. on pp. 40, 42).

[87] D. Tsarpalis, D. Vamvatsikos, and I. Vayas. "Seismic assessment approaches for mass-dominant sliding contents: The case of storage racks." In: *Earthquake Engineering & Structural Dynamics* n/a.n/a (2021). DOI: https://doi.org/10.1002/eqe.3592. eprint: https://onlinelibrary.wiley.com/doi/pdf/10.1002/eqe.3592 (cit. on p. 40).

[88] M. S. Shaheen and K. J. Rasmussen. "Development of friction-damped seismic fuses for steel storage racks." In: *Journal of Constructional Steel Research* 192 (2022), p. 107216. ISSN: 0143-974X. DOI: https://doi.org/10.1016/j.jcsr.2022.107216 (cit. on pp. 40, 45).

[89] B. P. Gilbert et al. "Determining the transverse shear stiffness of steel storage rack upright frames." In: *Journal of Constructional Steel Research* 78 (2012), pp. 107–116. ISSN: 0143-974X. DOI: https://doi.org/10.1016/j.jcsr.2012.06.012 (cit. on p. 41).

[90] H. Far, A. Saleh, and A. Firouzianhaji. "A simplified method to determine shear stiffness of thin walled cold formed steel storage rack frames." In: *Journal of Constructional Steel Research* 138 (2017), pp. 799–805. ISSN: 0143-974X. DOI: https://doi.org/10.1016/j.jcsr.2017.09.012 (cit. on p. 41).

[91] J. R. Maguire et al. "Equivalent static force method for selective storage racks with uplifting baseplates." In: *Journal of Constructional Steel Research* 165 (2020), p. 105821. ISSN: 0143-974X. DOI: https://doi.org/10.1016/j.jcsr.2019.105821 (cit. on pp. 41, 68).

[92] F. Freddi, C. A. Dimopoulos, and T. L. Karavasilis. "Rocking damage-free steel column base with friction devices: design procedure and numerical evaluation." In: *Earthquake Engineering & Structural Dynamics* 46.14 (2017), pp. 2281–2300. DOI: https://doi.org/10.1002/eqe.2904. eprint: https://onlinelibrary.wiley.com/doi/pdf/10.1002/eqe.2904 (cit. on p. 41).

[93] Z. Huang et al. "Determination of the flexural behavior of steel storage rack baseplate upright connections with eccentric anchor bolts." In: *Thin-Walled Structures* 160 (2021), p. 107375. ISSN: 0263-8231. DOI: https://doi.org/10.1016/j.tws.2020.107375 (cit. on p. 41).

[94] S. Di Benedetto, M. Latour, and G. Rizzano. "Chord failure resistance of 3D cut welded connections with CHS columns and through I-BEAMS." In: *Thin-Walled Structures* 154 (2020), p. 106821. ISSN: 0263-8231. DOI: https://doi.org/10.1016/j.tws.2020.106821 (cit. on pp. 42, 73).

[95] S. Di Benedetto et al. "Experimental response of a large-scale two-storey steel building equipped with low-yielding friction joints." In: *Soil Dynamics and Earthquake Engineering* 152 (2022). ISSN: 02677261. DOI: 10.1016/j.soildyn.2021.107022 (cit. on p. 42).

[96] G. Clifton. "Semi-rigid Joints for Moment Resisting Steel Framed Seismic-Resisting Systems." In: (Jan. 2005) (cit. on p. 42).

[97] A. M. Freitas, F. T. Souza, and M. S. Freitas. "Analysis and behavior of steel storage drive-in racks." In: *Thin-Walled Structures* 48.2 (2010), pp. 110–117. ISSN: 0263-8231. DOI: https://doi.org/10.1016/j.tws.2009.09.003 (cit. on p. 44).

[98] M. Shaheen and K. Rasmussen. "Seismic tests of drive-in steel storage racks in cross-aisle direction." In: *Journal of constructional steel research* 162 (2019), pp. 1–18 (cit. on p. 44).

[99] M. Mucciarelli and D. Liberatore. "Guest editorial: The Emilia 2012 earthquakes, Italy." In: *Bulletin of Earthquake Engineering* 12.5 (Oct. 2014), pp. 2111–2116. ISSN: 1573-1456. DOI: 10.1007/s10518-014-9629-6 (cit. on p. 45).

[100] F. Saitta et al. "Behaviour of industrial buildings in the Pianura Padana Emiliana Earthquake." In: *Energia Ambiente Innovazione* 4/5 (Nov. 2012), pp. 47–57 (cit. on p. 45).

[101] D. A. Bournas, P. Negro, and F. F. Taucer. "Performance of industrial buildings during the Emilia earthquakes in Northern Italy and recommendations for their strengthening." In: *Bulletin of Earthquake Engineering* 12.5 (Oct. 2014), pp. 2383–2404. ISSN: 1573-1456. DOI: 10.1007/s10518-013-9466-z (cit. on p. 45).

[102] A. Franco, S. Massimiani, and G. Royer-Carfagni. "Passive control of steel storage racks for Parmigiano Reggiano Cheese under seismic accelerations." In: *Journal of earthquake engineering* 19 (2015), pp. 1222–1259 (cit. on pp. 45, 46).

[103] L. Fiorino, V. Macillo, and R. Landolfo. "Shake table tests of a full-scale two-story sheathing-braced cold-formed steel building." In: *Engineering Structures* 151 (2017), pp. 633–647. DOI: 10.1016/j.engstruct.2017.08.056 (cit. on p. 48).

[104] Y. Hu et al. "Seismic responses and damage assessment of a mid-rise cold-formed steel building under far-fault and near-fault ground motions." In: *Thin-Walled Structures* 163 (2021), p. 107690. ISSN: 0263-8231. DOI: https://doi.org/10.1016/j.tws.2021.107690 (cit. on p. 48).

[105] M. Michele et al. "The Amatrice 2016 seismic sequence: A preliminary look at the mainshock and aftershocks distribution." In: *Annals of Geophysics* 59 (Nov. 2016). DOI: 10.4401/ag-7227 (cit. on p. 51).

[106] E. Valerio et al. "Ground Deformation and Source Geometry of the 30 October 2016 Mw 6.5 Norcia Earthquake (Central Italy) Investigated Through Seismological Data, DInSAR Measurements, and Numerical Modelling." In: *Remote Sensing* 10 (Nov. 2018), p. 1901. DOI: 10.3390/rs10121901 (cit. on p. 51).

[107] R. Sisti et al. "Damage assessment and the effectiveness of prevention: the response of ordinary unreinforced masonry buildings in Norcia during the Central Italy 2016-2017 seismic sequence." In: *Bulletin of Earthquake Engineering* (Aug. 2018). DOI: 10.1007/s10518-018-0448-z (cit. on p. 51).

[108] M. Dolce and D. Di Bucci. "Comparing recent Italian earthquakes." In: *Bulletin of Earthquake Engineering* 15 (May 2015). DOI: 10.1007/s10518-015-9773-7 (cit. on p. 51).

[109]   M. Savoia, N. Buratti, and L. Vincenzi. "Damage and collapses in industrial precast buildings after the 2012 Emilia earthquake." In: *Engineering Structures* 137 (2017), pp. 162–180. ISSN: 0141-0296. DOI: https://doi.org/10.1016/j.engstruct.2017.01.059 (cit. on p. 51).

[110]   R. S. Jangid and J. M. Kelly. "Base isolation for near-fault motions." In: *Earthquake Engineering & Structural Dynamics* 30.5 (2001), pp. 691–707. DOI: 10.1002/eqe.31 (cit. on p. 51).

[111]   F. McKenna, M. H. Scott, and G. L. Fenves. "Nonlinear Finite-Element Analysis Software Architecture Using Object Composition." In: *Journal of Computing in Civil Engineering* 24.1 (2010), pp. 95–107. DOI: 10.1061/(ASCE)CP.1943-5487.0000002 (cit. on pp. 60, 80).

[112]   M. Constantinou, A. Mokha, and A. Reinhorn. "Teflon Bearings in Base Isolation II: Modeling." In: *Journal of Structural Engineering* 116.2 (1990), pp. 455–474. DOI: 10.1061/(ASCE)0733-9445(1990)116:2(455) (cit. on p. 60).

[113]   D. D. Domenico, E. Gandelli, and V. Quaglini. "Effective base isolation combining low-friction curved surface sliders and hysteretic gap dampers." In: *Soil Dynamics and Earthquake Engineering* 130 (2020), p. 105989. ISSN: 0267-7261. DOI: https://doi.org/10.1016/j.soildyn.2019.105989 (cit. on p. 60).

[114]   E. Fagà et al. "Modelling curved surface sliding bearings with bilinear constitutive law: effects on the response of seismically isolated buildings." In: *Mater Struct* 49 (2016), pp. 2179–2196. DOI: https://doi.org/10.1617/s11527-015-0642-2 (cit. on p. 60).

[115]   S. Erlicher, L. Bonaventura, and O. Bursi. "The analysis of the Generalized α method for non-linear dynamic problems." In: *Computational Mechanics* 28 (Jan. 2002), pp. 83–104. DOI: 10.1007/s00466-001-0273-z (cit. on pp. 62, 82).

[116]   K. L. Ryan and J. Polanco. "Problems with Rayleigh Damping in Base-Isolated Buildings." In: *Journal of Structural Engineering* 134.11 (2008), pp. 1780–1784. DOI: 10.1061/(ASCE)0733-9445(2008)134:11(1780) (cit. on p. 62).

[117]   D. R. Pant, A. C. Wijeyewickrema, and M. A. ElGawady. "Appropriate viscous damping for nonlinear time-history analysis of base-isolated reinforced concrete buildings." In: *Earthquake Engineering & Structural Dynamics* 42.15 (2013), pp. 2321–2339. DOI: https://doi.org/10.1002/eqe.2328. eprint: https://onlinelibrary.wiley.com/doi/pdf/10.1002/eqe.2328 (cit. on p. 62).

[118]   D. Vamvatsikos and C. A. Cornell. "Incremental dynamic analysis." In: *Earthquake Engineering & Structural Dynamics* 31.3 (2002), pp. 491–514. DOI: 10.1002/eqe.141 (cit. on pp. 63, 83).

[119]   M. Latour, V. Piluso, and G. Rizzano. "Cyclic Modeling of Bolted Beam-to-Column Connections: Component Approach." In: *Journal of Earthquake Engineering* 15.4 (2011), pp. 537–563. DOI: 10.1080/13632469.2010.513423 (cit. on p. 73).

[120]   M. Latour et al. "Experimental analysis and mechanical modeling of T-stubs with four bolts per row." In: *Journal of Constructional Steel Research* 101 (2014), pp. 158–174. ISSN: 0143-974X. DOI: https://doi.org/10.1016/j.jcsr.2014.05.004 (cit. on p. 73).

[121]   X. Zhu and Z. Wu. "Study on New Bolted T-Stub Connection with Inserted Plates under Axial and Cyclic Loads." In: *Applied Sciences* 10.7 (2020). ISSN: 2076-3417. DOI: 10.3390/app10072631 (cit. on p. 75).

[122]   M. Menegotto and P. Pinto. "Method of analysis of cyclically loaded RC plane frames including changes in geometry and non-elastic behavior of elements under normal force and bending." In: *Preliminary Report IABSE* 13 (1973) (cit. on p. 78).

[123] F. Filippou, E. Popov, and V. Bertero. "Effects of Bond Deterioration on Hysteretic Behavior of Reinforced Concrete Joints." In: *Report EERC 83-19, Earthquake Engineering Research Center, University of California, Berkeley* (1983) (cit. on p. 78).

[124] G. Kiymaz. "Investigations on the bearing strength of stainless steel bolted plates under in-plane tension." In: *Steel and Composite Structures* 9 (Mar. 2009). DOI: 10.12989/scs.2009.9.2.173 (cit. on p. 78).

[125] J. W. Hu, R. T. Leon, and T. Park. "Mechanical modeling of bolted T-stub connections under cyclic loads Part I: Stiffness Modeling." In: *Journal of Constructional Steel Research* 67.11 (2011), pp. 1710–1718. ISSN: 0143-974X. DOI: https://doi.org/10.1016/j.jcsr.2011.04.009 (cit. on p. 79).

[126] P. Galli, S. Castenetto, and E. Peronace. "The Macroseismic Intensity Distribution of the 30 October 2016 Earthquake in Central Italy (Mw 6.6): Seismotectonic Implications." In: *Tectonics* 36.10 (2017), pp. 2179–2191. DOI: https://doi.org/10.1002/2017TC004583. eprint: https://agupubs.onlinelibrary.wiley.com/doi/pdf/10.1002/2017TC004583 (cit. on p. 85).

Books and Codes

[127] FEMA 460. *Seismic considerations for steel storage racks located in areas accessible to the public*. Federal Emergency Management Agency, Washington, DC., 2005 (cit. on pp. 18, 20, 27, 35).

[128] ANSI MH 16.1. *Specification for the Design, Testing and Utilization of Industrial Storage Racks*. American National Standard, US, 2009 (cit. on p. 19).

[129] EN 16681. *Steel Static Storage Systems – Adjustable Pallet Racking Systems – Principles for Seismic Design*. European Committee for Standardization, Brussels, 2016 (cit. on pp. 19–21, 27, 41, 64, 68, 70, 71).

[130] Standards New Zealand. *Structural Design Actions, Part 5: Earthquake Actions*. New Zealand, NZS 1170.5:2004, Standard. NZS, 2004 (cit. on p. 19).

[131] G.J. Beattie, B.L. Deam. *Seismic Design of High Level Selective Storage Racking Systems with Public Access*. BRANZ Design Guide, BRANZ Ltd, Judgeford, New Zealand, 2006 (cit. on p. 19).

[132] Eurocode 3. *Design of Steel Structures*. European Committee for Standardization, Brussels, 2005 (cit. on pp. 19–21, 40, 71, 75).

[133] ANSI/AISC 360-16. *Specification for structural steel buildings*. American Institute of Steel Construction, US, 2016 (cit. on pp. 19, 20, 74, 75).

[134] EN 15512. *Steel Static Storage Systems – Adjustable Pallet Racking Systems – Principles for Structural Design*. European Committee for Standardization, Brussels, 2021 (cit. on pp. 19, 20, 41, 48, 71, 79, 88).

[135] SEISRACK. *Storage racks in seismic areas*. European Commission et al., 2009. DOI: doi/10.2777/60886 (cit. on pp. 19, 41).

[136] FEM 10.2.08. *Recommendations for the design of static steel storage pallet racks in seismic conditions*. Federation Européenne de Manutention, version 1.00, 2010 (cit. on pp. 19, 20).

[137] EN1998-1. *Eurocode 8 - Design of Structures for Earthquake Resistance-Part 1: General Rules, Seismic Actions and Rules for Buildings*. European Committee for Standardization CEN, EN1998-1, 2005 (cit. on pp. 20, 41, 69, 73).

[138] A. Preumont. *Vibration Control of Active Structures: An Introduction*. Springer International Publishing, 2018 (cit. on p. 22).

[139] SEAOC - Vision 2000 Committee. *Performance based seismic engineering of buildings, vols. I and II: Conceptual framework*. Sacramento, CA: Structural Engineers Association of California, 1995 (cit. on p. 23).

[140] I. Avramidis et al. *Eurocode-Compliant Seismic Analysis and Design of R/C Buildings*. $1^{s}t$. Vol. 38. Geotechnical, Geological and Earthquake Engineering. Springer International Publishing, 2016 (cit. on p. 23).

[141] C. Christopoulos and A. Filiatrault. *Principle of Passive Supplemental Damping and Seismic Isolation*. Eucentre, Jan. 2006 (cit. on pp. 25, 29).

[142] A. K. Chopra. *Dynamics of Structures: theory and applications to earthquake engineering*. 4th ed. Reading, Mass.: Prentice Hall, 2012, p. 843 (cit. on pp. 26, 29, 72, 81).

[143] EN 15129. *Anti-seismic devices*. European Committee for Standardization, Brussels, 2009 (cit. on pp. 27, 54, 91).

[144] S. Braun. *Encyclopedia of Vibration:* Academic Press, San Diego, 2001, p. 1595. ISBN: 0-12-227085-1. DOI: 10.1115/1.1470670 (cit. on p. 29).

[145] S. G. Kelly. *Mechanical vibrations: theory and applications*. Cengage learning, 2012 (cit. on p. 29).

[146] CEB-FIB. *Seismic design of precast concrete building structures, State-of-art report prepared by Task Group 7.3*. Fib, 2003 (cit. on p. 30).

[147] F. M. Mazzolani and V. Gioncu. *Seismic Resistant Steel Structures edited by Federico M. Mazzolani, Victor Gioncu*. eng. 1st ed. 2000. CISM International Centre for Mechanical Sciences, Courses and Lectures, 420. Vienna: Springer Vienna : Imprint: Springer, 2000. ISBN: 3-211-83329-3 (cit. on p. 40).

[148] I. Vayas, J. Ermopoulos, and G. Ioannidis. *Design of Steel Structures to Eurocodes*. Springer International Publishing, 2019. DOI: 10.1007/978-3-319-95474-5 (cit. on p. 40).

[149] C. Faella, V. Piluso, and G. Rizzano. *Structural Steel Semirigid Connections: Theory, Design, and Software*. Boca Raton, FL, USA: CRC Press, 1999 (cit. on p. 72).

[150] EN 10346. *Continuously hot-dip coated steel flat products for cold forming - technical delivery conditions*. British Standards Institution, London, 2015 (cit. on p. 73).

Book Chapters

[151] F. Naeim and J. M. Kelly. "Theoretical Basis of Seismic Isolation." In: *Design of Seismic Isolated Structures*. John Wiley & Sons, Ltd, 2007. Chap. 2, pp. 25–45. ISBN: 9780470172742. DOI: 10.1002/9780470172742.ch2 (cit. on pp. 25, 29, 38, 60).

[152] R. Paolucci et al. "Record Processing in ITACA, the New Italian Strong-Motion Database." In: *Earthquake Data in Engineering Seismology: Predictive Models, Data Management and Networks*. Ed. by S. Akkar, P. Gülkan, and T. van Eck. Dordrecht: Springer Netherlands, 2011, pp. 99–113. ISBN: 978-94-007-0152-6. DOI: 10.1007/978-94-007-0152-6_8 (cit. on p. 83).

Proceedings

[153] M. Simoncelli, B. Tagliafierro, and R. Montuori. "Seismic devices for steel storage structures." In: vol. 2021-June. National Technical University of Athens, 2021 (cit. on pp. 8, 21, 40).

[154] B. Taglafierro et al. "Experimental testing campaign and numerical modelling of an innovative base-plate connection for pallet racking systems." In: vol. 2021-June. National Technical University of Athens, 2021 (cit. on pp. 8, 73).

[155]   B. Tagliafierro et al. "A new open source solver for modelling fluid-structure interaction: Case study of a point-absorber wave energy converter with power take-off unit." In: ed. by P. C. Papadrakakis M. Fragiadakis M. Vol. 1. European Association for Structural Dynamics, 2020, pp. 657–668. ISBN: 9786188507203 (cit. on p. 8).

[156]   B. Tagliafierro and E. Nastri. "Seismic design lateral force distributions based on elastic analysis of structures." In: ed. by T. C. Simos T.E. Vol. 2116. American Institute of Physics Inc., 2019. ISBN: 9780735418547. DOI: 10.1063/1.5114273 (cit. on p. 8).

[157]   C. Chen et al. "Behavior of steel storage pallet racking connection - A review." In: vol. 30. 2019, pp. 457–469. DOI: http://dx.doi.org/10.12989/scs.2019.30.5.457 (cit. on p. 27).

[158]   C. Chadwell, J. Stanley, and M. J.M. "Nonlinear Analytical Modeling and System Verification of a Wine Barrel on a Portable Steel Rack Subject to Seismic Excitation." In: 8th National Conference of Earthquake Engineering. San Francisco, California, Oct. 2006 (cit. on p. 39).

[159]   C. Chadwell, K. Brennan, and M. Porter. "Seismic Isolation of Wine Barrel Stacks on Portable Steel Racks." In: WCEE 14th World Conference on Earthquake Engineering. Beijing, China, Oct. 2008 (cit. on p. 39).

[160]   A. Mensah et al. "Probabilistic Combination of Earthquake and Operational Loads for Wind Turbines." In: Jan. 2012. DOI: 10.13140/2.1.2212.1928 (cit. on p. 40).

[161]   M. D. Titirla and P. Papadopoulos. "Finite Element Investigation of a New Seismic Energy Absorption Device through Simultaneously Yield and Friction." In: COMPDYN 2015, 5th ECCOMAS Thematic Conference on Computational Methods in Structural Dynamics and Earthquake Engineering. Crete Island, Greece, May 2015 (cit. on p. 40).

[162]   Z. Tang et al. "Increasing seismic resilience of pallet racking systems using sliding friction baseplates." In: 2017 NZSEE conference. New Zeland, 2017 (cit. on pp. 42, 43, 68).

[163]   T. Takeuchi and K. Suzuki. "Performance-based design for truss-frame structures using dissipation devices." In: 4th International speciality conference. Naples, Italy, 2003 (cit. on pp. 43, 44).

[164]   M. Shaheen and K. Rasmussen. "Design methods of drive-in steel storage racks." In: 8th Eurosteel2017. Copenhagen, Denmark, 2017 (cit. on p. 45).

Miscellaneous

[165]   R. Michael. *Design and development of a seismic isolation system for commercial storage rack*. [Retrieved from https://etd.ohiolink.edu/]. (Electronic Thesis or Dissertation). 2013 (cit. on p. 34).

[166]   MATLAB Release 2019a. *The MathWorks*. 2019 (cit. on p. 50).

[167]   MATLAB Release 2021b. *The MathWorks*. 2021 (cit. on p. 83).

[168]   ITACA 3.2. *Italian Accelerometric Archive v3.2 - Istituto Nazionale di Geofisica e Vulcanologia*. 2022. DOI: 10.13127/itaca.3.2 (cit. on p. 83).